NJPST

NIGERIAN JOURNAL OF POLYMER SCIENCE AND TECHNOLOGY

A PUBLICATION OF THE POLYMER INSTITUTE OF NIGERIA

Vol. 12, 2017. ISSN 1119-4111

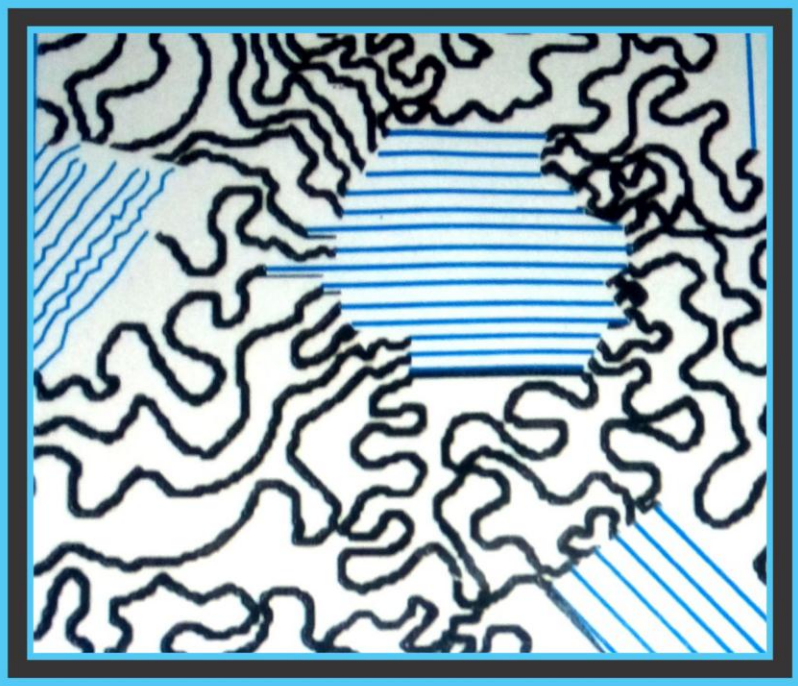

POLYMER INSTITUTE OF NIGERIA

Nigerian Journal of Polymer Science and Technology

Volume 12, 2017

ISSN: 1119-4111

A PUBLICATION OF THE POLYMER INSTITUTE OF NIGERIA

Nigerian Journal of Polymer Science and Technology

ISSN: 1119-4111 Volume 12, 2017

EDITORIAL BOARD

NATIONAL OFFICERS AND COUNCIL MEMBERS OF THE POLYMER INSTITUTE OF NIGERIA (PIN)

POLYMER INSTITUTE OF NIGERIA BOARD OF DIRECTORS

NATIONAL OFFICERS AND COUNCIL MEMBERS OF THE POLYMER INSTITUTE OF NIGERIA (PIN)

POLYMER INSTITUTE OF NIGERIA BOARD OF DIRECTORS

Chief Alexis N. Ajuebon, FPIN	Chairman, Board of Directors
Dr. J. T. Dawha, FPIN	Immediate Past Board Chairman
Prof. P. A. P Mamza, FPIN, FICCON	President
Dr. J. E Imanah, FPIN	Immediate Past President
Prof B. T Nwufo,FPIN	Secretary to the Board
Dr. (Mrs) C. D Igwebike-Ossi	Vice President (Operations)
Dr. F. O Biotidara, FPIN	Vice President (Finance)
Engr. (Dr.) F. P Momoh	General Secretary
Engr. (Dr.) N. C Iheaturu	Assistant Secretary General
Dr. P. M Ejikeme	Treasurer
Dr. M. B Dalen	Publicity Secretary
Engr. (Mrs) G. O Ihekweme	Membership Secretary
Dr. F. O Biotidara, FPIN (Acting)	Lagos District
Prof. O. Akaranta, FPIN	Port Harcourt District
Mr. F. Inegbedion	Auchi District
Dr. Owen Egharevba	Benin District
Mr. V. Nwadike, FPIN	Warri District
Engr. (Dr.) N. C Iheaturu	Owerri District
Mr. Yakubu Embu (Acting)	Zaria District
Prof. Pius Ukoha	Anambra/Enugu/Ebonyi District

Mr. Ishaya G. Kure	Jos District
Mr. Noble Alu (Acting)	Abuja District
Dr. (Mrs) Doris Boryo (Acting)	Adamawa/Bauchi/Gombe Chapter
Prof. D.S Oguniyyi (Acting)	Kwara Chapter
Mr. Saleh I. Sani (Acting)	Kano/Jigawa Chapter
Prof. S. Achi (Acting)	Kaduna Chapter
Dr. O. Turoti (Acting)	Osun Chapter
Dr. Misbahu M. Ladan (Acting)	Sokoto/Kebbi/Zamfara Chapter
Dr. Micheal Eneji (Acting)	Kogi/Niger Chapter

PAST & PRESENT PRESIDENT(S) OF THE POLYMER INSTITUTE OF NIGERIA

1. Chief Engr. K. Ogunade, FPIN	1989 – 1995
2. Ms. May Ikokwu, FPIN	1995 – 1998
3. Dr. T. O Odozi, FPIN	1998 – 2001
4. Dr. P. C. O Nzelu, FPIN	2001 – 2005
5. Dr. E. J Asore, FPIN	Oct., 2005 – Dec., 2005
6. Prof. B. T Nwufo, FPIN	Dec., 2005 – Oct., 2011
7. Dr. J. E Imanah, FPIN	2011 – 2015
8. Prof. P. A. P Mamza, FPIN, FICCON	2015 – till date

CORRESPONDENCE

Editor-in-Chief
Prof. S. M Gumel
(smgumel.chm@buk.edu.ng)

Published by:
POLYMER INSTITUTE OF NIGERIA

Nigerian Journal of polymer Science and Technology

Information to Authors

Scope of the Journal

The Journal is devoted to publishing original research and short communications in all aspects of Polymer Science and Technology (Engineering). Articles in the related discipline of Materials Science Technology will also be considered for publication.

Preparation of Manuscript

Manuscript should be written in the third person in an objective, formal and impersonal style. The SI system should be used for all scientific and laboratory data. The full stop should not be included in abbreviations, example m (not m.) ppm not (p.p.m.). All mathematical expressions should be included in the manuscript. Care should be taken to distinguish between capital and lowercase letters, between zero (0) and letter (O), between the numeral (1) and letter (I), etc. Mathematical expressions should fit into a single column when set in type. Fractional powers are preferred to root signs and should always be used in more elaborate formulas. The solids (/) should be used instead of the horizontal lines for fractions whenever possible. Numbers that identify mathematical expressions should be enclosed in parentheses. Refer to equations in the text as "Eq. (1)", etc., or "Equation (1)", etc., at the beginning of a sentence.

Content

All pages must be numbered consecutively. A manuscript would normally include a title, abstract, keywords, introduction, materials and methods, results and discussion, conclusions and references.

i. **Title page**: A short title which should be concise but informative must be provided. This should be followed by the names and full addresses of all authors. E-mail addresses of the corresponding authors must be included.

ii. **Abstract**: The abstract should not be more 220 words. It should give concise factual information about objectives of the work, the methods used, the results obtained and the conclusions reached.

iii. **Keywords**: The authors should list below the abstract keywords for information retrieval purposes. The

keywords should identify with main point in the paper.

iv. **Abbreviations and Notations**: Nomenclature must be listed at the beginning of the paper and should conform to the system of standard SI units. Acronyms and abbreviations should be spelt out in full at their first appearance in the text.

v. **Text**: Papers should be typed single column, with double line spacing on one side of the paper only with ample margins on all sides. The text should be divided into sections each with a separate heading, numbered consecutively. The section heading be typed on a separate line and should be bold.

vi. **Conclusions and Recommendations**: The conclusions should summarise the findings, clearly stating the contributions and their relevance. Recommendations for implementation or for areas of further work on the subject matter should be made.

vii. **Acknowledgements**: These should be brief and relevant. The names of funding organizations should be written in full. Dedications are not permitted.

viii. **References**: References to publish work should be indicated at the appropriate place in the text, according to the Harvard system (i.e. using author(s)' name(s) and date), with a reference list in alphabetical order, at the end of the manuscript. All references in this list should be indicated at some point in the text and vice versa. Papers by more than two authors but with same first author should be listed by year sequence and alphabetically within each year.

Examples of layout of reference are given below:

Book

Onyeyili, I.O. (2003) Analysis of statistically Determine Structures. El' Demak Publishers, Enugu.

Thesis

Ihueze, C.C. (2005) Optimum Buckling Response Model of GRP Composites. Ph.D. Thesis, University of Nigeria, Nsukka.

Journal

Umerie, S.C., Ogbuagu, A.S., Ogbuagu, J.O. (2004) Stabilisation of palm oils by using Ficus exasprata leaves in local processing methods. *Bioresources Technology*, 94: 307-310.

Conference

Menkiti, M.C., Ugodulunwa, F.X.O., Onukwuli, O.D. (2007) studies on the coagulation and flocculation of coal washery effluent. *Proceedings of the 37th annual conference of the Nigerian Society of Chemical Engineers*, Enugu, 22-24 November, pp169-184.

ix. **Illustrations**: All figures whether line drawings, graphs or photographs should be given a figure number be Arabic numeral in ascending order as reference is first made to them in the text (e.g. Fig. 1). Tables are to be similarly numbered. Captions of figures should be below the respective figures while captions of table should be above the respective tables. The measured quantity with the units, usually in brackets, and the numerical

scale should be given alongside the ordinate and abscissa of every graph. All illustrations including chemical structures should be placed in the appropriate places within the text.

x. **Submission of Manuscript**: Manuscript should be submitted to the Editor-in-Chief via pineditor2017@gmail.com.
Manuscripts are considered for acceptance on the understanding that the work described is original and has not been published or submitted for consideration elsewhere and that the author has obtained necessary authorization for publication of the material submitted. Submission of a multi-authored manuscript implies the consent of all the participating authors. A processing fee of N3,000.00 (Three thousand naira only) is charged per manuscript. Make payment to PIN National Account, Polymer Institute of Nigeria account number **0006664735** at Union Bank Plc. A publication fee for accepted manuscript of **NGN10, 000.00** (Ten Thousand Naira) is charged and should be remitted to Polymer Institute of Nigerian Account number **0006664735** at Union Bank Plc.

xi. **Copyright**: By submitting a manuscript, the authors agree that the copyright for the article is transferred to the Polymer Institute of Nigeria, if and when the article is accepted for publication.

xii. **Disposal of Material**: Once published, all copies of the manuscript, and correspondence will be held for three months before disposal. Authors must contact the Technical secretary if they wish to have any material retu

Contents

Kinetic Analysis of Thermal Stability and Activation Energies of Agricultural Waste Residues Using Flynn-Wall-Ozawa and Coats-Redfern Models
Ogah, A.O., Ikelle, I.I., Nworie, F.S., and Ilochi, N.O 1

Synthesis and Characterization of Silver Nanoparticles-Embedded Alkyd Resins Derived from Castor Seed Oil
Haruna Musa and Abubakar A. Abubakar 9

Effect of solvent annealing on the morphology, optical and electrical properties of in-situ deposited polyaniline thin films.
N. Alu, P.A.P. Mamza, C.E. Gimba 20

Modified three-step Synthesis and Polymerization of Monofunctional 1, 3-Benzoxazine
Abdullahi Usman G/Gabbas 27

Studies of *Luffa cylindrica* Fiber Reinforced Waste Low Density Polyethylene Composite
Y. Adamu, M.T. Isa, J.A. Mohammed, T.K. Bello 38

Synthesis of Carbon nanotube Macroinitiator of Atom Transfer Radical Polymerization by Esterification Reaction
Umar Ali and Sani Muhammad Gumel 45

The Reinforcing Potentials of White Sand as Filler in Natural Rubber Vulcanizates.
E. Osabohien and N .O. Ojeifo. 53

Utilization of Waste Glass Powder as a Pozzolanic Material for Partial Replacement of Cement in Concrete.
Gambo H.I, Mamza P.A.P. and Gonah C.M. 63

Mechanical and Cryo-Fracture Properties of *Core-Shell* Clay Filled Epoxy Composites
Nnamdi Chibuike Iheaturu 74

Comparative Study of Conventional Paver Block with Coir Fibre Filled Waste Low-Density Polyethylene Paver Blocks
Yibowei, Moses E, Biotidara Frank O., Ichetaonye Simon I., Ugo Kingsley U., Adekoya, Joseph G., Idemudia, Lawrence O, Nwigwe, Uzoma S. 85

Nigerian Journal of Polymer Science and Technology, 2017, Vol. 12, pp1-8

Received: 13 Nov. 2017 Accepted: 17 June 2018

Kinetic Analysis of Thermal Stability and Activation Energies of Agricultural Waste Residues Using Flynn-Wall-Ozawa and Coats-Redfern Models

[1*]Ogah, A.O., [1]Ikelle, I.I., [1]Nworie, F.S., and [2]Ilochi, N.O

[1]Department of Industrial Chemistry, Faculty of Science, Ebonyi State University, PMB 053, Abakaliki, Ebonyi State, Nigeria

[2]Department of Industrial Chemistry, Evangel University, Okpoto, Ebonyi State, Nigeria

[*]Corresponding author E-mail address: anselmogah@gmail.com

Abstract

The objective of the study was to determine the thermal degradation mechanisms and apparent activation energies of agro waste residues using thermo gravimetric analysis. Thermal degradation behaviors of corncob (CCF), rice hull (RHF), walnut shell (WSF) and oil palm (OPF) fibrous wastes under N_2 atmosphere were evaluated to derive their kinetic parameters at various heating rates of 5, 10, 20 and 40^{o}C/min. Kinetic parameters were calculated using Flynn-Wall-Ozawa (F.W.O) and Coats Redfern models. The thermo gravimetric analysis (TGA) results showed that activation energies of the fibers varied significantly with the extent of degradation indicating a multistage mechanism involving a variety of compounds. Higher heating rate affected not only the temperature of maximum weight loss, but also the activation energies and degradation conversions of the agro fibers during decomposition. Activation energies of the agro waste residues decomposition appeared to peak around 40-50% conversion. The apparent activation energies (E_a) of the agro waste residues according to (F.W.O) and Coats Redfern models was found to be in the range between 184.74/183.87 kJ/mol for rice hull, 184.18/180.73 kJ/mol for walnut shell, 162.37/161.33 kJ/mol for corncob and 141.64/140.54 kJ/mol for oil palm fiber.

Keywords: Apparent activation energy, Thermal stability, Agro-residues, Thermo gravimetric analysis, Flynn-Wall-Ozawa, Coats Redfer

Introduction

Nowadays, it is not enough for products to meet technical and economical requirements, it is also important that they have sustainable characteristics. This necessity motivates academic and industrial researches to develop innovative solutions, which can be noted from the large number of technical papers investigating the use of agro-industrial residues as raw materials for producing energy, biofuels, and composites (Kumar *et al.* 2008; White *et al.* 2011). A further example found in the technical literature about the uses of agro waste feedstock is the production of composites, regarded as promising materials that can replace petrochemical based composites (Lv *et al.* 2010).

[*]Department of Industrial Chemistry, Faculty of Science, Ebonyi State University, PMB 053, Abakaliki, Ebonyi State, Nigeria (Ogah, A.O, anselmogah@gmail.com)

Agro-industry is an economic sector that generates immense amounts of agro residues. This renewable biomass usually comes from non-edible plants or parts of them (Goyal *et al.* 2008). Agro residues find applications in the automotive, packaging and building industries. Agro residues are composed of lignocellulosics and as such they are subjected to thermal degradation during composites production (Zhang *et al.* 2010).

Therefore, understanding the thermal degradation characteristics of these agro resources will help in the design and application of composites. Slopiecka *et al.* (2012) examined the kinetic study of the decomposition of poplar wood by a comparison of Kissinger and FWO methods with a good agreement value 153.92 kJ/mol and 158 kJ/mol. Corradini *et al.* (2009) studied the activation energy of several cotton fibers with thermogravimetric analysis (TGA) and Flynn-Wall-Ozawa method, and it was 150 kJ/mol. They concluded that these methods were efficient for the description of the degradation mechanism of solid state reactions.

Nada and Hassan, (2000) investigated cellulose and some cellulose derivatives and obtained their activation energies of 53-182 kJ/mol. Kinetic analysis of the dynamic TGA data can offer an estimation of activation energy as a function of the conversion rate and can also predict the degradation time in an isothermal mode (White *et al.*, 2011).

The objective of the study was to determine the thermal degradation mechanisms and apparent activation energies of agro waste residues using the models approach analyses.

Materials and methods

Materials: The corncob fiber was obtained from Mt. Pulaski Products, LLC Mt. Pulaski, IL, USA. The rice hull fiber was supplied by Rice Hull Specialty Products, Stuttgart, AR, USA. The walnut shell fiber was obtained from Composition Materials Co. CT, USA. Samples were oven dried at 105 ℃ for 24 h. The samples were of 60 to 100 mesh particle size. The fibers were used as supplied by the manufacturers. The oil palm fiber (OPF) was collected from the rural farmers of Ebonyi State, Nigeria. The fibers were soaked in hot water with detergent for three days in order to remove the residual oil and other impurities. The fibers were dried in the sun for one week to obtain a dry mass and bagged in black polythene. A 40-mesh Wiley grinder was used to reduce the fiber particle prior to TG analysis.

Methods Thermogravimetric analysis: The thermal stability of agro fibers was investigated using a thermal gravimetric analyzer (SDT Q600, TA Inst.). 5-10mg of sample was weighed in a platinum pan and operated under a continuous flux of nitrogen (60ml/min). Under dynamic analysis, all of the samples were heated from room temperature to 500^{o}C with 5, 10, 20 and 40^{o}C/min ramp; under isothermal conditions (Sathasivam and Haris 2012; Elkhaoulani *et al.* 2013)

Kinetic modeling: The isoconversional Flynn-Wall-Ozawa method is an integral method, which leads to $-E_a/R$ from the slope of the line determined by plotting log β against 1/T at any certain conversion rate (Flynn and Wall 1966). The modified Coats-Redfern method is a multiple-heating rate application of the Coats-Redfern equation (Coats and Redfern 1964). Plotting the left-hand side for each heating rate against 1/T at that heating rate gives a family of straight lines of slope $-E_a/R$.

Activation energy of thermal decomposition: To evaluate activation energy, Flynn-Wall-Ozawa and Coats-Redfern expressions were used as follows (Yao *et al.* 2008):

Flynn Wall Ozawa expression (Yao *et al.* 2008)

$$\ln(\beta_i) = \ln(A_aE_a/Rg(\alpha)) - 5.331 - 1.052E_a/RT_{\alpha i} \quad \ldots\ldots\ldots\ldots\ldots\ldots\ldots\ldots\ldots\ldots(i)$$

where g(α) is constant at a given value of conversion. The subscripts i and α denotes given value of heating rate and given value of

conversion, respectively. The activation energy E_a is calculated from the slope - 1.052Eα/R.

Coats Redfern expression (Yao *et al.* 2008):

$\ln(\beta/T^2) = \ln(K_oR/E_g(x) - E_a/RT$ ……(ii)

where, E_a = activation energy of thermal decomposition, R = gas constant, β = heating rate, and T = absolute temperature. For activation energy (E_a), a linear relationship between log β and 1/T, log β/T^2 and 1/T at selected fraction of thermal decomposition was displayed and E_a was then evaluated from the slope. The selected fraction ranged from 0.05 to 0.5 and the resulting values of the activation energy for each fraction were compared.

Results and discussion

Thermal stability of agro fibers and weight loss of agro fibers: The weight loss as a function of temperature for the four studied agro fibers and their derivatives are shown in Figs. 1(a and b). The oil palm fiber degradation initiated earlier starting from 150^{o}C and there are three major degradation peaks in the derived weight loss curve, 210^{o}C (43%), 275^{o}C (42%) and 360^{o}C (52.5%). By contrast, rice hull fiber had its degradation occurring from above 250^{o}C and there are three major degradation peaks in the derived weight loss curve, 310^{o}C (60%), 350^{o}C (50%) and 410^{o}C (10%). Corncob fiber degradation started from below 200^{o}C with two major degradation peaks in the derived weight loss curve, 300^{o}C (48%) and 350^{o}C (80%).Walnut shell fiber degradation started very close to 250^{o}C with two major degradation peaks in the derived weight loss curve, 270^{o}C (38%) and 350^{o}C (60%). Walnut shell fiber degradation started very close to 250^{o}C with two major degradation peaks in the derived weight loss curve, 270^{o}C (38%) and 350^{o}C (60%).

From the results obtained it could be said that rice hull agro residue has better thermal stability as evidenced by the higher activation energies of 184.74 and 183.87 kJ/mol according to FWO and Coats Redfern models. This could be attributable to the chemical composition of the rice hull agro residues, which according to Yao et al. (2008) contained a higher silica content.

Degradation kinetics and activation energy of agro fibers

To obtain activation energy of thermal decomposition, the data obtained were converted to a log β and 1/T, ln (β/T^2) and 1/T as presented in Tables 1-4. Figs. 2 (a and b) show the activation energy of thermal decomposition as a function of conversion rate using F-W-O and Coats Redfern models. Figs. 3(a, b, c and d) Fig. 4(a, b, c and d) represent the isoconversional curves of corncob, rice hull, walnut shell and oil palm fibers by FWO and Coats Redfern models respectively. Because decomposition at the early stage was affected by the moisture, the fixed conversions (α) were selected from 0.05 to 0.5.The activation energy for each (α) was calculated from the slope of each straight line. It was found that as thermal decomposition proceeded in the rice hull fiber, the activation energy increased from (175 kJ/mol) at 5% conversion decreased steeply at 30 % conversion and it then increased to (194 kJ/mol) at 50% conversion. This finding is similar to the result obtained by Alwani *et al.* (2014). The activation energy of thermal decomposition for corncob fiber increased from (147 kJ/mol) at 5 % conversion and increased linearly to (177 kJ/mol) at 50 % conversion. The activation energy of thermal decomposition for walnut shell fiber increased from (179 kJ/mol) at 5 % conversion, experienced a reduction between 10 to 20 % conversion and thereafter increased to (179 kJ/mol) at 50 % conversion.

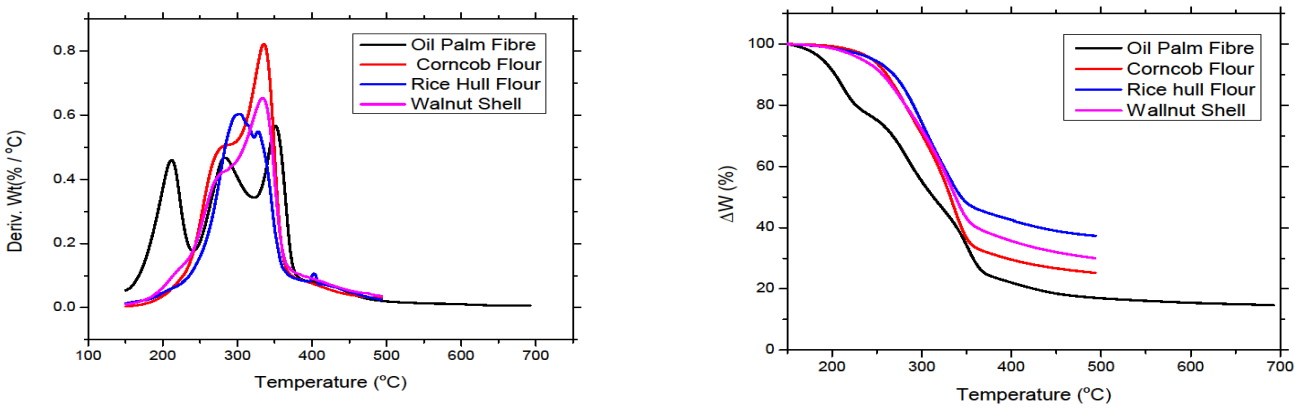

Fig.1: Thermograms showing (a) derivative of the weight loss curves and (b) weight loss curves

Compared with the other agro fibers, oil palm fiber shows larger changes in (E_a) and a higher overall (E_a) at 50 % conversion. The (E_a) of oil palm fiber shows a three-stage increase, which in turn suggests a complex multi-step degradation mechanism. It was found that the average (E_a) of oil palm fiber (141kJ/mol) is lower compared to the other three agro fibers. This indicates the lower thermal stability of the oil palm fiber compared to the other three agro fibers as shown by the Flynn-Wall-Ozawa and Coats Redfern models.

The differences in kinetic parameters can be attributable to complicated nature of agro residues constituted by a mixture of cellulose, hemicelluloses, lignin and extractives, with proportion reactivity and chemistry affected by variety. Based on the studied parameters it could be stated that the rice hull, corncob and walnut shell agro waste fibers qualify as good or potential composite materials. This agrees with the work of Yao *et al.* (2008) in which apparent activation energies of 160-170 kJ/mol was obtained for ten natural fibers throughout the polymer processing temperature range.

Table 1: Degradation kinetics and Activation Energy Parameters for Corn Cob Fiber at 1000K

(β)	log β	ln(β/T²)	α									
			0.05	0.1	0.15	0.2	0.25	0.3	0.35	0.4	0.45	0.5
5	0.699	-11.212	1.932	1.872	1.835	1.802	1.771	1.741	1.714	1.691	1.670	1.653
10	1.000	-10.557	1.894	1.835	1.798	1.765	1.735	1.707	1.680	1.657	1.638	1.621
20	1.301	-9.904	1.858	1.768	1.768	1.730	1.701	1.674	1.648	1.625	1.589	1.589
40	1.602	-9.247	1.821	1.725	1.725	1.668	1.668	1.643	1.618	1.595	1.577	1.560

Table 2: Degradation kinetics and Activation Energy Parameters for Oil Palm Fiber at 1000K

log β	ln(β/T²)	α									
		0.05	0.1	0.15	0.20	0.25	0.30	0.35	0.40	0.45	0.50
0.699	-11.263	2.164	2.098	2.053	2.001	1.909	1.849	1.811	1.778	1.744	1.706
1.000	-10.608	2.114	2.044	1.997	1.953	1.878	1.818	1.779	1.747	1.713	1.677
1.301	-9.949	2.063	1.987	1.939	1.896	1.839	1.783	1.746	1.716	1.684	1.649
1.602	-9.302	2.011	1.927	1.878	1.840	1.798	1.748	1.710	1.681	1.653	1.621

Table 3: Degradation kinetics and Activation Energy Parameters for Walnut Shell Fiber at 1000K

Log β	$\ln(\beta/T^2)$	α									
		0.05	0.1	0.15	0.2	0.25	0.3	0.35	0.4	0.45	0.5
0.699	-11.199	1.975	1.888	1.840	1.801	1.765	1.733	1.704	1.679	1.657	1.637
1.000	-10.543	1.937	1.853	1.807	1.770	1.736	1.705	1.677	1.652	1.631	1.611
1.301	-9.898	1.900	1.816	1.772	1.735	1.702	1.672	1.644	1.621	1.601	1.581
1.602	-9.237	1.884	1.793	1.745	1.707	1.674	1.645	1.618	1.594	1.573	1.554

Table 4: Degradation kinetics and Activation Energy Parameters for Rice Hull Fiber at 1000K

Log β	$\ln(\beta/T^2)$	α									
		0.05	0.1	0.15	0.2	0.25	0.3	0.35	0.4	0.45	0.5
0.699	-11.104	1.928	1.846	1.804	1.774	1.748	1.724	1.670	1.674	1.649	1.620
1.000	-10.445	1.896	1.814	1.772	1.743	1.717	1.692	1.668	1.643	1.618	1.590
1.301	-9.782	1.868	1.785	1.743	1.714	1.688	1.663	1.638	1.613	1.588	1.560
1.602	-9.126	1.834	1.755	1.713	1.684	1.660	1.634	1.611	1.587	1.564	1.534

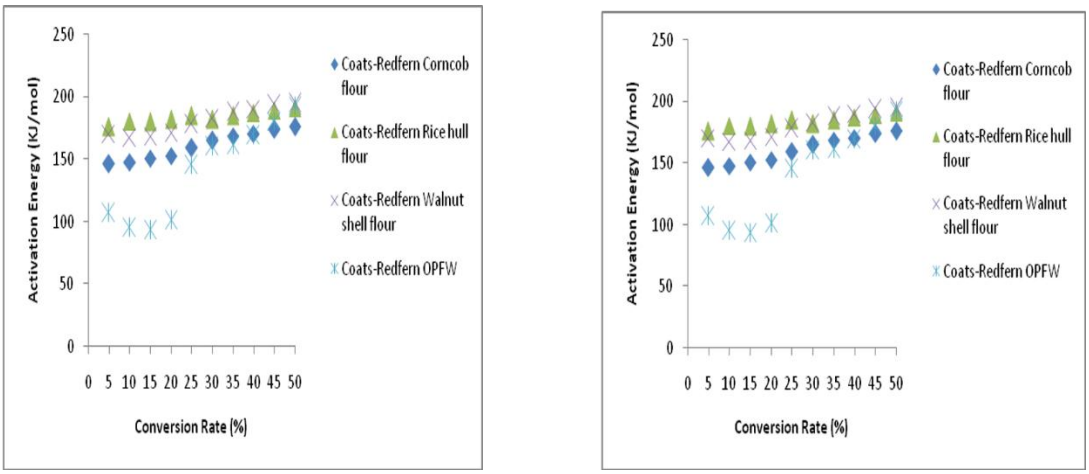

Fig.2: Comparison of activation energy of thermal decomposition of agro fibers by (a) F-W-O and (b) Coats Redfern

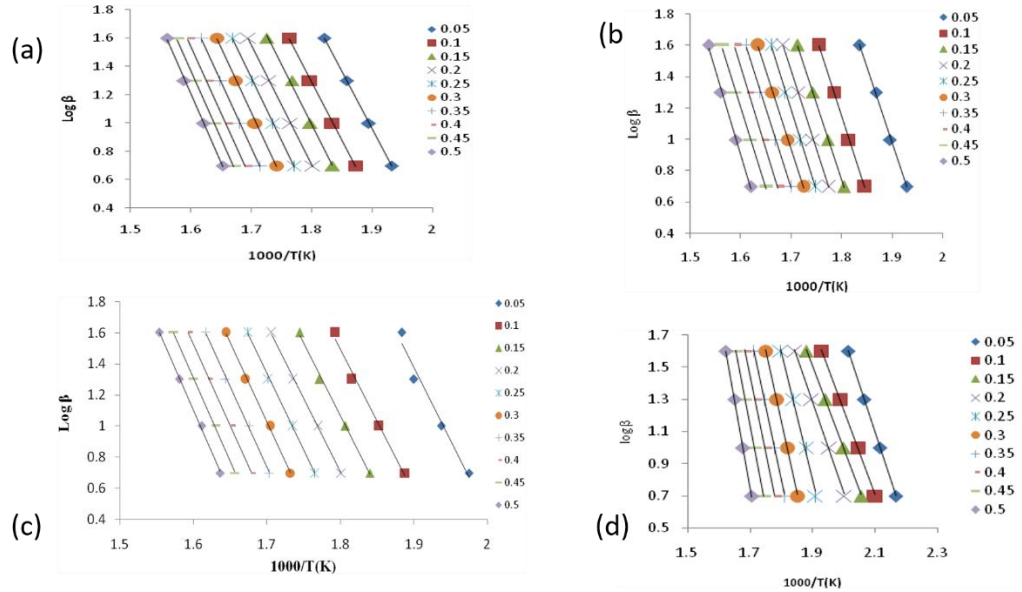

Fig. 3: Isoconversional curves of (a) corncob (b) rice hull (c) walnut shell and (d) oil palm fibers by Flynn-Wall-Ozawa expression.

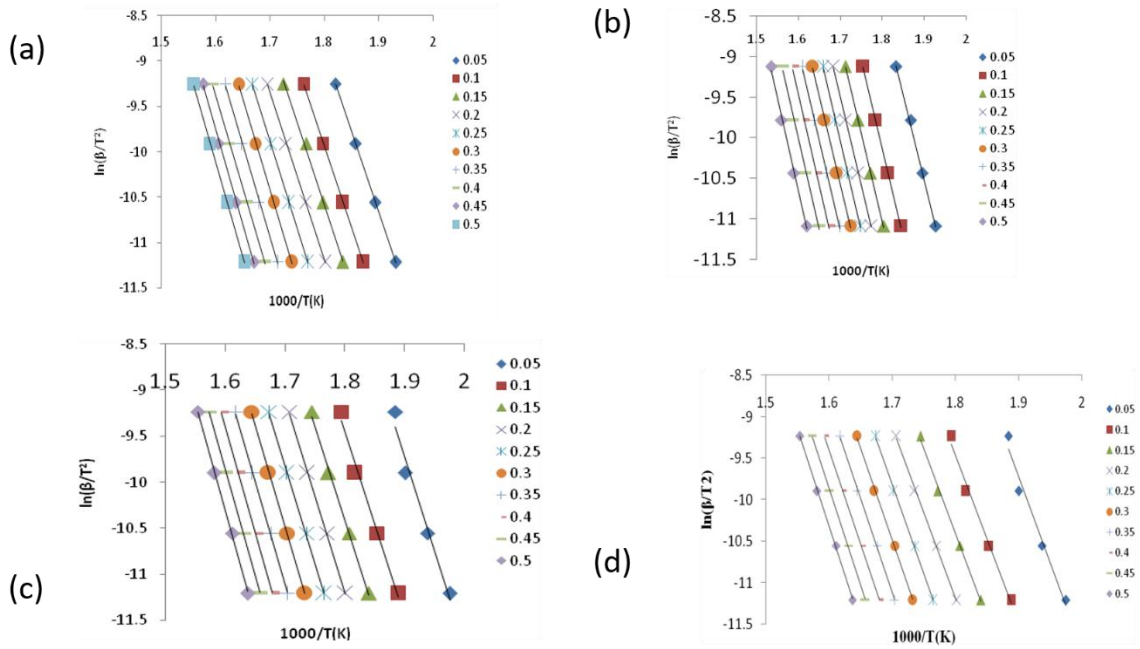

Fig. 4: Isoconversional curves of (a) corncob (b) rice hull (c) walnut shell and (d) oil palm fibers by Coats Redfern expression.

Conclusion

The thermal degradation (weight loss curves and derivative weight loss curves), thermal stability and apparent activation energies of four agro waste residues were characterized using TGA and model free approaches. The agro waste residues displayed different degradation profiles in their TGA/DTG curves respectively. The rice hull was the most thermally stable followed by walnut shell and corncob fibers, whereas the oil palm fiber showed the least thermal stability as confirmed by the average activation energies using the Flynn-Wall-Ozawa and Coats Redfern models. The study has confirmed that the evaluation of the thermal degradation and activation energies of the agro residues indicate their potential as composite materials.

Recommendations

The authors recommend that further work be done on the effect of coupling agents on the thermal stability and apparent activation energies of the studied agro residues.

References

Alwani, M.S., Abdul Khalil, H.P.S., Sulaiman, O., Md Nazrul Islam, and Rudi Dungani, (2014) An Approach to Using Agricultural Waste Fibers in Biocomposites Application: Thermogravimetric Analysis and Activation Energy Study, *BioResources* **9** (1), 218-230.

Coats, A.W. and Redfern, J.P. (1964) Kinetic Parameters from Thermo gravimetric Data, *Journal of Nature*, 201, 68-69. Corradini, E., Teixeira, E., Paladin, P.,

Agnelli, J., Silva, O.R., Mattoso, L.H. (2009)Thermal Stability and Degradation Kinetic Study of White and Colored Cotton Fibers by Thermo gravimetric Analysis, *J. Therm. Anal. Calorim*. **97(**2), 415-419.

Elkhaoulani, A., Arrakhiz, F., Benmoussa, K., Bouhfid, R., and Qaise, A. (2013) Mechanical and Thermal Properties of Polymer Composite Based on Natural Fibers: Moroccan Hemp Fibers/Polypropylene, Mater. Design 49, 203-208.

Flynn, J.H., and Wall, L.A. (1966) A Quick, Direct Method for the Determination of Activation Energy from Thermo gravimetric Data, *Journal Polymer Lett*ers, **4(**5), 323-328.

Goyal H., Seal D., Saxena R., (2008) "Bio-fuels from Thermochemical Conversion of Renewable Resources: A Review", Renewable and Sustainable Energy Reviews, **12(**2), 504-517.

Kumar A., Wang L., Dzenis Y., Jones D., Hanna M., (2008) "Thermogravimetric Characterization of Corn Stover As Gasification and Pyrolysis Feedstock", Biomas and Bioenergy,**32(**5) , 460-467.

Lv G., Wu ., Lou R., (2010) "Kinetic Study of Thermal Decomposition of Hemicelluloses Isolated From Corn Stalk", BioResources, **5(**2), 1281-1291.

Nada, A.M.A., and Hassan, M.L. (2000) Thermal Behavior of Cellulose and Some Cellulose Derivatives, *Journal Polymer Degradation and Stability,* 67,111-115.

Sathasivam, K., and Haris, M. R. H. M. (2012) Thermal Properties of Modified Banana Trunk Fiber, J. Therm. Anal. Calorim. **108(**1), 9-17.

Slopiecka, K., Bartocci, P. and Fantozzi, F. (2012) Thermogravimetric Analysis and Kinetic Study of Poplar Wood Pyrolysis, *Appl. Energy*, **97**, 219-497.

White, J.E., Catallo, W.J., and Legendre, B.L. (2011) Biomass Pyrolysis Kinetics: A Comparative Critical Review with Relevant Agricultural Residue Case Studies, *J. Anal. Appl. Pyrol.* **91**(1), 1-33.

Yao, F., Wu, Q. Lei, Y., Guo, W., and Xu, Y.

(2008) Thermal Decomposition Kinetics of Natural Fibers: Activation Energy with Dynamic Thermogravimetric Analysis, *Journal Polymer Degrad. Stabil*. **93** (1), 90-9.

Zhang L., Xu C., Champagne P. (2010) "Overview of Recent Advances in Thermo-chemical Conversion of Biomass", Energy Conversion and Management, **51** (5), 969-982.

Nigerian Journal of Polymer Science and Technology, 2017, Vol. 12, pp 9-20

Received: 06 March 2018 Accepted: 21 August 2018

Synthesis and Characterization of Silver Nanoparticles-Embedded Alkyd Resins derived from Castor Seed Oil

[†]Haruna Musa and Abubakar A. Abubakar

Department of Pure and Industrial Chemistry, Bayero University, P.M.B. 3011, Kano, Nigeria.

Abstract

Alkyd resin (CSOR) was prepared from castor seed oil (CSO) by alcoholysis with glycerol to form monoglyceride and polycondensation with phthalic anhydride to form the alkyd resin (CSOR). The formation of resin was monitored by drop in acid value as the reaction progresses. Silver nanoparticles (AgNPs) were also synthesized from silver benzoate solution (SBS) by one step *in-situ* reduction method. The nanoparticles were mixed with CSOR in toluene to form a homogeneous mixture of silver nanoparticles-embedded alkyd resin (AgNPs-CSOR). The formation of AgNPs was confirmed by colour change, surface plasmon resonance at 455 nm as observed by UV-visible spectrophotometry and the presence of Ag-O band at 696 cm^{-1} as shown by FTIR spectroscopy. The antimicrobial activity of SBS, CSO, CSOR, and AgNPs-CSOR were evaluated against *Escherichia coli, Salmonella typhi, Staphylococcus aureus, Aspergillus flavus, Aspergillus fumigatus and Mucor species* in nutrient agar using the disc diffusion method. The appearance of higher zone of inhibition in AgNPs-CSOR clearly indicated a higher antimicrobials activity when compared to SBS, CSO and CSOR. The performance characteristics of the CSOR and Ag-NPs-embedded alkyd resins as ingredients in surface coatings were further evaluated. The results obtained revealed that the paint films air-dried faster, show good solvent resistance and excellent light fastness which suggest the potentiality of AgNP-CSOR as binder in the formulation of antimicrobial surface coatings.

Keywords: Castor seed oil, Alkyd resin, Silver nanoparticles, Plasmon resonance, Antimicrobacterial, Antifungal.

Introduction

The National Nanotechnology Initiative (NNI) of the United State defined nanoparticles as microscopic particles with at least one of the three dimensions having less than 100 nm (Behera *et al.*, 2013). In recent years, the study of nanoparticles has received enormous attention especially in the creation and manipulation of products at nanoscale level having novel properties (Hussain *et al.*, 2005). The properties of nanoparticles entirely differ from conventional macroscopic materials. These unique characteristic properties of nanoparticles arise from their high surface to volume ratio (Premanathan *et al.*, 2011).

Silver nanoparticles (AgNPs) are widely used in variety of applications. For many years silver nanoparticles had been used as a colloidal material in the preparation of many consumer products (Srivastava *et al.*, 2012). Nowadays, AgNPs are used in many fields such as surface coating, drug delivery, biosensing, nanodevice fabrication, nanomedicine, imaging, catalysis etc. These applications can be attributed to their unique properties such as surface enhanced raman scattering, antibacterial and antifungal properties (Kim *et al.*, 2006).

Silver nanoparticles have potential (Nagy *et al*., applications in cosmetics, clothing,

[†] Department of Pure and Industrial Chemistry, Bayero University Kano (Haruna Musa, hmusa.chm@buk.edu.ng)

sunscreen and food industries due to their antibacterial properties 2011). Several physical, chemical and biological methods have been used in synthesis and stabilization silver nanoparticles. Biological methods using algae, fungi, yeast and bacteria as reducing and stabilization agents have been reported (Sintubin *et al.,* 2012).
Photochemical methods using UV radiation and aqueous solution containing Triton X-100 as stabilization agent have been used to synthesise a stable and monodisperse AgNPs (Gosh *et al.,* 2003). Similarly, physical method involving thermal application have been employed in the synthesis of AgNPs Jung *et al.,* (2006). Among the existing methods of AgNPs synthesis, chemical method is the most versatile technique especially using polymers as stabilization agents (Sun and Xia, 2002; Kim *et al*., 2006). Alkyd resins have been used as a popular binder for surface coatings and paints formulations. Vegetable oil is an important raw material for alkyd resin production. Alkyds are polyester products formed from the polymeric condensation of polyhydric alcohol, polybasic acid and monobasic fatty acids. Surface coatings such as alkyd paints and varnishes are finishes applied to the surfaces of materials to decorate and protect the surfaces (Kyenge *et al.,* 2012; Odetoye *et al.,* 2012).

Several researchers have reported the preparation of nanoparticles-embedded antimicrobial coatings with strong activity against some selected bacterial isolate (Cornelia *et al.,* 2013; Rivero *et al.,* 2011; Musa and Sharif, 2016).

The aim of this research work is to synthesize and characterize, silver nanoparticles-embedded alkyd resins from castor seed oil by *in situ* reduction method with the oil triglyceride serving as green and eco-friendly reducing agent, determine the antibacterial and antifungal properties of the resin and also evaluate its performance properties when used as binder in formulation of surface coatings.

Materials and Methods

Materials

Silver benzoate salt (SBS) (Sigma-Aldrich) was used as a precursor for the synthesis of silver nanoparticles (AgNPs). Castor seed oil (CSO) was donated by National Research Institute for Chemical Technology (NARICT) Basawa, Zaria, Nigeria. All chemicals and solvents used were of analytical grade and used without further purification. The glassware used were washed thoroughly and dried overnight in a vacuum oven prior to use. All weighing was carried out on an electric Metter balance model H30AR. FTIR spectra of the castor seed oil, alkyd resins and silver nanoparticles samples were acquired using FTIR spectrophotometre Agilent Technologies recorded in the transmittance mode in the range of 4000-650 cm^{-1}, viscosity measurements of alkyd resin and formulated paints samples were carried out in the Instruments Laboratory of the Department of Pure and Industrial Chemistry, Bayero University, Kano, Nigeria. Antibacterial and antifungal activity studies were carried out at the Postgraduate Research Laboratory of the Department of Microbiology, Bayero University, Kano, Nigeria.

Decolorization of Castor Seed Oil (CSO)

Castor seed oil (100g) was mixed with 10 g of activated charcoal and stirred for 30 minutes and then heated at 100°C for 1hour. The mixture was cooled to room temperature and activated charcoal was removed by filtration using Whatman No. 1 filter paper.

Determination of Physicochemical Parameters of Castor Seed Oil (CSO)

The physicochemical properties of CSO such as refractive index, iodine value, saponification number, acid value, percentage free fatty acid and specific gravity were determined according to standard methods (AOCS, 1996).

Synthesis of Castor Seed Oil Alkyd Resin (CSOR)

The synthesis was carried out using a modified procedure reported by Oladipo *et al*., (2013); Onukwli and Igbokwe (2008). Castor seed oil (98 g) was poured into a three-necked flask equipped with Dean and Stark apparatus and condenser. The oil was heated on a hot plate equipped with a magnetic stirrer bar at 120 ^{o}C for 3 hours to remove moisture. Glycerol (20 g) as added at 120 ^{o}C temperature before raising the temperature to 230 ^{o}C. After 40 minutes, aliquot of the reaction mixture was taken to check for solubility in methanol. The formation of a clear solution indicated the formation of monoglyceride which marked the end of the first stage. At the onset of the second stage, the temperature was lowered to about 180 ^{o}C and 44 g phthalic anhydride was added, followed by the addition of 10% xylene into the reaction mixture to aid the distillation of water of esterification by forming an azeotrope. The temperature was gradually increased to 240 ^{o}C and the reaction was maintained for further 4 hours. Aliquots were withdrawn from the reaction mixture at intervals of thirty minutes to check for drop in acid value of the mixture as the reaction progresses. The reaction was stopped when the acid value was found to be below 10 mg KOH/ml and the alkyd resin was allowed to cool. The acid values were determined by titrating with 0.1M KOH solution to the phenolphthalein end point after dissolution in a mixture of toluene and ethanol (1:1). Nitrogen gas was used to blanket the surface of the reaction mixture during the reaction.

Syntheis of Silver Nanoparticles Embedded-Castor Seed Oil Alkyd Resin (AgNP-CSOR)

Silver benzoate (0.068 g) as dissolved in 75 ml of toluene. Castor seed oil alkyd resin (4.8 g) was added, mixed thoroughly to form a homogeneous mixture and kept in the dark for 12 hours.

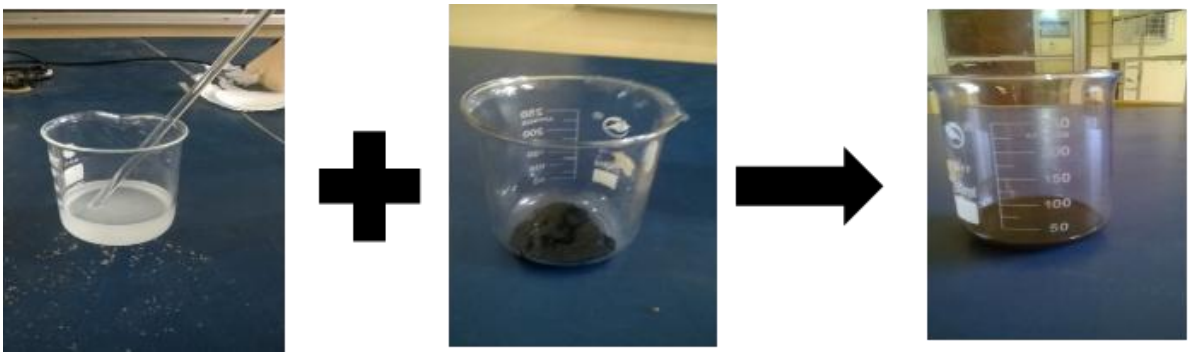

Figure 1: Synthesis of Silver Nanoparticles (AgNPs) using Silver Benzoate as Precursor

Characterisation of AgNP and AgNP-CSOR

FTIR of Castor Seed Oil (CSO)and Silver Nanoparticles embedded Alkyd Resin (AgNPs-CSOR)

The FTIR spectra of CSO and AgNPs-CSOR were acquired using FTIR spectrophotometre Agilent Technologies. The spectra were recorded in the frequency range of 4000-600 cm^{-1} to identify the absorption peaks.

UV-Visible Spectrophotometry of Silver Benzoate Salt (SBS) and Silver Nanoparticles embedded Alkyd Resin (AgNPs-CSOR)

The UV-visible absorption profile of silver benzoate salt (SBS) and silver nanoparticles embedded alkyd resin samples (AgNPs-CSOR) were determined using UV-visible spectrophotometre at wavelength range of 200-750 nm.

Antibacterial and antifungal activity of SBS, CSO, CSOR and CSOR-AgNPs

Disc diffusion method was used to evaluate the antimicrobial properties of the compounds. Agar plates were incubated with test organisms i.e. *Eschericia coli, Salmonella typii, staphylococcus aureus* and *Aspergillus flavus, Aspergillus fumigatus and Mucor species by* spreading the test compounds uniformly. The discs were incubated for 24 hours at 37^{o}C. Standard drugs were also used as control i.e. Ampicillin for bacteria and Ketoconazole for fungi. After 24 hours of incubation, the antibacterial and antifungal activity of the test compounds and that of the standard drugs were evaluated by measuring the zone of inhibition (mm) in each disc.

Formulation of Paint Using the Synthesised CSOR as Binder

A surface coating (paint) was formulated using the synthesized resin as binder. 10 g each of CSOR and AgNPs-CSOR (10 g) were separately used in the formulation. In each formulation, iron (II) oxide was mixed with solvents before adding to the alkyd resins. Also, paint additives such as extenders and thickeners were added and stirred to obtain a homogeneous mixture. The composition of the surface coating is presented in Table 1.

Table 1: Composition of Surface Coating (Paint) Formulation

Component	Weight (g)		
	Blank	CSO	AgNPs-CSOR
Alkyd Resin	0.00	10.00	10.0
Iron (II) Oxide (Pigment)	7.50	7.50	7.50
Toluene	30.0	30.0	30.0
Talc	0.80	0.80	0.80
Nitrosol	0.30	0.30	0.30
Pigment Volume Concentration (PVC)	0.0	0.039	0.40
% PVC	0.0	3.9	4.0

Performance Evaluation of the Paint Film

The performance characteristics of the films were determined using ASTM standard methods (ASTM D5895-03, 2003).

The properties analysed include chemical resistance, drying schedule, and light fastness. Films of paints derived from CSOR and AgNPs-CSOR binders were prepared by applying a thin spread of the paint on a clear glass panel and dried at room temperature. The drying processes were monitored in terms of the time of set-to-touch, surface-dry and dry-through. The chemical resistance of the film in different solvent media (H_2O, KOH, H_2SO_4, and aqueous NaCl) was also determined at room temperature

Results and Discussion

Physicochemical Characterisation of Castor Seed Oil (CSO)

The results of the physicochemical analysis of CSO is presented in Table 2. The acid value of CSO was found to be 10.36 mgKOH/g and the value indicates a measure of the extent to which the triglycerides in the oil have been decomposed by lipase action. The iodine value of CSO was found to be 40.8 mg/g which indicates lower degree of unsaturation and also classified the oil as non-drying. Similarly, the saponification value of CSO was obtained as 159.90 mg/g which suggests the presence of higher molecular weight fatty acids. The peroxide value of 12.34 meq/kg indicates the non-rancid nature of the oil and the % free fatty acid of 5.18 suggests the low amount of hydrolysed triglyceride molecules in the sample.

Table 2: Physicochemical Properties of CSO

Property	Value
Colour	Yellow
Acid Value (mgKOH/g)	10.36
Iodine Value (mg/g)	40.88
Saponification Value	159.90
Free Fatty Acid (FFA) (%)	5.18
Refractive Index	1.46
Specific Gravity g/cm^3 at 25 ℃	0.9314
Peroxide Value (Meq/kg)	12.34
Viscosity (MPa) at 28^{o}C	89.41
Moisture Content (%)	0.26

Titrimetric Determination of Acid Value

Moreover, the titrimetric determination of acid value as the alcoholysis reaction progresses shows a sharp decrease in the acid value of the reaction mixture at the initial stage as presented in Fig 2. This as a result of reaction of primary and secondary hydroxyl groups of glycerol with phthalic anhydride

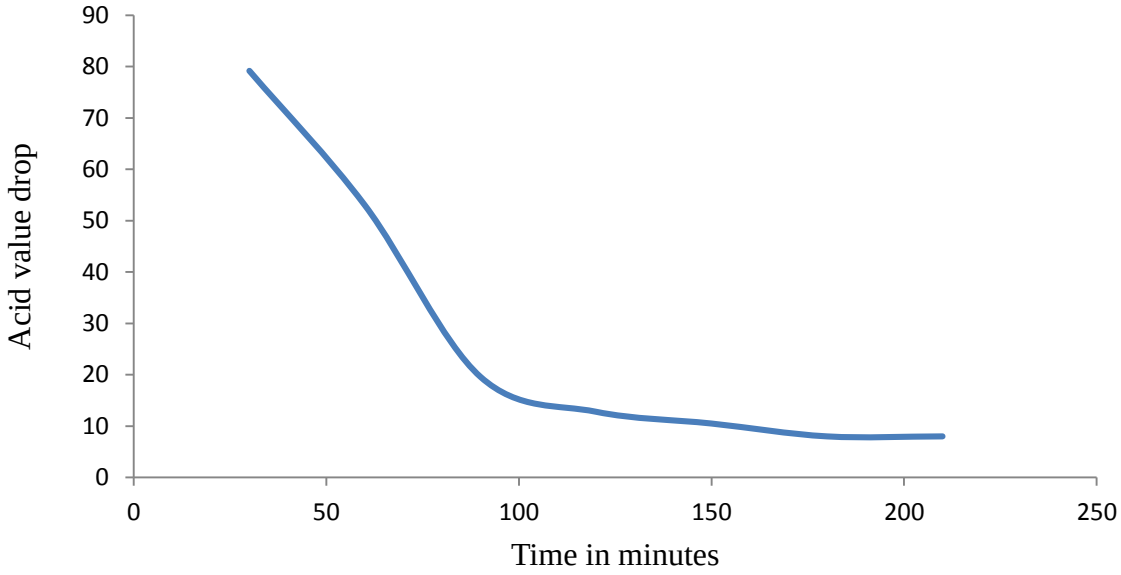

Figure 2: Plot of Acid Value drop with Reaction Time (minutes)

IR Analyses

Figures 3 and 4 represent the FTIR spectra of CSOR and AgNPs-CSOR respectively. The absorption bands at 1739 cm^{-1} in Figure 3 and 1778cm^{-1} in Figure 4, are as a results of C=O stretching vibrations, the peak observed at 1158 and 1259cm^{-1} in Fig. and 4 respectively is as a results of C–O stretching of an ester while the peaks that appears at 1601cm^{-1} is due to C=C stretching of aromatics. Comparig the CSOR and AgNPs-CSOR spectra, a new peaks is observed at 696cm^{-1} in Fig. 4. This is ascribed to the presence of Ag-O bond as a result of incorporating AgNPs in to the resin. The peak due to Ag-O bond was not observed in the CSOR spectrum (Fig 3). Similar results were reported by Patel (2007); Bora *et al.*, (2014); Guran *et al.*, (2013).

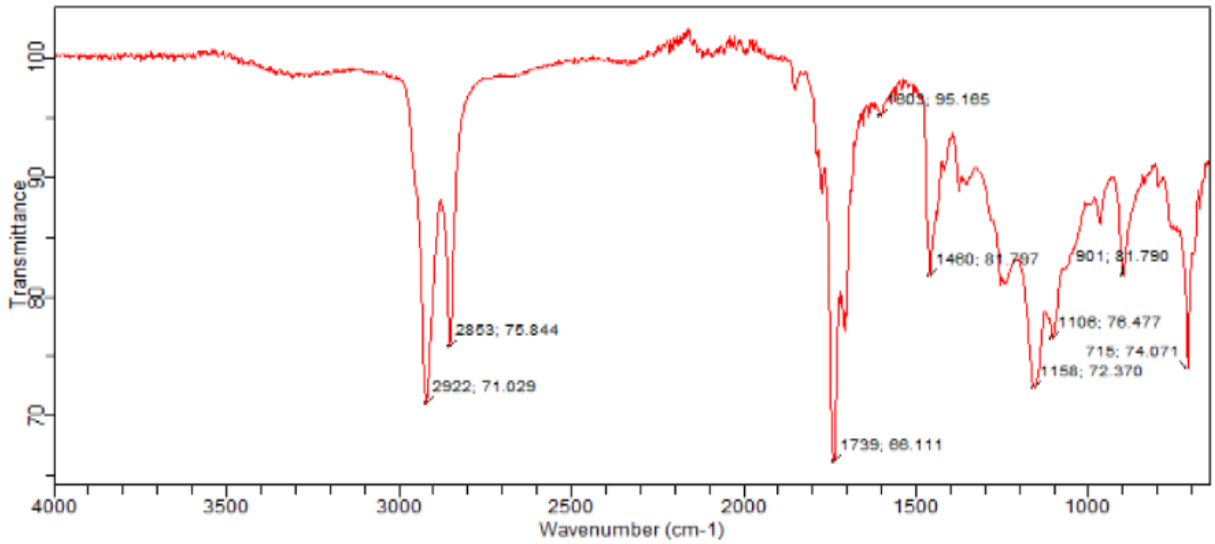

Figure 3: FTIR of Castor Seed Oil Alkyd Resin (CSOR)

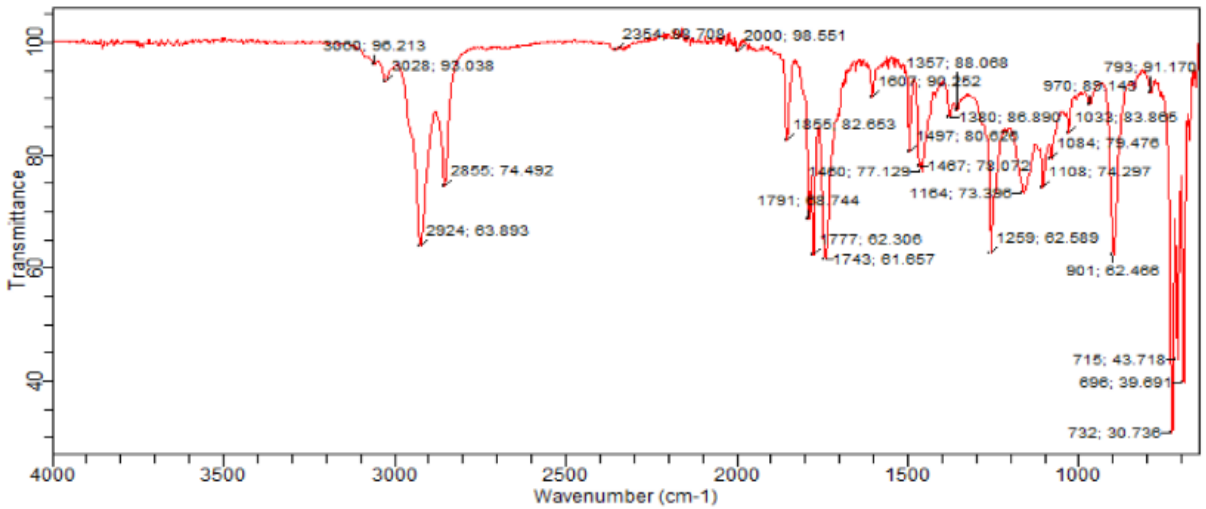

Figure 4: FTIR of Silver Nanoparticles-embedded Castor Seed Oil Alkyd Resin (CSOR-AgNPs)

UV-visible Spectrophotometry

Figure 5 shows the results of wavelength of maximum absorption of silver benzoate solution (SBS) and silver nanoparticles-embedded castor seed oil alkyd resin AgNPs-CSOR). SBS solution shows a wavelength of maximum absorption of

205nm, as expected for Ag ions and AgNPs-CSOR with distinct light yellow colour in the solution phase shows an absorbance 455 nm in which increases as a function of time. This peak is due to the surface plasmon resonance of AgNPs originating from the quantum size of the AgNPs. This also confirms the formation of silver particles at nanoscale dimensions. The absorbance maximum does not change over a period, indicating that the silver particles are prevented from coagulating owing to stabilization of nanoparticles by fatty acids, which are essential constituents of the CSO. Similar results reported by Patel, (2007); Dhand *et al.*, (2015).

Antibacterial and Antifungal Activity Evaluation by Disc Diffusion Method

Figure 6 shows the antibacterial and antifungal activities of SBS, CSO, CSOR, and AgNPs-CSOR. The diameter of zones of inhibition was measured (mm) for each treatment. The antibacterial and antifungal activity was evaluated against three different pathogenic bacteria namely; *E.coli, Salmonella typii and Staphylococcus aureus* and three different pathogenic fungi namely; *Aspergillus flavus Aspergillus fumigatus* and *Mucor specie*. Ampicillin was used as the standard drug (control) for bacteria while Ketoconazole was used as the control for fungal species. SBS, CSO, CSOR, JSOR and AgNPs-CSOR of different concentrations were prepared in µg/ml using dimethyl sulfoxide (DMSO) as solvent. It is clear from the results of zone of inhibition presented in Fig. 6 that AgNPs-CSOR has higher antibacterial and antifungal activities when compared to SBS, CSO and CSOR.

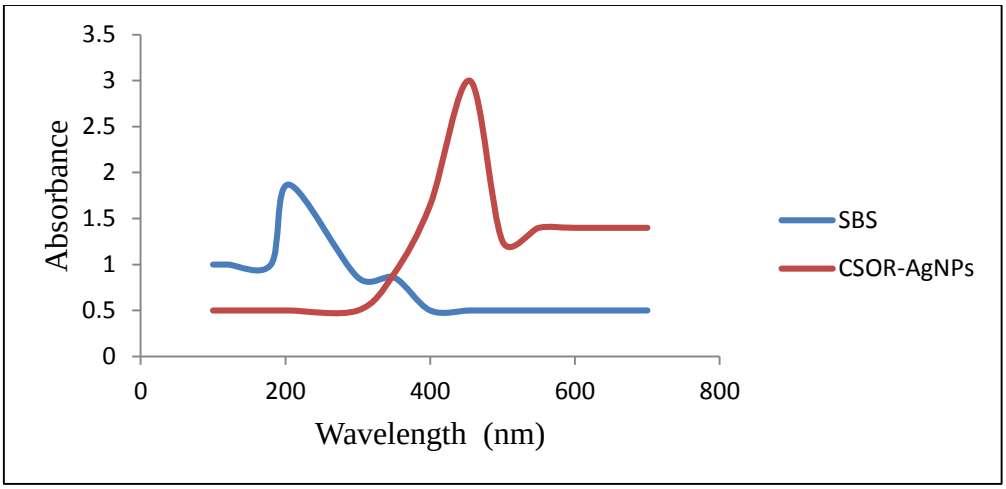

Figure 5: Wavelength of maximum absorption of silver benzoate and CSOR-AgNPs

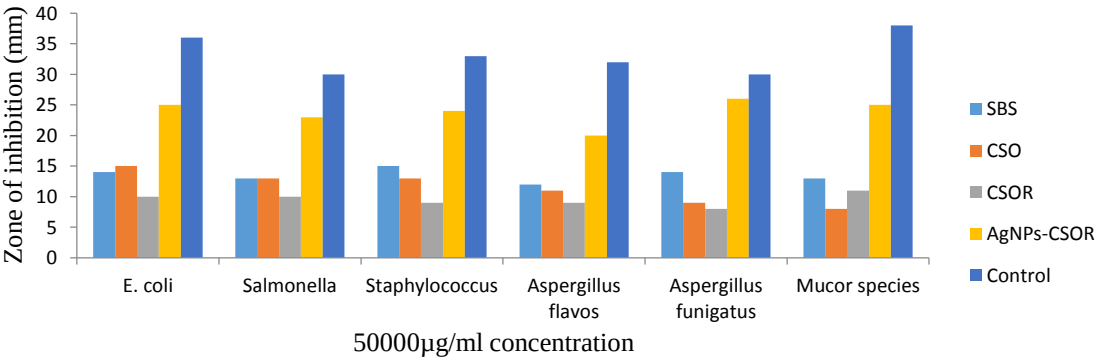

Figure 6: Antibacterial and Antifungal activities of SBS, CSO, CSOR and AgNP-CSOR

Performance Evaluation of the Prepared Paint Films

Three different paints were formulated blank (without binder), CSOR (using castor seed oil alkyd resin as binder) and AgNPs-CSOR (using silver nanoparticles embedded castor seed oil alkyd resin as binder). The percentage pigment volume concentration (% PVC) of the paints derived from CSOR and AgNPs-CSOR as binders are 3.9 and 4.0 % respectively. PVC is an important parameter in determining the quality of paints**.** The lower the PVC, the higher the durability and gloss of paint. High PVC can cause a decrease in adhesion as well as durability of paint. If the volume increases as compared to the volume of binder, the film will lose cohesion with time. The blank sample has little durability owing to the absence of binder.

Drying Schedule Analysis

Figure 7 shows the drying schedule of the different formulated paints i.e Blank, CSOR, and AgNPs-CSOR paints respectively. The results show that all blank samples have very fast drying property owing to the absence of binder. AgNPs-CSOR based paint was exhibited an excellent drying property when compared to CSOR based pain

Chemical Resistance Test

Table 3 shows the chemical resistance characteristics of Blank, CSOR and CSOR-AgNPs based paint films. From the results, the blank films show poor resistance to acid, brine and alkali, whereas CSOR and CSOR-AgNPs based films show excellent resistance to acid, brine and water but poor resistance to alkali which could be due to the presence of an ester group in the alkyd resin binder.

Light Fastness Rating

Table 4 show the results of light fastness test, of Blank, CSOR and AgNPs-CSOR derived paints. The test was carried out by exposing the paint films simultaneously with a standard blue wool in an intense artificial light source in a light fastness tester for 120 hours. The light fastness was then assessed by comparing the degree of fading of paint film with that of standard blue wool. From the results, CSOR and CSOR-AgNPs show an excellent light fastness property while the blank sample has moderate light fastness property due to the absence of binder in the blank. This result suggests that alkyd resin binder plays a significant role in enhancing the light fastness property of paints.

Table 3: Chemical/Solvent Resistance Test of Paint Films

Test	**Sample**		
	Blank	**CSOR**	**AgNPs-CSOR**
Alkali (0.1M KOH)	2	2	2
Acid (0.1M H_2SO_4)	2	1	1
Brine (5% w/v)	2	1	1
Distilled water	1	1	1

Key: 1 = Film not removed after solvent/chemical treatment
2 = Film removed after solvent/chemical treatment

Table 4: The light fastness test of the formulated paints

Sample	Grade	Degree of Fading	Light Fastness Rating
Blank	4	Appreciable fading	Moderate
CSOR	7	Very slight fading	Excellent
CSOR-AgNPs	7	Very slight fading	Excellent

Conclusion

In the present study, locally available castor seed oil (CSO) has been successfully converted to alkyd resin (CSOR) by alcoholysis and polycondensation reactions. Silver benzoate salt (SBS) have also been successfully converted to silver nanoparticles (AgNPs) by *in-situ* reduction method. The AgNPs-embedded alkyd resin shows positive antibacterial and antifungal activity. Performance evaluation of the resins show that AgNPs– embedded alkyd resins have excellent coating properties such as drying schedule, solvent/chemical resistance and light fastness property, hence AgNPs-CSOR has promising application as surface coatings for various substrates to impart antibacterial and antifungal properties.

Acknowledgments

The authors would like to thank Bayero University Kano, Nigeria for providing the chemicals and equipments used in this research. Also, the authors gratefully acknowledge the Department of Microbiolgy, Bayero University Kano for conducting the antimicrobial test of the samples prepared in this research.

References

AOCS, (1996) Sampling and analysis of commercial flats and triglycerides official methods of analysis of the American triglycerides chemist *SOC.*, 801-855.

ASTM D5895-03 (2003) Standard method for evaluating Drying or curing during film formation of Organic Coatings. Annual book of ASTM Standardsm.06 (01).

Behera, S. S., Jha, S., Arakha, M., and Panigrahi, T. K. (2013) Synthesis of Silver Nanoparticles from Microbial Source-A Green Synthesis Approach, and Activity of its Antimicrobial Activity against Escherichia coli. *International Journal of Engineering Research and Applications (IJERA), 3*(2), 058-062.

Bora, M. M., Gogoi, P., Deka, D.C., Kakati, D.K. (2014) Synthesis and characterization of yellow oleander (Thevetia peruviana) seed oil-based alkyd resin Industrial Crops and Products. 52,721-728.

Cornelia G., Alexandra P., Denisa F., Anton F. and Cezar C. (2013) Antimicrobial coatings obtaining and characterization. *Mater. Sci*. 36(2), 183–188.

Dhand, V., Soumya, L., Bharadwaj, S., Chakra, Bhatt, S. D., and Sreedhar, B. (2015) Green synthesis of silver nanoparticles using Coffea arabica seed extract and its antibacterial activity. *Materials Science and Engineering, 58*(2016),36-43.

Ghosh S. K. Kundu S. Mandal M. Nath S. and Pal T. (2003) "Studies on the evolution of silver nanoparticles in micelle by UV photoactivation," *Journal of Nanoparticle Research*, 5(5- 6), 577–587.

Guran, C., Pica, A., Fical, D, Ficai, A., and Comanescu, C (2013) Antimicrobial coatings— obtaining and characterization. *Bull. Mater. Sci., 36*(2), 183-188.

Hussain, S.M., Hess, K.L., Gearhart, J.M., Geiss, K.T. and Schlager, J.J (2005) in vitro toxicity of nanoparticles in BRL 3A rat liver cells. *Toxicol In-Vitro, 19 (7)*, 975-983.

Jung J. H. Cheol Oh H. H. Soo Noh J. and S. Soo Kim H. J (2006) "Metal nanoparticles generation using a small ceramic heater with a local heating area," *Journal of Aerosol Science*, 37(12), 1662–1670.

Kim D., Jeong S. and Moon J. (2006) "Synthesis of silver nanoparticles using the polyol process and the influence of precursor injection," *Nanotechnology*, 17(16), 4019–4024.

Kyenge, B. A., Anhawange, B.A., Ageh, J.T., and Igbum, G.O. (2012) Comparative analysis of soybean seed oil-modified alkyd resin and epoxidised soybean seed oil-modified alkyd resin. *International Journal of. Modern Organic Chemistry*, 1(2), 66-71.

Musa H. and Sharif N. S. (2016) Preparation and Antimicrobial Evaluation of Neem Oil Alkyd Resin and Its Application as Binder in Oil-Based Paint, *Environmental and Natural Resources Research*, 6(2): 92-98

Nagy, A., Harrison, A., Sabbani, S., Munson,

R.S., Jr., Dutta, P.K. and Waldman, W.J (2011). Silver nanoparticles embedded in zeolite membranes:release of silver ions and mechanism of antibacterial action. *International Journal of Nanomedicine*, 6, 1833-1852.

Odetoye,T.E , Ogunniyi, D.S. and Olatunji, G.A. (2012) Improving Jatropha curcas Linneaus seed oil alkyd resins, *Progress in Organic Coatings*, 73(4), 374–381.

Oladipo, G. O., Eromosele, I. C., & Folarin, O. M. (2013) Formation and Characterization of Paint Based on Alkyd Resin Derivative of *Ximenia americana* (Wild Olive) Seed Oil. *Environment and Natural Resources Research, 3*(3), 52.

Onukwli, O. D., and Igbokwe, P.K. J. (2008) Production and characterization of castor oil-modified Alkyd resins. *Engineering and Applied Sciences*, 3(2),161-165.

Patel, V. C., Varughese, J., Krishnamoorthy, P.A., Jain, R.C., Singh, A.K. and Ramamoorty, M. (2007) Synthesis of alkyd resin from jatropha and rapeseed oils and their applications in electrical insulation. *Journal of Applied Polymer Science*, 107(3), 1724-1729.

Premanathan, M., Karthikeyan, K., Jeyasubramanian, K. and Manivannan, G. (2011) Selective toxicity of ZnO nanoparticles toward gram-positive bacteria and cancer cells by apoptosis through lipid peroxidation. Nanomedicine, 7(2), 184-192.

Rivero, P. J., Urrutia, A., Goicoechea, J., Zamarreño, C. R., Arregui, F. J., and Mat, I. R. (2011) An antibacterial coating based on a polymer/solgel hybrid matrix loaded with silver nanoparticles. *Nanoscale Research Letters 6*, 305.

Sintubin L. Verstraete W. and Boon N, (2012) "Biologically produced nanosilver: current state and future perspectives," *Biotechnology and Bioengineering*,109(10), 2422–2436.

Srivastava, M., Singh, S. and Self, W.T. (2012) Exposure to silver nanoparticle inhibits selenoprotein synthesis and the activity of thioredoxin reductase. *Environ Health Perspect*, 120 (1), 56-61.

Sun Y. and Xia Y. (2002) "Shape-controlled synthesis of gold and silver nanoparticles," Science, 298 (5601), 2176-2179

Nigerian Journal of Polymer Science and Technology, 2017, Vol. 12, pp21-27

Received: 06 March 2018 Accepted: 07 September 2018

Effect of solvent annealing on the morphology, optical and electrical properties of in-situ deposited polyaniline thin films.

‡[1]N. Alu, [2]P.A.P. Mamza, [2]C.E. Gimba

[1]Physics Advanced Laboratory, Sheda Science & Technology Complex, P.M.B. 181, Garki - Abuja

[2]Department of Chemistry, Ahmadu Bello University, Zaria

Abstract

Sulfuric acid doped polyaniline thin films were grown on glass substrates by in-situ polymerization of Aniline with Ammonium peroxydisulfate as oxidant. The effect of solvent annealing on the electrical, mechanical and optical property as well as the morphology of the films were studied by profilometry, four-point probe, nano indentation and UV-visible spectroscopy respectively. It was found by profilometry that the films had an average thickness of 300nm with a roughness of 98nm. Nano indentation put the Elastic modulus at 12.77 GPa. Moreover, UV- visible spectroscopy at 328 and 636 nm indicates conformational changes due to extension of the conjugated polymer chains caused by the solvent annealing. Four points-probe resistivity measurements gave sheet resistance of 1.5 x 10^3, 3.6 x 10^3, 8.3 x 10^4 and 8.0 x 10^6 Ωsq. for the films annealed in diethyl Ether, chloroform and propanol respectively. The film annealed in diethyl ether had the best performance of 1.5 x 10^3 Ωsq. which is over 62% improvement over the 2.4 x 10^3Ωsq obtained for the pristine polyaniline.

Key words: conducting polymers; polyaniline; solvent annealing.

Introduction

Conducting polymers has emerged as attractive materials for the fabrication of optoelectronic devices and as replacement for metals in certain applications. In addition, the interesting optoelectronic property and redox chemistry of conducting polymers have opened up new applications such as for instance, all polymer batteries and OLEDS. Polyaniline (PANI) is particularly interesting in this regard because it combines ease of synthesis, excellent stability, interesting redox chemistry, and good electronic conductivity (Choi & Park, 2002). PANI can be doped to the metallic state either chemically or electrochemical by the charge transfer reaction with the conjugated backbone and protonation of the nitrogen, (Chiang & MacDiarmid, 1986). li et al. (2009) demonstrated that PANI possesses adequate electro-catalytic activity to promote, catalytic regeneration of iodide (I_3^-) to iodine in a DSSC. In addtion, stretch-oriented doped PANI possesses conductivity in excess 670 ± 55S/cm (Adams et al., 1998). A great deal of the usefulness of PANI is predicated on the posibility to form it into thin highly conductive films, which is the preferred form for optoelectronics. Often, post deposition treatments such as annealing are employed to obtain the required characteristics. Generally, PANI is synthesized from Aniline or its derivatives through oxidative polymerization but straightforward synthesis of PANI often produces particulate products with irregular shapes, which are very difficult to process. Therefore, methods have been developed to make nanostructures of polyaniline (with diameters smaller than

‡ Physics Advanced Laboratory, Sheda Science and Technology Complex (N. Alu, noble.alu@gmail.com)

100 nm) by introducing "structural directing agents" (Yu et al., 2006) during the chemical polymerizing reaction. A great variety of such agents have been reported in the literature, including surfactants (Michaelson & McEvoy, 1994; Bhowmick et al., 2011) liquid crystals, polyelectrolytes (Yu et al., 2006) nanowire seeds and aniline oligomers (Zhang and Manohar, 2004) and relatively complex and bulky organic dopants (Wan and Nalwa, 2005).

It is believed that such functional molecules can either directly act as templates (*e.g*., polyelectrolytes) or promote the self-assembly of ordered "soft templates" (*e.g.* micelles, emulsions) that guide the formation of polyaniline nanostructures. Other areas of active research are in the incorporation of functional dopants in the polymer matrix itself as it eliminates the use of volatile dopants and the use of polyacids to improve the selected properties, solubility, processability, and electrical conductivity (Tarver et al., 2018). Aniline undergoes oxidative polymerization in acidic medium (Stejskal & Gilbert, 2002) where it exists as an anilinium cation, suitable oxidants include Ammonium peroxydisulfate, ferric chloride, and hydrogen peroxide. In basic or neutral environment, it is even possible to polymerize aniline with air usually with the aid of transition metal catalyst.

A very interesting property of PANI is the in-situ adsorption polymerization on suitable substrates to yield highly adherent films. The utility of this simply technique lies in its wide applicability and low cost. The electrical and optical property of such films may be tuned by suitable doping and annealing treatments as reported by several authors. This method circumvents the difficulty in processing PANI as noted earlier which is due to a combination of polyconjugated structure and the presence of benzene rings in the backbone, which pose thermodynamic barriers, and imparts rigidity to the chains.

Materials and Methods

Materials

Aniline (merck) was used as received. Ammonium peroxydisulfate (sigma-aldrich), 30% hydrogen peroxide(sigma-aldrich), hydrochloric acid (bdh), sulfuric acid (bdh), chromic acid (bdh), absolute ethanol (merck), propanol (merck), chloroform (merck), diethyether (merck), hexane (sigma aldrich), toluene (sigma aldrich), dimethyldichlorosilane (sigma aldrich) were analytical grade and used without further purification. distilled water was used in all experiments.

Deposition of polyaniline thin films

Films of polyaniline where deposited on microscope slides as follows.

Glass slides preparations

A total of 20 glass slides were cleaned by treatment for 40min with piranha solution (prepared by slowly adding 30 % hydrogen peroxide to concentrated sulfuric acid in a ratio of 3:7) The treatment also hydroxylates the glass surface and prepares it for subsequent silanization prior to chemical bath deposition of polyaniline. The slides are then rinsed thoroughly with distilled water from a wash bottle and dried in a hot air oven at 70^0C for 1hr, they are then rendered hydrophobic by treatment with 5% dimethydichlorosilane in toluene for 1hr according to a procedure by Huang et al, (1997).

Preparation of polyaniline precursor

The polyaniline precursor is a two-part composition that are mixed just before use and contained; Part A, 4ml Aniline in 200ml, 1M $H2SO_4$ and Part B, 4.6g Ammonium persulfate ($(NH_4)_2S_2O_8$) in 200ml1M H_2SO_4. The rinse bath contained 4ml Aniline in 200ml 1M H_2SO_4.

In-situ deposition of polyaniline

The cleaned glass slides in sets of four denoted (A_1 to A_4; B_1 to B4; C_1 to C_4; D_1 to D_4 and E_1 to E_4) are subsequently suspended in a 250 cm^3 open beaker equipped with a magnetic stirring bar and thermometer. Deposition of PANI commenced with the beaker filled to the 200cm3 marks with equal volume of Part A and B of the polyaniline precursor and briefly stirred at 600 rpm for 10second at room temperatures. The substrates were taken out after 5 min and placed in the rinse bath for 30min to reduce the oxidation state of polyaniline from the pernigraniline to the emeraldine and finally rinsed with distilled water followed by drying with a hot air blower.

Post –deposition solvent anneal

Each slide is scribed with a diamond tipped scriber and divided into five equal sized pieces and are then subjected to solvent anneal at the boiling point of the solvents in closed Erlenmeyer flask immersed in a hot water bath for 2 hours.

Characterization of the polyaniline films

The pristine and solvent annealed PANI films were characterized by, 4-Point Probe (Signatone QuadPro Resistivity System). Surface profiling (Veeco Dektak 150 Stylus Surface Profiler). Nanomechanical Test. (HYSITRON INC, TI 750 Ubi System with nanometer resolution imaging capability). UV-visible spectrophotometer (UV-Vis-NIR Spectrophotometer (Avantes).

Results and Discussions

Micro-structural features

In other to understand the microstructural features of the as formed PANI film, it was subjected to imaging using HYSITRON INC, TI 750 Ubi System in the imaging mode the micrograph is shown in figure 3.1 and shows a pinhole free film.

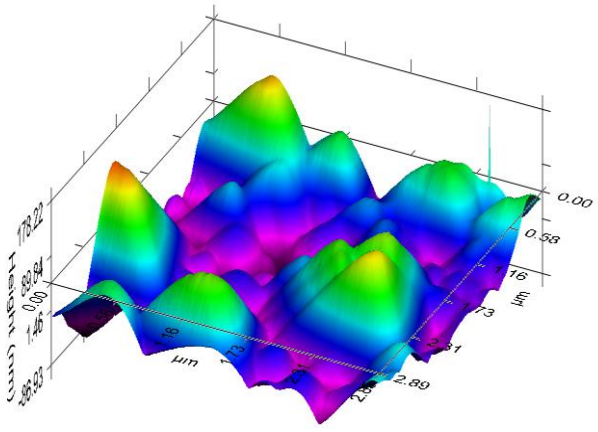

Figure 1 Image of the as formed polyaniline film.

Surface profiling with Veeco Dektak 150 Stylus Surface Profiler

As measured with a Veeco Dektak 150 Stylus Surface Profiler the thickness of the film is 300nm with a mean roughness value of approximately 98nm, the acquisitions were performed with a scan rate of 45 µm/s, a sampling rate of 60 Hz, and a sensor range of 600 µm with a Stylus force of 35.7 mg.

Nanomechanical Test with HYSITRON INC, TI 750 Ubi System Nanoindenter

Nano indentation offers a convenient method for assessing the physical properties of thin film samples that are not amenable to manipulation with conventional methods, Nanomechanical tests were carried out using a Hysitron TI-75 which performs nano-indentation on the test samples, to do this, the machine presses a hard diamond tip whose mechanical properties are known into a sample whose properties are unknown. The load placed on the indenter tip is increased as the tip penetrates further into the specimen until a preset value is reached, at this point, the load may be held constant for a period or removed. The output of this test is in the form of a force displacement curve from which the rigidity, hardness, elastic modulus modules other physical parameters of the sample are extracted. Proprietary software, Triboscan interprets these data to generate the hardness and reduced modulus of the films from which the elastic modulus is extracted. Figure 3.2 show typical load–displacement curves at indentation load of 80.03, and strain rate of 5.6nm/s for the pristine film.

From the load– displacement curves, the reduced modulus (*E*r) and hardness (*H*) values were extracted. Table 3.1 presents the summary of the nano indentation for locations 002 and 003 the loading is 80.03 µN while for 004 it is 30.02 µN. in all cases, the strain rate was 7 % of the maximum loading.

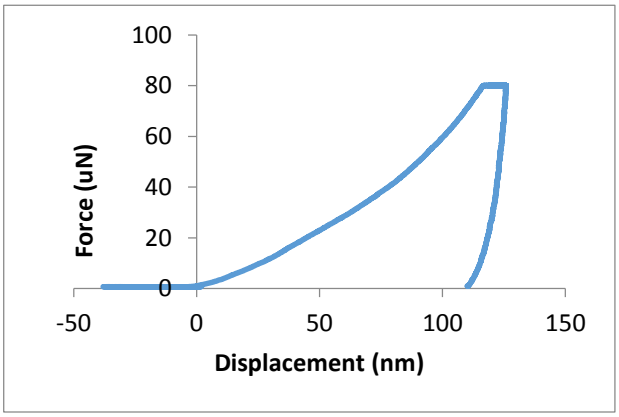

Figure 2: Force displacement curve for sample point 01 at indentation load of 80.03µN, strain rate of 5.6nm/s and for 24 iterations.

Table 1: presents the summary of the nano indentation for locations 002 and 003 the loading is 80.03 µN while for 004 it is 30.02 µN.

location	v_{ind}	V_{PANI}	Displ.(nm)	Loading force(uN)	Er	Hardness (MPa)
002	0.07	0.38	121.5	80.03	16.61	162.68
003	0.07	0.38	145.3	80.03	11.96	117.73
004	0.07	0.38	56.1	30.02	15.64	225.07
Average					14.73	168.49
Standard deviation					2.453	53.91

It shows that the measured data for the *E*r and H are consistent with a mean value of 14.73 and 168.49MPa respectively. Commonly reported literature value for the hardness of polymers lie within 100 to 600MPa.

Resistivity studies by the 4-Point Probe technique

Solvent annealing induces conformational changes in the PANI film, leading to changes in the electrical properties of the film as confirmed by 4-point probe resistivity measurements. These results are presented in Table 3.2. Some of the samples actually had decreased conductivity values after the solvent treatment while others where much improved.

The ethanol and propanol annealed samples appear to have been degraded by the treatment as evidenced by the large increase in sheet resistance. But diethyl ether annealed PANI gave the best result with sheet resistance of 1542.00 ± 4.47 which is 62.5% improvement over the conductivity of pristine PANI.

UV- visible spectroscopy

The UV- visible spectra of pristine as well as treated PANI thin films are shown in (Figure 3.3), as seen, post deposition solvent annealing had a remarkable effect on the optical characteristics of the film, indicative of profound change in the conformation of the polymer chains.

These results reveal a disappearance or lack of a characteristic polaron band centered at 550nm which normally occurs in dispersions of polyaniline in non-polar solvents and arises from isolated or loosely coupled polarions. In none polar solvents, the polarons of individual tetrameric units are normally isolated from each other because of twist defects between aromatic rings (McManus, Yang and Cushman, 1985) Therefore, the disappearance of this band is indicative of a highly extended conformation allowing overlap between polarions of adjacent polymer units. Also, it is observed that the three absorption peaks in the UV-visible spectrum normally assigned to transitions from π band to π* band, polaron band to π* band, and π band to polaron band are replaced with intraband transitions within the half-filled polaron bands further confirming a solvent induced extension of the PANI conformation.

Table 2 Electrical property of the solvent annealed PANI measured by the four Point-probe technique

Sample	Sheet resistance (Ω/Sq)	Conductivity (S/m)
Pristine PANI	2410	1338.508901
Diethyl Ether Annealed PANI	1542	2091.962679
Chloroform annealed PANI	3682	876.1016979
Propanol annealed PANI	83200	38.77171216
Ethanol annealed PANI	8018400	0.402300515

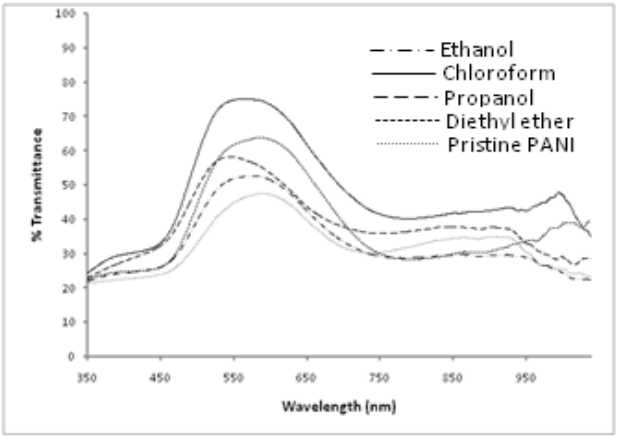

Figure 3: UV-visible spectra showing the effect of different post deposition solvent anneal treatment on the transmittance of PANI thin film.

CONCLUSIONS

In conclusion, solvent annealing of PANI has a profound effect on not only its electrical conductivity but also the optical band gap, which is a strong indication of conformal changes taking place on the hydrocarbon backbone. Furthermore, there is also a strong possibility of de-doping by the polar solvent ethanol and propanol at the annealing temperature leading to degradation in the film property. Noteworthy is the ease with which the optical, electrical, and mechanical properties of PANI may be tuned by simple solvent annealing which has obvious implication in a wide range of applications.

References

Adams, P., Devasagayam, P., Pomfret, S., Abell, L. and Monkman, A. (1998). A new acid-processing route to polyaniline films which exhibit metallic conductivity and electrical transport strongly dependent upon intrachain molecular dynamics.

Journal of Physics: Condensed Matter, 10(37), pp.8293-8303.

Bhowmick, B., Bain, M., Maity, D., Bera, N., Mondal, D., Mollick, M., Maiti, P. and Chattopadhyay, D. (2011). Synthesis of dendritic polyaniline nanofibers by using soft template of sodium alginate. *Journal of Applied Polymer Science*, 123(3), pp.1630-1635.

Chiang, J., & MacDiarmid, A. (1986). 'Polyaniline': Protonic acid doping of the emeraldine form to the metallic regime. *Synthetic Metals*, *13*(1-3), pp.193-205.

Choi, S., & Park, S. (2002). Electrochemistry of Conductive Polymers. XXVI. Effects of Electrolytes and Growth Methods on Polyaniline Morphology. *Journal of the Electrochemical Society*, *149*(2), E26.

Huang, Z., Wang, P., MacDiarmid, A., Xia, Y., & Whitesides, G. (1997). Selective Deposition of Conducting Polymers on Hydroxyl-Terminated Surfaces with Printed Monolayers of Alkylsiloxanes as Templates. *Langmuir*, *13*(24), pp. 6480-6484.

Li, Z., Ye, B., Hu, X., Ma, X., Zhang, X. and Deng, Y. (2009). Facile electropolymerized-PANI as counter electrode for low cost dye-sensitized solar cell. *Electrochemistry Communications*, 11(9), pp.1768-1771.

McManus, P., Yang, S. and Cushman, R. (1985). Electrochemical doping of polyaniline: effects on conductivity and optical spectra. *Journal of the Chemical Society, Chemical Communications*, (22), p.1556.

Michaelson, J. and McEvoy, A. (1994). Interfacial polymerization of aniline. *Journal of the Chemical Society, Chemical Communications*, (1), p.79.

Stejskal, J. and Gilbert, R. (2002). Polyaniline. Preparation of a c onducting polymer (IUPAC Technical Report). *Pure and Applied Chemistry*, 74(5), pp.857-867.

Tarver, J., Yoo, J., Dennes, T., Schwartz, J. and Loo, Y. (2018). *Polymer Acid Doped Polyaniline Is Electrochemically Stable Beyond pH 9*.

Wan, M. and Nalwa, H. (2005). cyclopedia of nanoscience and nanotechnology. *Choice Reviews Online*, 42(05), pp.42-2552a-42-2552a.

Yu, Y., Zhihuai, S., Chen, S., Bian, C., Chen, W. and Xue, G. (2006). Facile Synthesis of Polyaniline−Sodium Alginate Nanofibers. *Langmuir*, 22(8), pp.3899-3905.

Zhang, X. and Manohar, S. (2004). Polyaniline nanofibers: chemical synthesis using surfactants. *Chemical Communications*, (20), p.2360

Nigerian Journal of Polymer Science and Technology, 2017, Vol. 12, pp 28-38

Received: 24 March 2018 Accepted: 30 August 2018

Modified three-step Synthesis and Polymerization of Monofunctional 1, 3-Benzoxazine

[§]Abdullahi Usman G/Gabbas

Department of Science Laboratory Technology, Hussaini Adamu Federal Polytechnic

Kazaure, Jigawa State, Nigeria.

Abstract

A monofunctional 1,3-benzoxazine was synthesized via three-step technique involving condensation of 4-nitroaniline with 2-hydroxybenzaldehyde to obtain an Imine compound which is reduced using $NaBH_4$ to obtain 2-hydroxybenzylamine that undergo ring-closure reaction with methylene bromide to obtain the target monofunctional 1,3-benzoxazine. The structure of the monofunctional 1,3-benzoxazine was confirmed by FT-IR, ^{1}H and ^{13}C NMR spectra and Mass spectroscopy. The 1,3-benzoxazine compound was polymerized via thermally activated ring opening which affords a polybenzoxazine with 5% and 10% weight loss temperatures of 208 and 237°C, degradation temperature of 322°C and a char yield of 34% at 800°C indicating overall moderate thermal properties for the synthesized polybenzoxazine.

Keywords: Monofunctional 1,3-benzoxazine, Modified three-step synthesis, Thermally activated ring opening, Polybenzoxazine

Introduction

The synthesis of monofunctional 1,3-benzoxazine dates back to 1940's [Burke, 1949] but the potentials of these compounds were only realized in the last two decades [Demir *et al.*, 2013]. These compounds were initially synthesized from phenols and primary amines using various solvents [Burke *et al.*, 1952]. They are addition cure phenolic resins that have attracted the attention of researchers in the last few decades because of their advantages of the traditionally known polymers. These advantages including low melt viscosity, no harsh catalyst required no volatile release during cure and minimal cure shrinkage [Li, 2010; Zhang *et al.*, 2015; Zuniga *et al.*, 2012]. Polybenzoxazines also exhibit good dielectric properties and low water absorption at saturation and thus are excellent candidates for electronic packaging applications. They also have a good thermal stability that is demonstrated by their high glass transition temperatures, degradation temperatures, and char yields [Agag, 2006]. These compounds were the base for the production of a new class of phenolic materials namely polybenzoxazines, possessing high performance [Allen and Ishida, 2009]. Polybenzoxazines can thus be regarded as a new class of heterocyclic high-performance polymers with high thermal stability and high mechanical strength. They are a type of addition-cure phenolic resins with unique features that overcome the shortcomings associated with traditional

[§]Department of Science Laboratory Technology, Hussaini Adamu Polytechnic Kazaure (Abdullahi U. G. abduusmangbs@gmail.com)

phenolic resins [Chernykh *et al*., 2009]. The major advantages of polybenzoxazines over traditional resins include high char yield, no catalyst or acid needed for cure, higher glass transition temperatures, very low water absorption and no volumetric change upon cure [Baqar *et al*., 2011]. Perhaps, the most important advantage of this type of polymers is the rich molecular design flexibility which allows the tailoring of molecular structures to suit desired properties [Zhang and Ishida, 2015]. Furthermore, a survey of existing literature has revealed that compounds containing 3,4-dihydro-1,3-oxazine ring systems exhibit a wide range of pharmacological and antibacterial activities [Mathew *et al*., 2010; Manikannan and Muthusubramanian, 2010]. These heterocyclic compounds are also studied extensively for the synthesis of biologically active compounds ranging from herbicides and fungicides to therapeutically usable drugs [Shakil *et al*., 2010; Pasternak *et al*., 2009; Petrlikova *et al*., 2010; Tang *et al*., 2012].

In this paper, formaldehyde which has been classified as a suspected human carcinogen and a confirmed animal carcinogen [Lewis, 2008] was replaced with methylene bromide for ring-closure reaction as in the conventional three step procedure.

Materials and Methods

Materials

2-hydroxybenzaldehyde 98%, 4-nitroaniline 97%, Sodium borohydride 98% [Sigma Aldrich Chemicals]. Absolute Ethanol 99.8%, Methanol 98.5% [Fisher Scientific Chemicals Company]. Methylene bromide 99.5% [Acros Organics Chemicals Company].

Methods

Synthesis of 3-(4-nitrophenyl)-3,4-dihydro-2H-1,3-benzoxazine

0.05M (6.1g) of the 2-hydroxyaldehyde and 0.05M (7.4g) of 4-nitroaniline were slowly added into a round bottomed flask containing 150ml of absolute ethanol and the mixture was thoroughly shaken. This mixture was refluxed for 5h under nitrogen atmosphere and the resulting solution was allowed to cool to room temperature. 100 ml of water was then added and the resulting product was extracted with ethyl acetate, washed with water and dried over anhydrous sodium sulphate. The solution was then concentrated to dryness to give the imine compound 2-{(E)-[(4-nitrophenyl)imino]methyl}phenol.

0.02M (5.0g) of the imine compound was then dissolved in 100 ml of methanol contained in a 250 mL conical flask. In a separate conical flask, 0.1M (3.7g) of $NaBH_4$ was added into 100ml of methanol at room temperature. This solution was slowly added to the solution of the imine compound in portions while stirring over two hours. When the reduction is complete, 100 ml of water was added and the resulting product is extracted with ethyl acetate, washed with water, dried over anhydrous Na_2SO_4 and concentrated to dryness to obtain the 2-hydroxybenzylamine, 2-[(4-methylanilo)methyl]phenol. 0.02M (5.0g) of 2-[(4-methylanilo)methyl]phenol and an excess of methylene bromide were added to 150 ml of absolute ethanol in a 250 ml round bottomed flask and the reaction mixture was refluxed for 18-24h. The mixture was allowed to cool to room temperature and the solvent was removed using rotary evaporation. The product was dissolved in ethyl acetate and washed with 1M NaOH solution. The organic layer was dried over anhydrous Na_2SO_4 and concentrated to dryness to obtain 3-(4-nitrophenyl)-3,4-dihydro-2H-1,3-benzoxazine. This product

was finally purified by recrystallization in 50:50 water: ethanol mixture.

Polymerization of 3-(4-nitrophenyl)-3,4-dihydro-2H-1,3-benzoxazine

It has been reported in literature that 1, 3-benzoxazines exhibit exothermic ring opening reaction around 160°C-220°C (Ishida and Agag, 2011) and 200-250°C (Kiskan et. al., 2009). The polybenzoxazine was therefore simply synthesized by subjecting the 3-(4-nitrophenyl)-3,4-dihydro-2H-1,3-benzoxazine to a step curing procedure in a vacuum oven using the following protocol: 160°C (2h), 180°C (2h), 200°C (2h) and 250°C (2h). After the step-curing, the sample was allowed to freely cool to room temperature before further analysis.

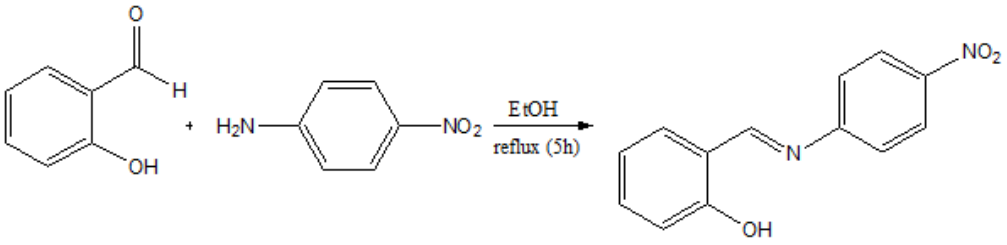

2-{(E)-[(4-nitrophenyl)imino]methyl}phenol

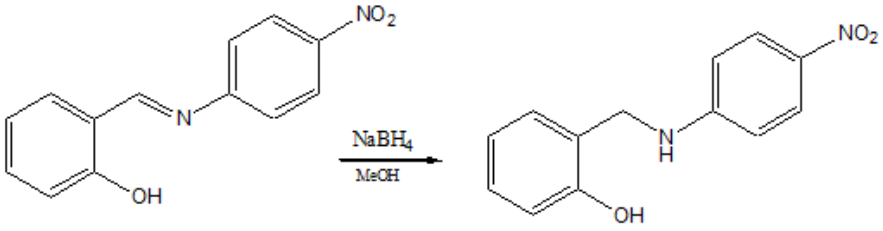

2-[(4-methylanilo)methyl]phenol.

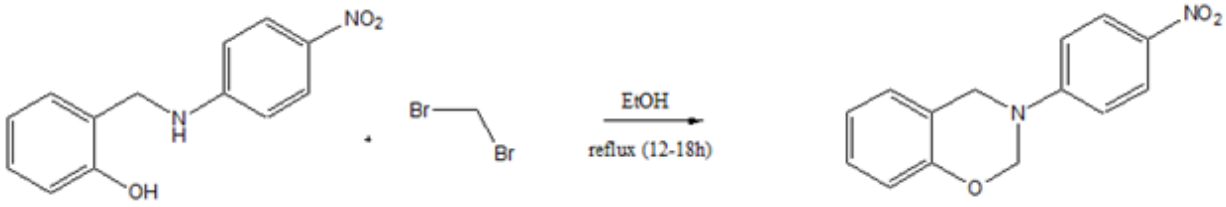

3-(4-nitrophenyl)-3,4-dihydro-2H-1,3-benzoxazine

Scheme 1. Synthesis of 3-(4-nitrophenyl)-3,4-dihydro-2H-1,3-benzoxazine

Characterization of 3-(4-nitrophenyl)-3,4-dihydro-2H-1,3-benzoxazine

Melting temperature (T_m) of the synthesized compound was determined using a Barnstead electrothermal melting point instrument 9100 Model. Fourier transform infrared spectroscopy (FT-IR) was used to recorded spectra in the region 280–4000 cm^{-1} on spectrophotometer Perkin Elmer FT-IR model 100 series (KBr Pellet). ^{1}H and ^{13}C nuclear magnetic resonance (NMR) spectral analysis was conducted on a JEOL 500 MHz NMR spectrometer using acetone-d_6 as the NMR solvent. Gas chromatography-mass spectrometry (GC-MS) analysis was carried out using a Shimadzu model QP 5050A GC-MS analyzer. Elemental analysis was performed with a Leco CHNS-932 Elemental Analyzer. Differential scanning calorimetry (DSC) measurements were realized using a Mettler Toledo DSC 822$_e$ calorimeter. TGA analysis was conducted using a Mettler Toledo TGA/DSC 1 STAR$_e$ System.

Results and Discussion

3-(4-nitrophenyl)-3,4-dihydro-2H-1,3-benzoxazine showed bands at 952 and 1488 cm^{-1} which are characteristic modes related to benzoxazine ring. Asymmetric Ar-H stretching vibration appears at 3077 cm^{-1} and aliphatic CH_2 stretching bands appear between 2936 and 2857 cm^{-1} while asymmetric stretching for C-O-C are located at 1224 cm^{-1}.

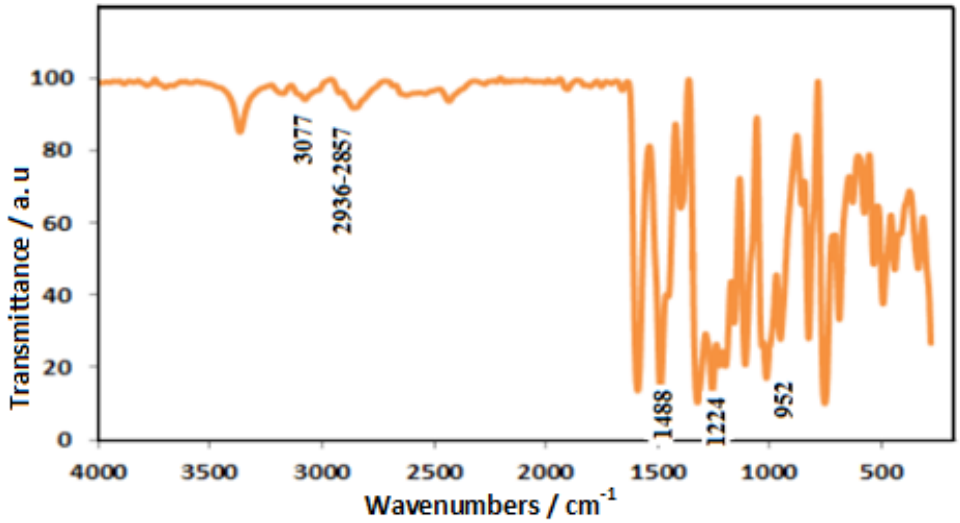

Figure 1. FT-IR spectrum of the 3-(4-nitrophenyl)-3,4-dihydro-2H-1,3-benzoxazine

Figure 2. ^{1}H NMR spectrum of the 3-(4-nitrophenyl)-3,4-dihydro-2H-1,3-benzoxazine in acetone.

The two distinct chemical shifts at 4.90 and 5.48 ppm are assigned to the newly formed 1,3-oxazine ring methylene protons (O-CH_2-N) and (Ar-CH_2-N) (Imran et. al., 2013, Kiskan et. al., 2009, Li et. al., 2014, Andronescu et. al., 2012). The chemical shifts in the range 6.78 – 8.16 ppm signify the presence of aromatic protons. The peaks at 2.09 and 2.94 ppm are due to CH_3 of acetone and H_2O, respectively which appear as solvent residual peak [Gottlieb et. al., 1997, Fulmer et. al., 2010].

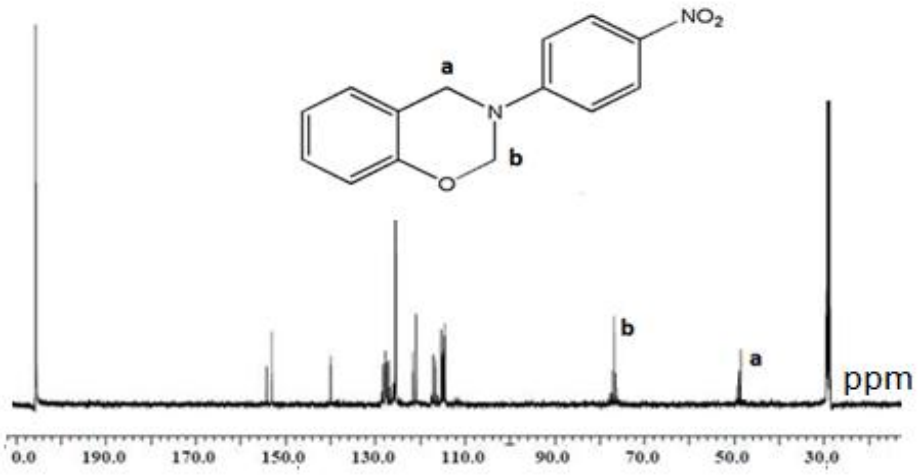

Figure 3. ^{13}C NMR spectrum of the 3-(4-nitrophenyl)-3,4-dihydro-2H-1,3-benzoxazine in acetone.

The carbon chemical shifts of the two methylene groups of the oxazine ring (N-CH_2-O) and (Ar-CH_2-N) are located at 76.9 ppm (N-CH_2-O) and 48.9 ppm (Ar-CH_2-N). The aromatic carbon chemicals shifts are located in the range 116.2-154.2 ppm. The peaks at 29.9 and 207.4 ppm represents the CH_3 and C=O chemical shifts of the solvent

(acetone) which appear as trace impurities [Gottlieb *et. al*., 1997, Fulmer *et. al*., 2010]

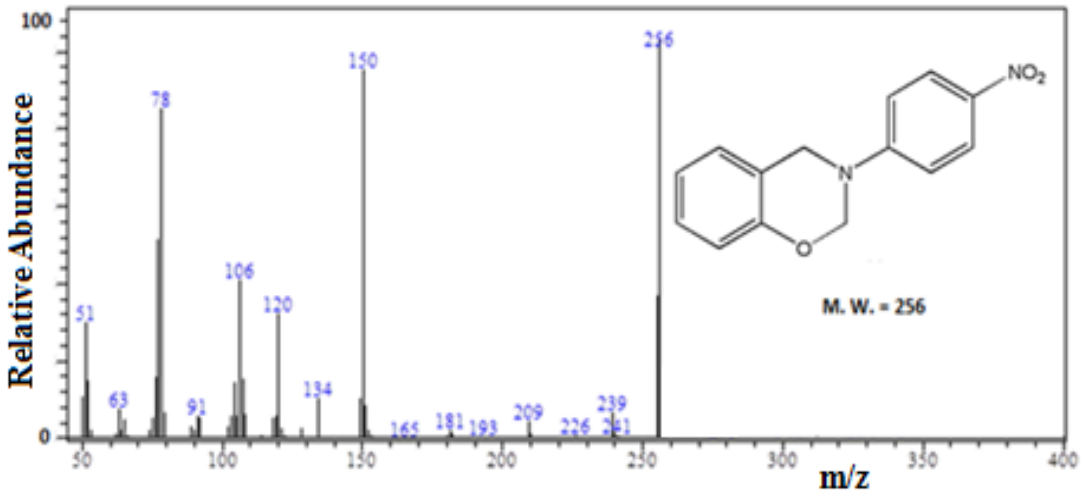

Figure 4. Mass spectrum of the monofunctional 1,3-benzoxazine derivative.

From the mass spectrum above, the molecular weight of the compound is given by the molecular ion peak with the highest m/z value (Lampman *et. al*., 2008). Thus, the molecular ion peak with the highest m/z value is 256 and this value is exactly the same as the calculated molecular weight.

Polymerization of 3-(4-nitrophenyl)-3,4-dihydro-2H-1,3-benzoxazine

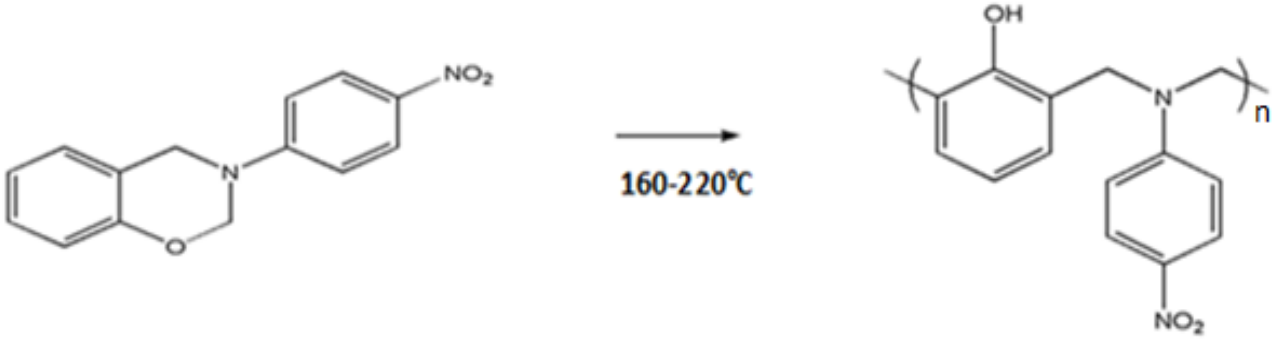

Figure 5. Polymerization of the 3-(4-nitrophenyl)-3,4-dihydro-2H-1,3-benzoxazine

Polymerization of 1,3-benzoxazine compounds is autocatalyzed (Ishida and Agag, 2011). This is so because the monomers contain phenolic materials and other benzoxazine oligomers that act as initiators or catalyst. Furthermore, the newly formed phenolic structure equally acts as initiators or catalysts. The purified monomers can therefore polymerize when their temperature is raised close to or more than their exothermic curing temperature normally in the range of 160-220 (Ning and Ishida, 1994). It is however important to note that the more the purity of the benzoxazine monomer, the more the polymerization temperature.

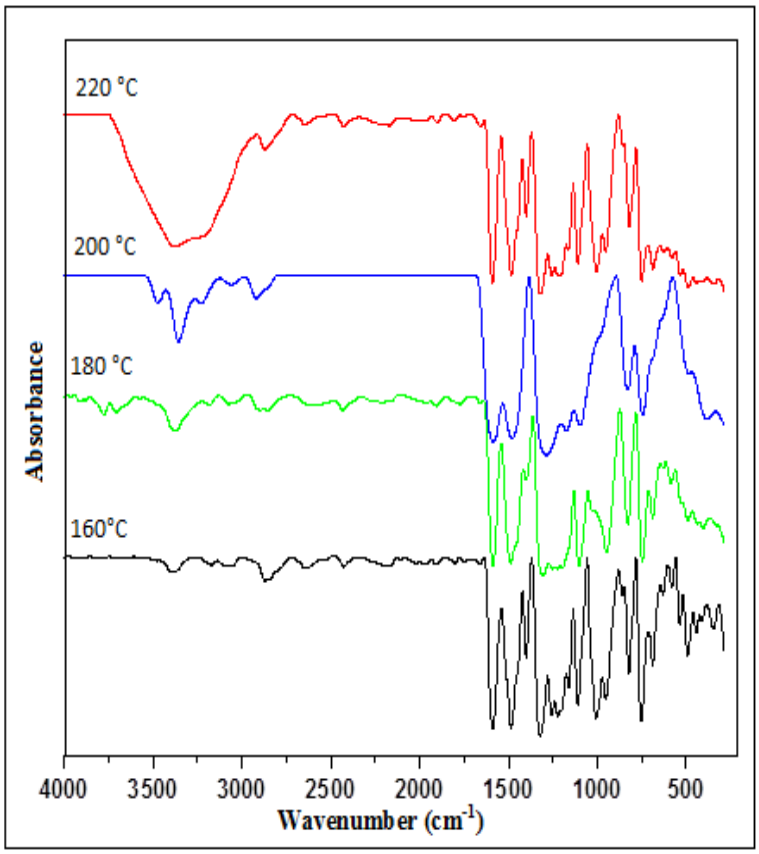

Figure 6. FT-IR spectra of poly (3-(4-nitrophenyl)-3,4-dihydro-2H-1,3-Benzoxazine after each heat treatment.

Figure 6 shows the FT-IR spectra of the 3-(4-nitrophenyl)-3,4-dihydro-2H-1,3-benzoxazine at each stage of the curing process. As the cure temperature is increased at each cure stage, there is a corresponding increase in the intensity of the absorption band at 3400 cm^{-1} which is assigned to OH and thus signifies the opening of the oxazine ring and therefore completion of polymerization.

TGA was used to deduce the thermal characteristics of the synthesized polybenzoxazine. Figure 7 gives the weight loss as the temperature is gradually increased. The 5% and 10% mass loss temperatures were found to be 208°C and 237°C while the degradation temperature was found to be 322°C. The char yield was found to be 34% at 800°C. Table 1 below gives the TGA result of the synthesized polybenzoxazine.

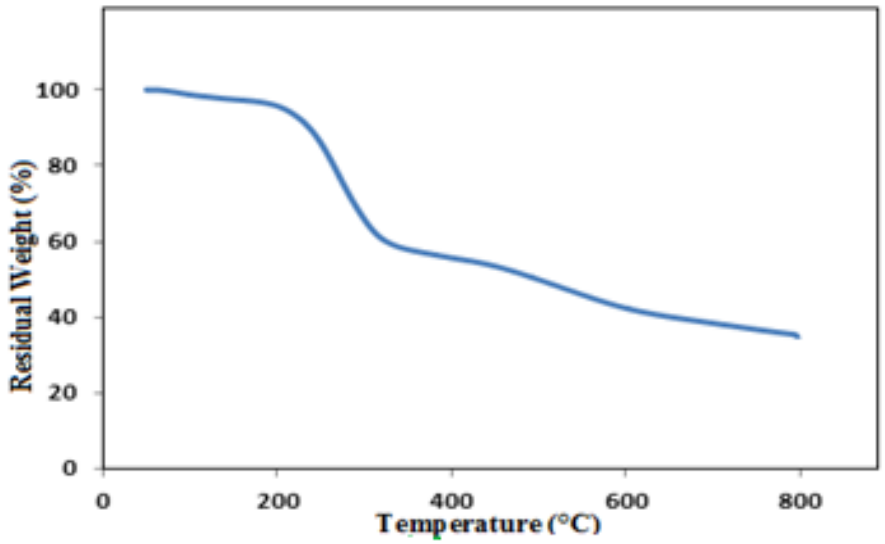

Figure 7. TGA thermogram of poly (3-(4-nitrophenyl)-3,4-dihydro-2H-1,3-benzoxazine).

Table 1: TGA result of poly (3-(4-nitrophenyl)-3,4-dihydro-2H-1,3-benzoxazine)

T_d5 (°C)	**T_d10 (°C)**	**T_d (°C)**	**Char Yield (%)** (at 800°C)
208	237	322	34

Conclusion

A monofunctional 1,3-benzoxazine was successfully synthesized using a modified three step synthetic technique in which formaldehyde was replaced with methylene bromide for ring closure reaction in the last synthetic step. The structure of the monofunctional compound was confirmed using appropriate spectral methods and finally polymerized through thermally activated ring opening to obtain the corresponding polybenzoxazine.

References

Agag, T. (2006). Preparation and properties of some thermosets derived from allyl-functional naphthoxazines. *Journal of Applied Polymer Science, 100*(5), 3769-3777.

Allen, D. J., & Ishida, H. (2009). Effect of phenol substitution on the network structure and properties of linear aliphatic diamine-based benzoxazines. *Polymer, 50*(2), 613-626.

Andreu, R., & Ronda, J. (2008). Synthesis of 3, 4-dihydro-2H-1, 3-benzoxazines by condensation of 2-hydroxyaldehydes and primary amines: Application to the synthesis of hydroxy-substituted and deuterium-labeledcompounds. *Synthetic Communications, 38*(14), 2316-2329.

Baqar, M., Agag, T., Ishida, H., & Qutubuddin, S. (2011). Poly (benzoxazine-co-urethane): A new concept for phenolic/urethane copolymers via one-pot method. *Polymer, 52*(2), 307-317.

Burke, W. (1949). 3, 4-dihydro-1, 3, 2H-benzoxazines. Reaction of p-substituted phenols with N, N-dimethylolamines. *Journal of the American Chemical Society, 71*(2), 609-612.

Burke, W., Kolbezen, M. J., & Stephens, C. W. (1952). Condensation of naphthols with formaldehyde and primary Amines1. *Journal of the American Chemical Society, 74*(14), 3601-3605.

Chernykh, A., Agag, T., & Ishida, H. (2009). Novel benzoxazine monomer containing diacetylene linkage: An approach to benzoxazine thermosets with low polymerization temperature without added initiators or catalysts. *Polymer, 50*(14), 3153-3157.

Chutayothin, P., & Ishida, H. (2011). Polymerization of p-cresol, formaldehyde, and piperazine and structure of monofunctional benzoxazine-derived oligomers.*Polymer, 52*(18), 3897-3904.

Demir, K. D., Kiskan, B., Aydogan, B., & Yagci, Y. (2013). Thermally curable main-chain benzoxazine prepolymers via polycondensation route. *Reactive and Functional Polymers, 73*(2), 346-359.

Elderfield, R. C. (1957). *Heterocyclic compounds: Six-membered*

heterocyclics containing two hetero atoms and their benzo derivatives J. Wiley.

Endo, T., & Sudo, A. (2009). Development and application of novel ring-opening polymerizations to functional networked polymers. *Journal of Polymer Science Part A: Polymer Chemistry, 47*(19), 4847-4858.

Lampman, G. M., Donald, L. Pavia, George, S. Kriz, & James, R. Vyvyan (2008). *Introduction to spectroscopy* Google books.

Gottlieb, H. E., Kotlyar, V., & Nudelman, A. (1997). NMR chemical shifts of common laboratory solvents as trace impurities. *The Journal of Organic Chemistry, 62*(21), 7512-7515.

Hemvichian, K., & Ishida, H. (2002). Thermal decomposition processes in aromatic amine-based polybenzoxazines investigated by TGA and GC–MS. *Polymer, 43*(16), 4391-4402

Imran, M., Kiskan, B., & Yagci, Y. (2013). Concise synthesis and characterization of unsymmetric 1, 3-benzoxazines by tandem reactions. *Tetrahedron Letters, 54*(36), 4966-4969.

Kawauchi, T., Murai, Y., Hashimoto, K., Ito, M., & Sakajiri, K. (2011). Synthesis and polymerization behavior of novel liquid-crystalline benzoxazines. Polymer, 52(12), 2150 – 2156.

Li, S. F. (2010). Synthesis of benzoxazine-based phenolic resin containing furan groups. *Chinese Chemical Letters, 21*(7), 868-871.

Lewis Sr, R. J. (2008). *Hazardous chemicals desk reference* John Wiley & Sons.

Mathew, B. P., Kumar, A., Sharma, S., Shukla, P., & Nath, M. (2010). An eco-friendly synthesis and antimicrobial activities of dihydro-2H-benzo-and naphtho-1, 3-oxazine derivatives. *European Journal of Medicinal Chemistry, 45*(4), 1502-1507.

Manikannan, R., & Muthusubramanian, S. (2010). Synthesis and biological activity of 6-alkyl/chloro-3-{4-(6-alkyl/chloro-2H-benzo [e][1, 3] oxazin-3 (4H)-yl) phenyl}-3, 4-dihydro-2H-benzo [e][1, 3] oxazines. *Indian Journal of Chemistry, 49*(8), 1083-1087.

Mireya, E., Carrajal, M., & Rincon, J. (1980). Synthesis of some benzoxazines and the study of their possible antibacterial activity. *Rev.Colomb.Cienc.Quim.Farm , 3*, 63-67.

Pasternak, A., Goble, S. D., Struthers, M., Vicario, P. P., Ayala, J. M., Di Salvo, J., Mills, S. G. (2009). Discovery of a potent and orally bioavailable CCR2 and

CCR5 dual antagonist. *ACS Medicinal Chemistry Letters, 1*(1), 14-18.

Petrlíková, E., Waisser, K., Divišová, H., Husáková, P., Vrabcová, P., Kuneš, J., Stolaříková, J. (2010). Highly active antimycobacterial derivatives of benzoxazine. *Bioorganic & Medicinal Chemistry, 18*(23), 8178-8187.

Shakil, N. A., Pandey, A., Singh, M. K., Kumar, J., Awasthi, S. K., Pandey, R. P. (2010). Synthesis and bioefficacy evaluation of new 3-substituted-3,4-dihydro-1,3-benzoxazines. *Journal of Environmental Science and Health Part B, 45*(2), 108-115.

Sini, N. K., Bijwe, J., Varma, I. K. (2014). Thermal behavior of bis-benzoxazines derived from renewable feed stock 'vanillin'. *Polymer Degradation and Stability, 109, 270*-277.

Tang, Z., Zhu, Z., Xia, Z., Liu, H., Chen, J., Xiao, W., & Ou, X. (2012). Synthesis and fungicidal activity of novel 2, 3-disubstituted-1, 3-benzoxazines. *Molecules, 17*(7), 8174-8185.

Zhang, K., & Ishida, H. (2015). Smart synthesis of high-performance thermosets based on ortho-amide–imide functional benzoxazines. *Frontiers in Materials, 2*, 5.

Zúñiga, C., Lligadas, G., Ronda, J. C., Galià, M., & Cádiz, V. (2012). Self-foaming diphenolic acid benzoxazine. *Polymer, 53*(15), 3089-3095.

Nigerian Journal of Polymer Science and Technology, 2017, Vol. 12, pp 39-45

Received: 12 July 2018 Accepted: 08 September 2018

Studies of *Luffa cylindrica* Fiber Reinforced Waste Low Density Polyethylene Composite

Y. Adamu, M.T. Isa[**], J.A. Mohammed, T.K. Bello

Department of Chemical Engineering, Ahmadu Bello University, Zaria

Abstract

Due to environmental concerns associated with synthetic fibers as reinforcement in composites, attention is now on the natural fibers that are biodegradable. While there are reported works on many natural fibers, *Luffa cylindrica* is an emerging fiber that requires attention in composite material development. In this research, *Luffa* fiber was used to reinforce waste low density polyethylene (wLDPE). The fiber loading was 5-30 wt% at interval of 5 wt%. The composite was compounded via a two-roll heat mixer operated at 150 ^{o}C for 10 mins. 15 wt% fiber loading recorded the highest tensile, impact and flexural strengths of 10.7 MPa, 32.2 mJ/mm^2 and 17.2 MPa respectively. The microstructural analysis however showed a low compatibility between the *Luffa* fiber and the waste polyethylene matrix thereby suggesting, a need for fiber modification for improved mechanical property.

Key words*:* Physical Properties, Mechanical Properties, Morphological Properties, *Luffa*, Polyethylene (wLDPE).

INTRODUCTION

Composite materials usually possess unique properties superior to its constituent elements. They are formed when two or more components combine to produce a new material with distinct interface. The interface separates the continuous phase called the matrix from the discontinuous phase (reinforcement/filler) embedded in it (Masuelli, 2013; Kant and Verma, 2017; Markovic and Visakh, 2017). The composites constituents can retain their respective properties within the composite formed (Bhargava, 2012). Figure 1 shows a schematic representation of a simple composite formed from a matrix reinforced with a fiber.

Over the years, composites have been produced from synthetic matrices and reinforcements (Mohanty *et al.*, 2002; Ubi and Abdul Rahman, 2015). These synthetic constituents exhibit non-biodegradable behaviors and hence constitute nuisances and hazards to the environment. Studies on non-biodegradable material for composite application which revealed negative environmental impact has prompted Scientists and Engineers to turn towards alternative materials that are cheap, lightweight, sustainable and environmentally friendly. The use of natural fibers (bio composites) as substitute for synthetic ones have recorded remarkable and impressive achievements (Meenakshi, 2012; Omar *et al.*, 2012; Dicker *et al.*, 2014; Ubi and Abdul Rahman, 2015).

Bio-composites are formed from bio-matrix and bio-reinforcement (Drzal *et al.*, 2003; Noël *et al.*, 2011). However, a synthetic matrix can be combined with bio-

[**] *Department of Chemical Engineering, Ahmadu Bello University, Zaria* (M.T. Isa, E-mail: **mtisaz@yahoo.com)**

reinforcement or a bio-matrix and synthetic fiber to make composite partially biodegradable. Among the most used synthetic matrix materials are polyester, epoxy, polyethylene, polypropylene etc. because of their low weight, low cost and ease of processing (Drzal *et al*., 2003; Paul *et al*., 2007; and Masuelli, 2013).

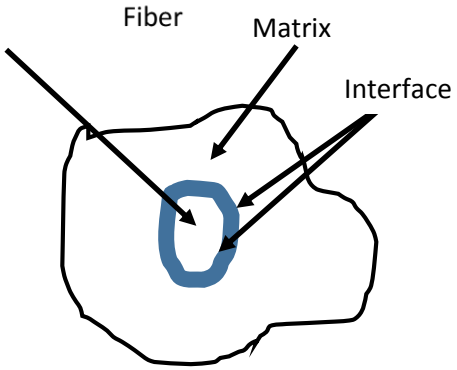

Figure 1: Schematic illustration of composite and its constituents.

Bio-reinforcements on the other hand includes wood, grass, agricultural residues, forestry wastes etc. (Perez *et al*., 2002; Mngomezulu and John, 2017). Martínez-López *et al*. (2013) studied the effect of the *Luffa* fibers on the mechanical properties of polymer (polyester resin) matrix. It was revealed that addition of *Luffa* fibers weakens the compressive strength, flexural strength and Young's modulus of the composite. Omar *et al*., (2012) also, in their review reported that, when *Abaca* fiber polypropylene (PP) composites were compared with jute and flax fiber PP composites at 40 wt% fiber loadings, *Abaca* fiber composites had the best mechanical properties.

There are few reported studies of *Luffa* reinforced polyethylene composites, however, this paper presents the physical and mechanical studies of waste low density polyethylene (wLDPE) reinforced with *Luffa cylindrica*l fibers.

Materials and Methods

The *Luffa* fruits (which were 150-170mm long and 100-120mm wide) were sourced from Ahmadu Bello University Zaria dam area while the waste low density polyethylene (wLDPE) sourced from Yus-Bol poly products in Barnawa, Kaduna State, Nigeria.

Methods

Preparation of *Luffa cylindrica* (*LC*) fibers

Luffa fiber was removed from its vein by cutting the ripe and matured fruit. The fiber was separated from the seeds and dried to achieve moisture free fiber.

The dried LC fibers were size reduced to 25mm x 25mm, to achieve even distribution of the fiber in matrix during compounding. A pre-sample (composite) was then formed to determine the amount of the reinforcement and matrix needed to fabricate composites.

Composites production

Waste low density polyethylene was first preheated in the two-roll mill, manufactured by Reliable Rubber and Machinery Company, North Berger New Jersey, U.S.A. Model No. 5183, thereafter chopped *Luffa* fibers was distributed into the matrix in the ratio 5/95 wt% (fiber to matrix ratio) and compounded at a temperature of 150^{o}C for 10 minutes period. After proper mixing, showed by the

consistency of the mix, the machine was stopped and the mixture scrapped off the rollers. The mixture was then placed in a mold and press at a temperature of 150^{o}C and pressure of 13.7895 MPa for a period of 4 minutes on a hydraulic press (Carver Incorporation New Jersey, U.S.A. Model No. 12000). The same procedure was used to produce composites of 10/90, 15/85, 20/80, 25/75 and 30/70 wt% fiber to matrix loading (Ubi and Abdul Rahman, 2015).

Composite Characterization

Tensile test was conducted according to ASTM D638 using the Instron machine model 3369, system number 3369K1781, capacity 50kN. Flexural test was conducted according to ASTM D790 using Universal materials testing machine, Norwood Instruments Ltd. 100 kN capacity. The impact test was conducted according to ASTM D256-78 using Charpy impact testing machine, Norwood Instruments Limited, Great Britain. Water absorption test and density tests were also conducted on the composite produced all based-on ASTM D570-98. A Phenom^{TM} (Pro X) Scanning Electron Microscopy (SEM) was used to examine the morphology and the composite surface topography produced from treated and untreated fibre. Three test samples were used in each test and the average was recorded, which was used to calculate the standard error as shown in figure 3-8 (Isa *et al.*, 2014).

$$SE = \frac{\sigma}{\sqrt{n}} \quad (1)$$

Where; SE = Standard error, σ = Standard deviation, n = Sample number

Results and Discussions

Mechanical Properties

This section presents tensile strength, percentage elongation, modulus of elasticity (MOE), flexural modulus and impact strength of the composite samples as shown from Figures 2-6 respectively.

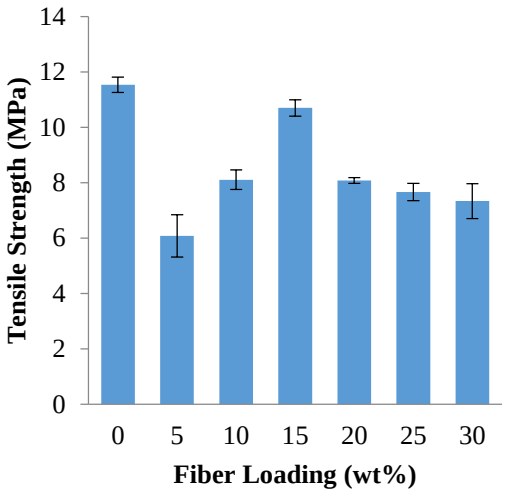

Figure 2: Effect of fiber loading on the tensile strength of *Luffa* reinforced wLDPE composite

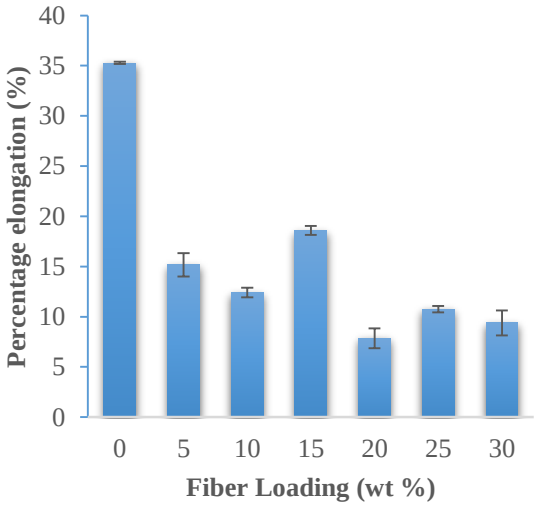

Figure 3: Effect of Fiber Loading on the percentage elongation of *Luffa* reinforced wLDPE composite

The tensile strength (T.S) increases with increase in fiber loading up to 15 wt% loading after which a drop was observed. The drop in T.S value is due to the effect of fiber-fiber contact when 15 wt% loading was exceeded, hence improper transfer of

load from matrix to fiber (Mwaikambo and Ansell, 2002). The 15 wt% also recorded the highest percentage elongation which support the highest loading amount of the fiber before its mechanical properties starts to deteriorate. A Similar trend was reported when LDPE matrix was reinforced with broom fiber (Paul *et al*., 2007).

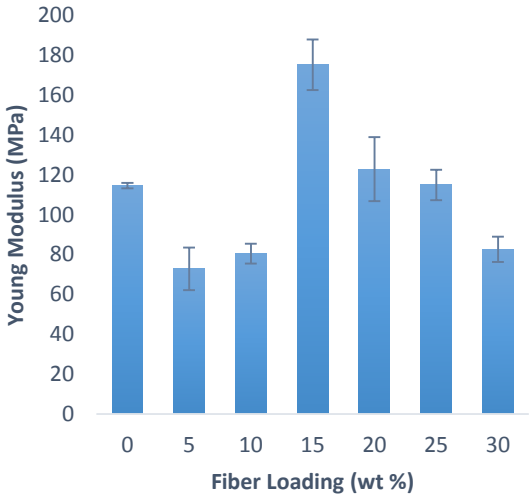

Figure 4: Effect of fiber loading on the Young Modulus of *Luffa* reinforced wLDPE composite

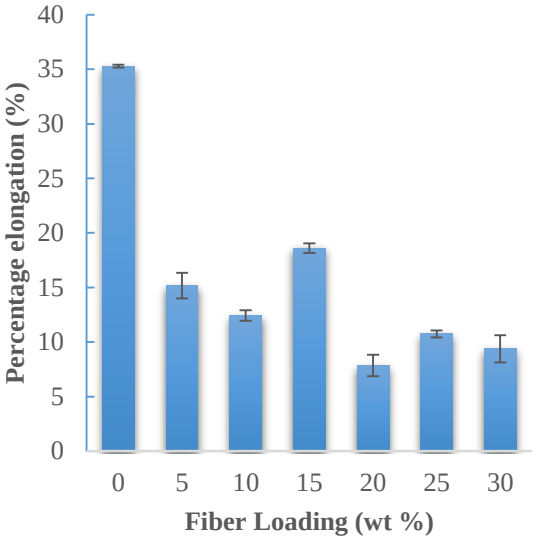

Figure 5: Effect of Fiber Loading on the Flexural Strength of *Luffa* reinforced wLDPE Composite

Modulus of elasticity (MOE) increases in similar trend as the T.S (Figure 4), which shows that 15 wt% fiber loading exhibited the highest MOE of 175.33 MPa. This suggests that the 15 wt% fiber loading exhibit higher degree of stiffness compare to the other fiber loadings. No improvement in the elongation at break was recorded, which was believed to be, due to the effect of improper distribution of fiber in the matrix at higher loading (Mwaikambo and Ansell, 2002). In Figure 5, there was a noticeable increase in the flexural strength value with increasing fiber loading until a peak of 15 wt% fiber loading was reached and a sharp decrease was observed. This may be also attributed to improper fiber-matrix-interaction at higher fiber content causing the composite to become weaker (Mwaikambo and Ansell, 2002). The highest value of flexural strength obtained at 15 wt% fiber loading (23.19 MPa) was slightly lower than 24.28 MPa for double layered *Luffa* fiber/epoxy composite (Sahu, 2013).

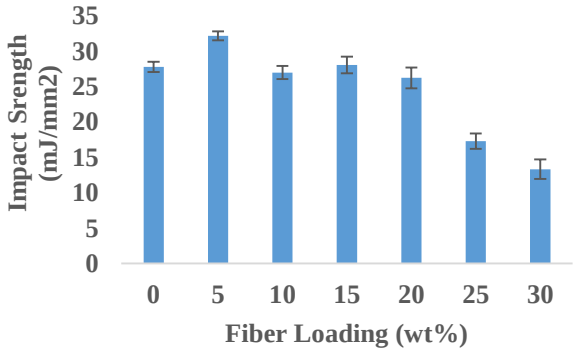

Figure 6: Effect of Fiber Loading on the Impact Strength of *Luffa* reinforced wLDPE Composite

For impact strength, 5 wt% fiber loading recorded the highest impact strength of 32.2 mJ/mm^2 followed by the 15wt % (28.08 mJ/mm^2). This could have been due to poor matrix-fiber interaction caused by improper mixing during compounding. A downward trend in impact was observed beyond 15 wt% fiber loading which could be predict fairly well for 40 wt % results as studied by Omar *et al*. (2012). In the study, *Abaca* fiber polypropylene (PP) composites were compared with jute and flax fiber PP composites at 40 wt% fiber loadings, *Abaca* fiber composites had the best impact strength of 4.5 mJ/mm^2, 3.0 mJ/mm^2 and 3.1 mJ/mm^2 respectively.

Physical Properties

This section presents percentage water absorption and density (Figures 7 and 8) of the compounded composites. Figure 7 shows the increase in water absorption as the filler increased. The affinity for water increased because of the hydrophilic nature of the fiber. The high-water absorption of lignocellulosic fibers is caused by hydrogen bonding between free hydroxyl groups on cellulose molecules and water molecules causing increase in water affinity (Demir *et al*., 2006). It was also observed from Figure 8 that the 10 wt% fiber loading exhibited the minimum density of 7.86 g/cm^3 which was about 14.6 wt% less than the control sample (0 wt% *Luffa* fiber) composite. But gradual increase was noticed. Even with the increase in density the highest value (8.31 g/cm^3) was still lower than the *Luffa* fiber density 9.2 g/cm^3 reported by Tanobe *et al*. (2014).

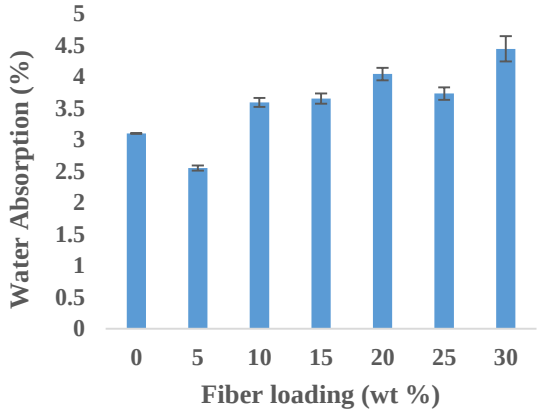

Figure 7: Effect of Fiber Loading on Water Absorption of *Luffa* reinforced wLDPE composite

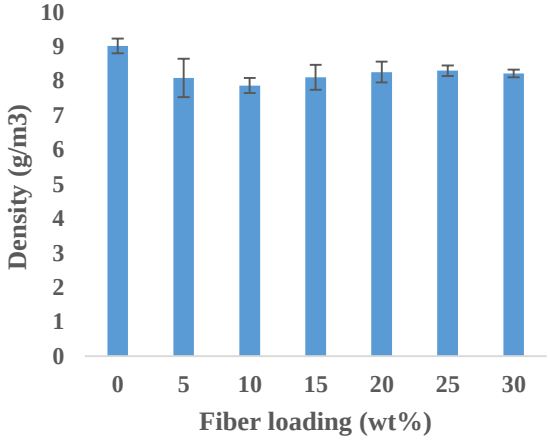

Figure 8: Effect of Fiber Loading on Density of *Luffa* reinforced wLDPE Composite

3.3 Surface Morphology

The scanning electron microscope (SEM) micrographs of the surface of composite specimens reinforced with 15 wt% *Luffa* fiber which has the highest mechanical properties is presented in Plate I. The wettability between *Luffa* fibers and waste low density polyethylene matrix seemed to be poor, due to the presence of larger void spaces as shown in Plate I (b). Despite the 15 wt% having the highest mechanical properties, there are still voids which can lead to reduced mechanical properties of the composite, causing failure. This is an indication that the fiber like any other natural fiber requires treatment for improved mechanical properties.

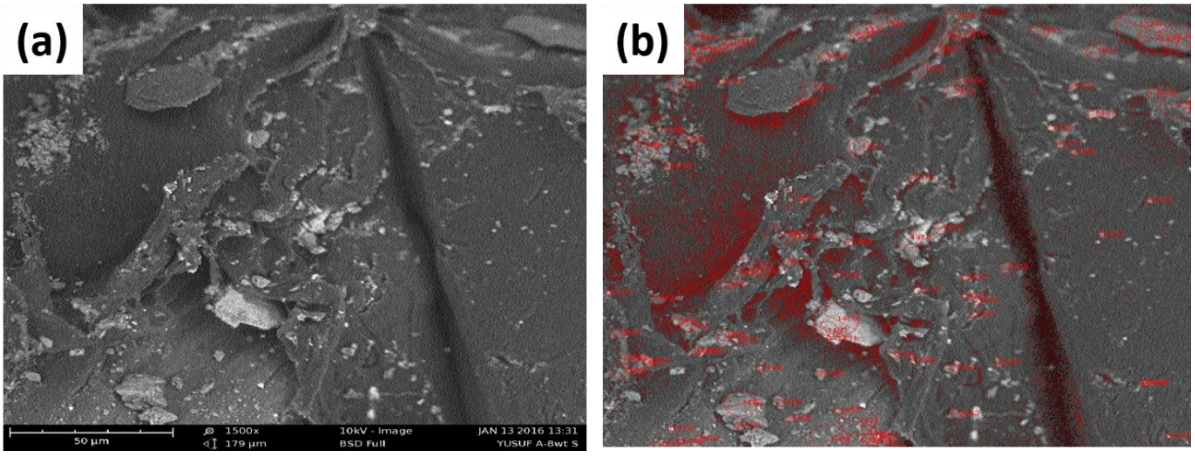

Plate I: SEM micrographs of 15 wt% *Luffa* fiber composite

Conclusion

Luffa fiber was successfully used to reinforce waste LDPE matrix in this work. The composite with 15 wt% *Luffa* fiber loadings gave the highest mechanical properties (tensile, MOE and flexural strength) with values 10.7 MPa, 175 MPa and 23.2 MPa respectively. The SEM morphology showed that, there were large void spaces present in the developed composite. Thus, this can be said to be responsible for the decrease in mechanical properties as observed.

References

Bhargava A.K., (2012). Engineering materials: Polymers, Ceramics and Composite 2nd Edition. PHI Learning Private Limited, New Delhi. pp. 267.

Demir, H., Atikler, U., Balköse, D., and Tıhmınlıoğlu, F. (2006). The effect of fiber surface treatments on the tensile and water sorption properties of polypropylene–*Luffa* fiber composites. *Composites Part A: Applied Science and Manufacturing*, ***37***(3), 447-456.

Dicker, M. P., Duckworth, P. F., Baker, A. B., Francois, G., Hazzard, M. K., and Weaver, P. M. (2014). Green composites: A review of Material attributes and complementary applications. *Comp osites part A: applied science and manufacturing*, ***56***, 280-289.

Drzal, L. T., Mohanty, A. K., and Misra, M. (2001). Bio-composite materials as alternatives to petroleum-based composites for automotive applications. *Magnesium*, Michigan State University, East Lansing, MI 48824. 2001, **40**, (60), 1-3.

Isa M. T., Usman S., Ameh A. O., Ajayi O. A., Omorogbe O., Ameuru S. U. (2014). The Effect of Fiber Treatment on the Mechanical and Water Absorption Properties of Short Okra/Glass Fibers Hybridized Epoxy Composites. International Journal of Materials Engineering, **4**, (5), 180-184.

Kant, S., and Verma, S. L. (2017). A Review on Analysis and Design of Bullet Resistant Jacket-Ballistic Analysis. *International Advanced Research Journal in Science, Engineering and Technology, 4(3)*, 71-80.

Markovic, G., and Visakh, P. M. (2017). Polymer blends: State of art. In *Recent Developments in Polymer Macro, Micro and Nano Blends* (pp. 1-15). Woodhead Publishing.

Martínez-López, M., Martínez-Barrera, G., and Martínez-Cruz, E. (2013). Effect of the Loofah-fibers on the mechanical properties of Polymer Concrete. In IOP Conference Series: Materials Science and Engineering (Vol. 45, No. 1, p. 012027). IOP Publishing.

Masuelli, M. A. (2013). Introduction of fiber reinforced polymers polymer and composites: concepts, properties and process. In Masuelli (Ed.) Fiber reinforced polymers: The technology applied for concrete repair. InTech Open, pp.1-24

Meenakshi, P. (2012). *Elements of environmental science and engineering*. PHI Learning Pvt. Ltd, New Delhi.

Mngomezulu, M. E., and John, M. J. (2017). Thermoset-cellulose nanocomposites: Flammability Characteristics. Wiley.

Mohanty, A. K., Misra, M., and Drzal, L. T. (2002). Sustainable bio-composites from renewable resources: opportunities and challenges in the green materials world. *Journal of Polymers and the Environment*, **10**(1-2), 19-26.

Mwaikambo, L. Y., and Ansell, M. P. (2002). Chemical modification of hemp, sisal, jute, and kapok fibers by alkalization. *Journal of applied polymer science*, ***84***(12), 2222-2234.

Noël M., Fredon E., Mougel E., Masson E., Masson D. (2011). Biopolymer as Reinforcement into Natural Matrices: a New Route to Bio-Composite Material. In Brahim Attaf (Ed.). Advances in composites materials-ecodesign and analysis. InTech Open, pp. 89

Omar F., Andrzej K.B., Hans-Peter F., Mohini S., 2012. Biocomposites reinforced with natural fibers: 2000–2010. *Progress in Polymer Science*, **37**, 1552-1596.

Paul A., Joseph K., Thorna S. (2007). Effect of surface treatments on the electrical properties of low density polyethylene composites reinforced with short sisal fibers. *Composites Science and Technology*, **51**(1), 67-79.

Perez J., Munoz-Dorado J., de la Rubia T., Martınez J. (2002). Biodegradation and biological treatments of cellulose, hemicellulose and lignin, an overview. *International Microbiology*, **5,** 53-63.

Sahu J. (2013). Study of tensile and flexural properties of *Luffa* fiber reinforced epoxy composites. B. Tech Thesis, National Institute of Technology, Rourkela, India, 39.

Tanobe V.O.A., Flores-Sahagun T.H.S., Amico S.C., Muniz G.I.B., Satyanarayana K.G. (2014). Sponge Gourd (*Luffa Cylindrica*) Reinforced Polyester Composites: Preparation and Properties. *Defence Science Journal*, **64**, (3), 273-280.

Ubi P.A., AbdulRahman S.A.R. (2015). Effect of Sodium Hydroxide Treatment on the Mechanical Properties of Crushed and Uncrushed *Luffa cylindrica* Fibre Reinforced rLDPE Composites. *World Academy of Sci., Engineering and Technology, International Journal of Chemical, Nuclear, Materials and Metallurgical Engineering*, **9**, (1), 303-308.

Nigerian Journal of Polymer Science and Technology, 2017, Vol. 12, pp 46-53

Received: 01 March 2018 Accepted: 03 September 2018

Synthesis of Carbon nanotube Macroinitiator of Atom Transfer Radical Polymerization by Esterification Reaction

Umar Ali[††1] and Sani Muhammad Gumel[2]

[1]*Department of Chemistry, Sule Lamido University, Kafin-Hausa, Jigawa, Nigeria*

[2]*Department of Pure and Industrial Chemistry, Bayero University Kano, Nigeria*

*Corresponding Author's Email Address: dumarali4@gmail.com

ABSTRACT

During atom transfer radical polymerization (ATRP) a halogen terminated initiator is necessary for the initiation of the polymerization and subsequent formation of the polymer chain in the propagation step. However, with the exception of *in situ* generation there was very limited or no studies on the carbon nanotube based macro-initiators for ATRP. Bromine terminated macro-initiator was synthesized by esterification reaction of hydroxyl group modified multiwalled carbon nanotubes and 2-bromoisobutyryl bromide. Characterization on the synthesized macro-initiator was performed by Fourier transform Infrared, X-ray photoelectron spectrometer, and ^{13}C-solid NMR spectroscopy. From the results, the 1735 cm^{-1} (C=O ester linkage), 788 cm^{-1} (C-Br), 177 ppm (ester linkage), biding peaks at 288.40 eV and 531 eV are all due to bromine terminated initiator. These exhibited a successful synthesis of the bromine terminated ATRP initiator.

Keywords: carbon nanotube, macro-initiator, esterification reaction, ATRP

Introduction

Carbon nanotubes (CNTs) was discovered by Sumio Iijima in early nineties, (Iijima, 1991) they have an outstanding mechanical, electrical, and thermal properties that make them attractive for applications in the field of polymer science and nanotechnology (Liu, 2005). The functionalization of CNT with polymer moieties could be achieved using ATRP method in a process called "*grafting from*" that involved the use of ATRP initiator or macro-initiator (De Falco et al., 2009). Well defined polymer chain with controlled composition and molecular architecture can be built on CNT surface with ATRP method (Baskaran et al., 2004; Hong et al., 2005; Kong et al., 2004a, 2004b; Matrab et al., 2006; Qin et al., 2004; Wu et al., 2007).

ATRP discovered by Matyjaszewski and Wang in 1995 (Wang & Matyjaszewski, 1995), is one of the controlled radical polymerization methods that was very powerful for the preparations of compositionally and structurally diverse polymers with general routes that include steps (i) CNT surface functionalization, (ii) incorporation of ATRP-initiating group to CNT surface, and (iii) Surface-initiating ATRP using various monomers and catalyst ligand system. The method relies on establishing an equilibrium between alkyl halide-type dormant species which could be

[††] Department of Chemistry, Sule Lamido University, Kafin-Hausa, Jigawa, Nigeria. (U. Ali, E-mail: dumarali4@gmail.com)

the CNT macro-initiator and propagating radical in the presence of transition metal complex ligand system (Liu & Chen, 2007; Tsarevsky & Jakubowski, 2011). The process involved lower oxidation state complex ($Cu^{I}L_n$; L= ligand) in which the transition metal Cu can exist in two different oxidation states (higher and lower) in a reversible redox process. The lower oxidation state (activator) transition metal reacts with the ATRP initiator (R-X) to yield the radical (R*) and the higher oxidation state (deactivator) metal complex then followed by the propagation stage (Tsarevsky & Jakubowski, 2011). The role of the ligand in the catalyst ligand system is to act as a reducing agent in which it makes the deactivator ($XCu^{II}L_n$) to reversibly react with the radical, converting it to the dormant alkyl halide while being reduced to activating complex $Cu^{I}L_n$ to promote a new redox cycle as illustrated in Figure 1.

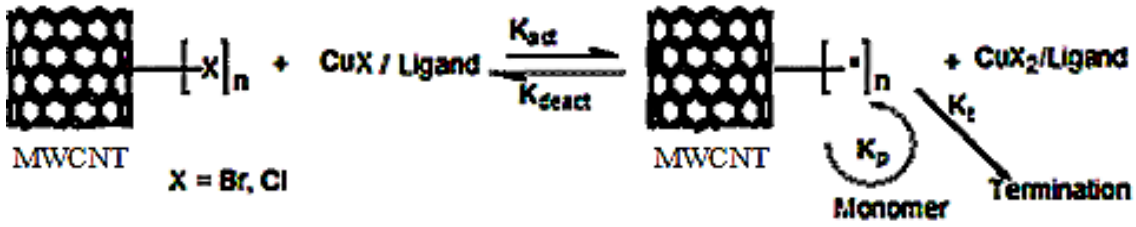

Figure 1: ATRP mechanism illustrating the equilibrium of activator and deactivator species.

The major advantages of using CNT based macro-initiators in ATRP is to; (i) have a living complex copolymers of CNT base, (ii) have unprecedented control over the chain topology of the complex copolymers (stars, combs, branched), and (iii) achieved high molecular weight with good polydispersity in CNT base copolymer preparations (Matyjaszewski Krzysztof 2002; Peng et al., 2015).

The work described the synthesis by esterification reaction and characterization of multiwalled carbon nanotube based ATRP macro-initiator. The successful synthesis may widen the applications of carbon nanotube in the field of polymer grafting, as it increases the opportunity of covalent attachment of well define living polymer chain with unprecedented control and desired topology on the surface of the CNTs.

Materials and Methods

Chemicals/Reagents

MWCNT with diameter 110-170 nm and purity of 90 % was obtained from Sigma Aldrich co.Ltd. Aluminium chloride 99.9% obtained from Fluka, potassium hydroxide 90% from QREC™, 2-bromoisobutyryl bromide 97% from Sigma Aldrich, and pyridine 99.8% from Sigma Aldrich. Other chemicals include chloroform 99% and methanol 99% from QREC™ Asia. All chemicals/reagents were used as received.

Preparation of Hydroxyl Functionalized MWCNT (MWCNT-OH)

MWCNT (0.2 g) and aluminium chloride (1.55 g) were ground in to powder form using pestle and mortar for 20 minutes. They were charged in to three-necked round bottom flask that contain excess chloroform, and then refluxed for 48 hrs under nitrogen gas (N_2). The yellowish-colored mixture was cooled to room temperature, then followed by slow addition of 50 ml of alkaline methanol using dropping funnel and stirred at 70°C for 20 hrs. Finally, the whole mixture was filtered through 0.2 µm PTFE membrane and washed repeatedly with distilled water, ether, and THF. The black powder was dried under vacuum (Choi et al., 2005).

Synthesis of MWCNT-Br Macro Initiator Using 2-bromoisobutyryl bromide

MWCNT-OH (0.16 g), 2-bromoisobutyryl bromide 8.5 ml (15.81 g, 0.07moles), and 0.3 ml (0.004 moles) pyridine were charged in to 100 ml three-necked round bottom flask. The mixture was refluxed for 12 hrs and the excess 2-bromoisobutyryl bromide was removed under reduced pressure. The resulting mixture was cooled to 0°C, and 40 ml of distilled water was added, followed by 1 hr stirring, 40 ml of chloroform (0.5 moles) was added then stirred for 1 hr. The chloroform layer containing MWCNT-OH was washed with distilled water three times and collected. Then the product was dried overnight under vacuum (Choi et al., 2005).

Characterization

Perkin Elmer infrared spectrometer, Spectrum ™ 400 was used for Fourier transform infrared (FT-IR) spectroscopy analysis of MWCNT-Br. Solid ^{13}C-NMR spectroscopic analysis of MWCNT-Br was done at ambient temperature on Bruker Avance III HD 400 MHz. A rotor of 4 mm in diameter was used to acquire the NMR spectra at spin frequency of 100.59 MHz. The high-resolution NMR spectrum was obtained with auto-correction of cross-polarization-magic angle spinning (CP-MAS) and dipolar decoupling.

The surface chemistry of MWCNT-Br was analyzed using X-ray photoelectron spectroscopy (XPS, Axis Ultra DLD Shimadzu). Al Kα (1486.6 eV) was the X-ray source, and the survey spectra was recorded in range of 0 to 1200 eV with pass energy of 20 eV in hybrid mode. Finally, the high-resolution scan spectra generated the C1s, and O1s peaks. The acquired data was converted to VAMAS format, further analyzed and deconvoluted using CasaXPS software.

Results and Discussion

Hydroxyl functionalized multi walled carbon nanotube (MWCNT-OH) was synthesized by electrophilic addition of chloroform and subsequent alkaline hydrolysis with alkaline methanol as illustrated in Figure 2. The essence of this modification is to make the MWCNT to undergo esterification reaction with an initiator for successful synthesis of ATRP macro-initiator.

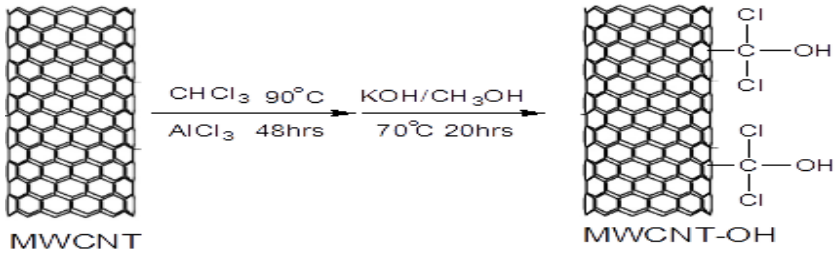

Figure 2: Synthesis of hydroxyl functionalized MWCNT

Figure 3 shows the FT-IR spectra of the functionalized MWCNT compares with the spectra of pristine MWCNT. As clearly evident, there was broad band absorption at 3475 cm^{-1} due to the free hydroxyl groups which was not observed on the pristine MWCNT spectra. Absorption due to C-Cl stretching was found at 759 cm^{-1}. The hydroxyl band from the spectra (b) (MWCNT-OH) indicates, a successful

introduction of OH group onto the MWCNT (Choi et al., 2005; Tagmatarchis et al., 2002; Tasis et al., 2006).

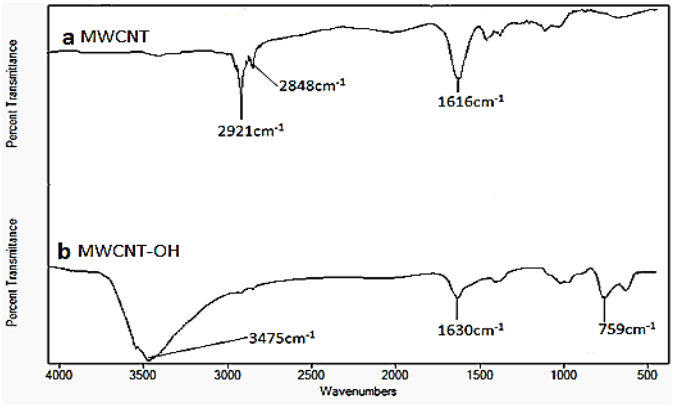

Figure 3: FT-IR Spectra of Hydroxyl Functionalized MWCNT

The esterification reaction between hydroxyl functionalized MWCNT and 2-bromoisobutyryl bromide in the presence of pyridine, followed by subsequent addition of distilled water at 0°C and chloroform with stirring yield the MWCNT-Br macro-initiator as represented in Figure 4.

Figure 5 represent the spectra of bromine terminated macro-initiator (MWCNT-Br) compare with that of hydroxyl functionalized MWCNT. From the spectrum of the macro-initiator appears at 2921 cm^{-1} for C-H stretching band aromatic, at 1735 cm^{-1} band due to C=O of aliphatic ester stretching it appeared too short due to shielding effect, band at 1614 cm^{-1} was for C=C aromatic from CNT, signal at 1111 cm^{-1} for C-O ester stretching, and band at 788 cm^{-1} was due to C-Br stretching for alkyl halide (Stuart).

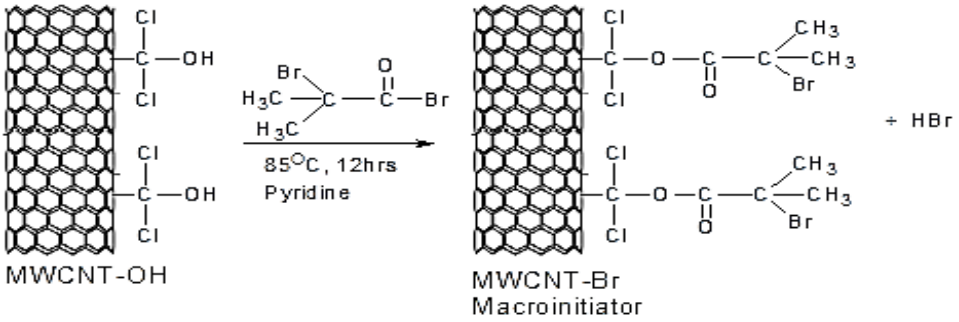

Figure 4: Synthesis of MWCNT-Br Macroinitiator from MWCNT-OH

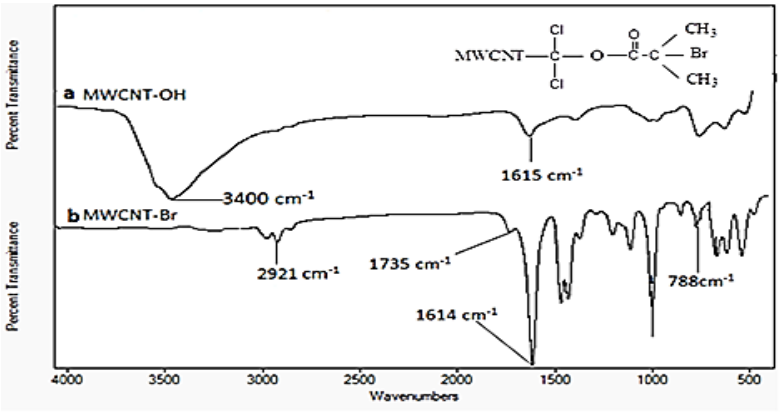

Figure 5: FT-IR Spectra of MWCNT-Br Macroinitiator

The MWCNT-Br macro-initiator was analyzed by 13C-solid NMR spectroscopy to confirm the ester linkage, -$C(CH_3)_2Br$, and C=C nuclei of MWCNT (Diniz & Tavares, 2004; Ibbett et al., 1992; Silvestri & Koenig, 1993; Souto-Maior et al., 2005). Figure 6 shows signals of 58.56, 80.44, 128, and 177.78 ppm which are attributed to –$C(CH_3)_2Br$, O-C-Cl, C=C, and C=O of ester respectively. From the results of the analysis, it covered all the major structural components of MWCNT-Br; hence, a successful synthesis of the macro-initiator.

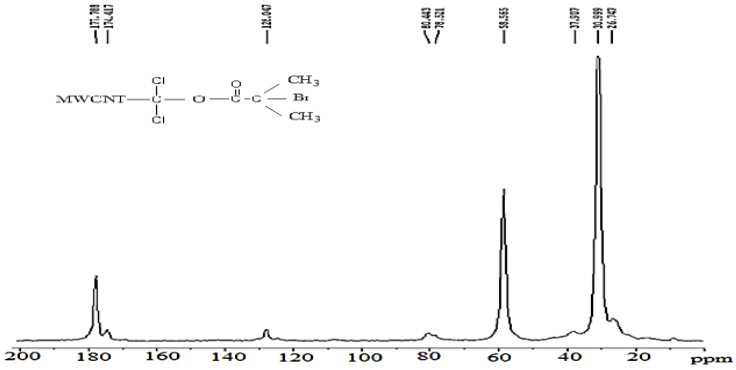

Figure 6: Solid-state[13] C-NMR Spectrum of MWCNT-Br

The aim of the XPS analysis of MWCNT-Br is to determine its surface chemistry. The high resolution XPS survey spectrum (see Figure 7) shows peaks at 288 and 531 eV for C1s and O1s respectively. Meanwhile, the high resolution C1s spectra in Figure 8 shows there are four fitted peaks in the main peak at 288.40, 289.1, 290.20, 290.80, and 294 eV corresponding to carbon links of C=C (MWCNT), C-Br, C-Cl, C-O (ester bridge), and O-C=O (ester carbonyl) respectively.

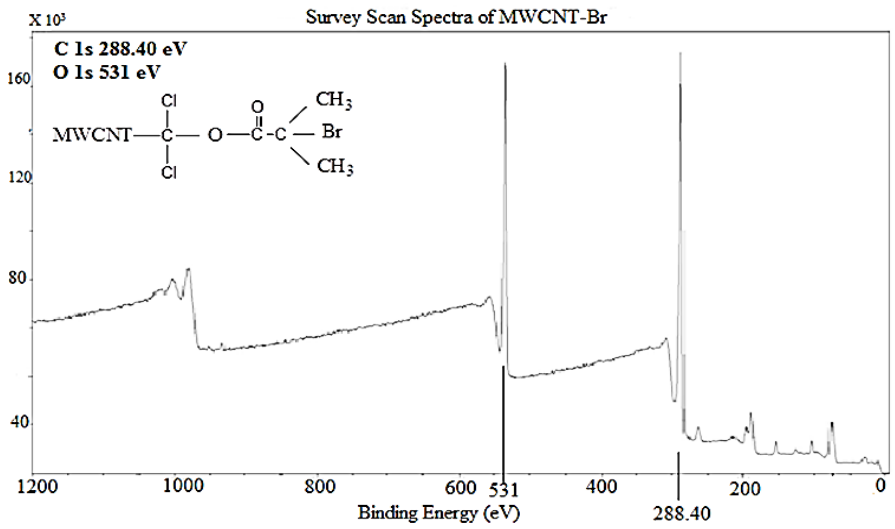

Figure 7: XPS Survey Spectrum of MWCNT-Br.

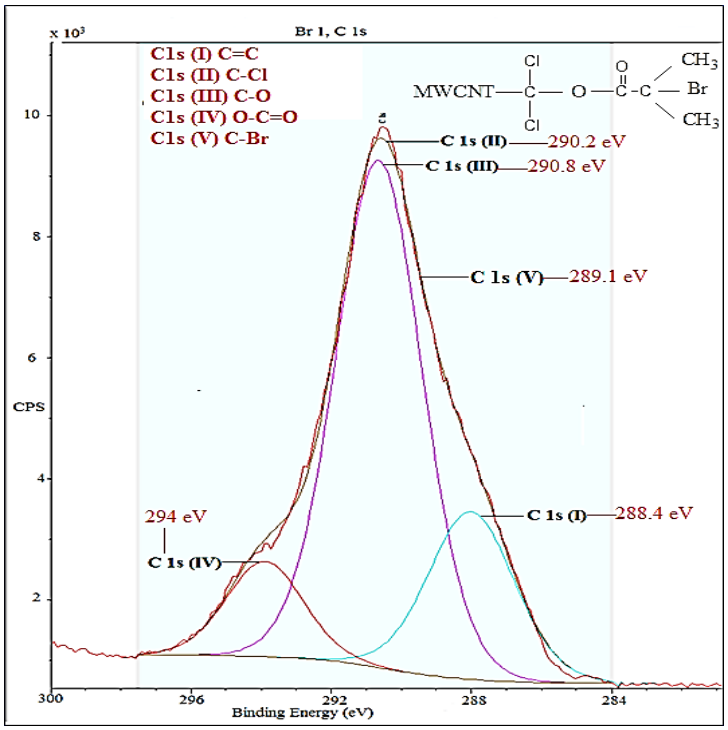

Figure 8: High-resolution XPS Spectra of C1s in different stents.

Conclusion

In conclusion, the bromine terminated MWCNT based macro-initiator of ATRP was successfully synthesized by esterification reaction. Henceforth, possess the potentials to simplify the covalent attachment of polymer moieties to the surface of the carbon nanotube by "*grafting from*" technique. It also provides, an opportunity of boosting the

applications of MWCNT especially in the field of nanocomposite.

References

Baskaran, D., Mays, J. W., & Bratcher, M. S. (2004). Polymer-Grafted Multiwalled Carbon Nanotubes through Surface-Initiated Polymerization. *Angewandte Chemie International Edition, 43*(16), 2138-2142.

Choi, J. H., Oh, S. B., Chang, J., Kim, I., Ha, C.-S., Kim, B. G., . . . Paik, H.-j. (2005). Graft Polymerization of Styrene from Single-Walled Carbon Nanotube using Atom Transfer Radical Polymerization. *Polymer Bulletin, 55*(3), 173-179.

De Falco, A., Fascio, M. L., Lamanna, M. E., Corcuera, M. A., Mondragon, I., Rubiolo, G. H., . . . Goyanes, S. (2009). Thermal treatment of the carbon nanotubes and their functionalization with styrene. *Physica B: Condensed Matter, 404*(18), 2780-2783.

Diniz, T. M. F. F., & Tavares, M. I. B. (2004). Solution and solid-state NMR investigation of poly(methyl methacrylate)/poly(vinyl pyrrolidone) blends. *Journal of Applied Polymer Science, 93*(1), 372-377.

Hong, C.-Y., You, Y.-Z., Wu, D., Liu, Y., & Pan, C.-Y. (2005). Multiwalled Carbon Nanotubes Grafted with Hyperbranched Polymer Shell via SCVP. *Macromolecules, 38*(7), 2606-2611.

Ibbett, R., Bucknall, D., & Higgins, J. S. (1992). Solid state 13C n.m.r. cross-polarization studies of a poly(methyl methacrylate)/solution chlorinated polyethylene blend. *Polymer, 33*(2), 423-425.

Iijima, S. (1991). Helical microtubules of graphitic carbon. *Nature, 354*(6348), 56-58.

Kong, H., Gao, C., & Yan, D. (2004a). Constructing amphiphilic polymer brushes on the convex surfaces of multi-walled carbon nanotubes by in situ atom transfer radical polymerization. *Journal of Materials Chemistry, 14*(9), 1401-1405.

Kong, H., Gao, C., & Yan, D. (2004b). Controlled functionalization of multiwalled carbon nanotubes by in situ atom transfer radical polymerization. *Journal of the American Chemical Society, 126*(2), 412-413.

Liu, P. (2005). Modifications of carbon nanotubes with polymers. *European Polymer Journal, 41*(11), 2693-2703.

Liu, Y.-L., & Chen, W.-H. (2007). Modification of Multiwall Carbon Nanotubes with Initiators and Macroinitiators of Atom Transfer Radical Polymerization. *Macromolecules, 40*(25), 8881-8886.

Matrab, T., Chancolon, J., L'hermite, M. M., Rouzaud, J.-N., Deniau, G., Boudou, J.-P., . . . Delamar, M. (2006). Atom transfer radical polymerization (ATRP) initiated by aryl diazonium salts: a new route for surface modification of multiwalled carbon nanotubes by tethered polymer chains. *Colloids and Surfaces A: Physicochemical and Engineering Aspects, 287*(1-3), 217-221.

Matyjaszewski Krzysztof , T. P. D. (2002). *Handbook of Radical Polymerization*. Canada: John Wiley and Sons,Inc., Hoboken.

Peng, K.-J., Wang, K.-H., Hsu, K.-Y., & Liu, Y.-L. (2015). Atom Transfer Radical Addition/Polymerization of Perfluorosulfonic Acid Polymer with the C–F Bonds as Reactive Sites. *ACS Macro Letters, 4*(2), 197-201.

Qin, S., Qin, D., Ford, W. T., Resasco, D. E., & Herrera, J. E. (2004). Polymer brushes on single-walled carbon nanotubes by atom transfer radical polymerization of n-butyl methacrylate. *Journal of the American Chemical Society, 126*(1), 170-176.

Silvestri, R. L., & Koenig, J. L. (1993). Applications of nuclear magnetic resonance spectrometry to solid polymers. *Analytica Chimica Acta, 283*(3), 997-1005.

Souto-Maior, R. M., Tavares, M. I. B., & Monteiro, E. E. (2005). Solid State 13C NMR Study of Methyl Methacrylate-Methacrylic Acid Copolymers. *Ann. Magn. Resson., 4*(3), 69-72.

Stuart, B. H. *Infrared Specroscopy: Fundamentals and Applications*. The Atrium, Southern Gate, Chichester, West Sussex, England.: John Wiley and Sons Ltd.

Tagmatarchis, N., Georgakilas, V., Prato, M., & Shinohara, H. (2002). Sidewall functionalization of single-walled carbon nanotubes through electrophilic addition. *Chemical Communications*(18), 2010-2011.

Tasis, D., Tagmatarchis, N., Bianco, A., & Prato, M. (2006). Chemistry of carbon nanotubes. *Journal of Chemical Review, 106*(3), 1105-1136.

Tsarevsky, N. V., & Jakubowski, W. (2011). Atom transfer radical polymerization of functional monomers employing Cu-based catalysts at low concentration: Polymerization of glycidyl methacrylate. *Journal of Polymer Science Part A: Polymer Chemistry, 49*(4), 918-925.

Wang, J.-S., & Matyjaszewski, K. (1995). Controlled/"Living" Radical Polymerization. Halogen Atom Transfer Radical Polymerization Promoted by a Cu(I)/Cu(II) Redox Process. *Macromolecules, 28*(23), 7901-7910.

Wu, H.-X., Tong, R., Qiu, X.-Q., Yang, H.-F., Lin, Y.-H., Cai, R.-F., & Qian, S.-X. (2007). Functionalization of multiwalled carbon nanotubes with polystyrene under atom transfer radical polymerization conditions. *Carbon, 45*(1), 152-159.

Nigerian Journal of Polymer Science and Technology, 2017, Vol. 12, pp 54-63

Received: 10 May 2018 Accepted: 13 October 2018

The Reinforcing Potentials of White Sand as Filler in Natural Rubber Vulcanizates.

‡‡E. Osabohien and N .O. Ojeifo.
Department of Chemistry, Delta State University, Abraka, Nigeria.

Abstract

Natural rubber with constant viscosity of 10, Standard Nigerian Rubber (SNR 10) was compounded with locally sourced white sand (WS) and standard silica (SS) as fillers. The WS was wet screened with a 75 µm stainless sieve and the screened sample was air-dried and pulverized for use as filler. The filler samples were characterized in terms of pH of aqueous slurry, loss on ignition, density, iodine adsorption number and moisture content. The cure characteristics, physico-mechanical and percentage swelling properties of the WS-SNR 10 in comparison with SS-SNR 10 vulcanizates were determined. The results showed that cure characteristics of WS-SNR 10 and SS-SNR 10 vulcanizates; scorch time, cure time and maximum torque increased as filler loading is increased. The tensile properties, tensile strength and modulus of WS-SNR 10 and SS-SNR 10 vulcanizates increased as filler loading increased to an optimum of 40 parts per hundred (phr) respectively, while elongation at break decreased as filler loading is increased. Abrasion resistance and hardness of WS-SNR 10 and SS-SNR 10 vulcanizates respectively increased to optimum level at 40 phr as filler loading is increased while compression set decreased as filler loading is increased. Percentage swelling in petroleum solvent is highest in gasoline, and lowest in diesel (gasoline>kerosene>diesel). The extent of reinforcement is in the order of SS-SNR 10 vulcanizates>WS-SNR 10 vulcanizates in cure characteristics, SS-SNR 10 vulcanizates>WS-SNR 10 vulcanizates in tensile-mechanical properties and SS-SNR 10 vulcanizates<WS-SNR 10 vulcanizates in percentage swelling properties.

Keywords: White sand, fillers, Natural rubber and reinforcement.

Introduction

Rubber manufacturing involves the addition to rubber many other materials called additives. These additives are to allow the rubber compounds to be processed satisfactorily and when vulcanized, help to improve the application properties of the rubber articles (Osabohien and Egboh,2007). Additives incorporated into rubber include; vulcanizing agents, accelerators, activators/retarders, anti-degradants, fillers, plasticizers and ancillary materials (Okoh, Osabohien and Egboh, 2014). The incorporation of these additives to the bulk properties of the raw polymer helps it to meet its service requirement.

Fillers are the second largest and one of the most important additives following the base polymers in rubber compounding. They help improve processability, physico-mechanical properties and reduce to a great extent the percentage swelling in petroleum solvents like gasoline, kerosene and diesel

‡‡ Department of Chemistry, Delta State University, Abraka, Nigeria (E. Osabohien, E-mail: eosabohien@delsu.edu.ng).

(Imanah, 2003; Okoh *et al.,* 2014). Research studies in the past have shown that without fillers, few polymers would have been adequate other than mere trivial applications (Boonstra, 1984; Hoffman, 1989; Okoh *et al.,* 2014; Osabohien, Okoh and Egboh, 2015). However, fillers can be classified as either reinforcing or non-reinforcing (Osabohien and Egboh, 2007; Okoh *et al.,* 2014). Reinforcing filler is one which increases the tensile strength, hardness and abrasion resistance of the rubber sample. Non-reinforcing fillers may not increase strength properties but can increase hardness, bulk and ultimately reduce cost of the rubber product (Osabohien, Okoh, Imanah and Egboh, 2011; Okoh *et al.,* 2014). The finer the particle size, the larger the surface area and the more reinforcing the filler is; commonly used reinforcing fillers are carbon black and silica. The non-reinforcing fillers are usually applied as extender or diluents e.g. $CaCO_3$ (whitings) and China clay. The present study evaluates the reinforcing potentials of white sand as filler in natural rubber vulcanizates in comparison with standard silica filler.

Materials and Methods

Materials: The fillers used for this study include standard silica which was bought from Onitsha main market, Anambra State, Nigeria. The white sand was sourced locally from Ethiope River, Abraka, Delta State, Nigeria. The filler characteristics were determined in the Department of Chemistry, Delta State University, Abraka, Nigeria, and the central laboratory of Obafemi Awolowo University, Ile-Ife, Nigeria. The SNR 10 was obtained from the Department of Polymer Technology, Auchi Polytechnic, Auchi, Edo State, Nigeria. The compounding of SNR 10 was carried out at the Department of Polymer Technology Workshop, Auchi Polytechnic, Auchi, Edo State, Nigeria and the rubber vulcanizate testing were performed at the Rubber Research Institute of Nigeria (RRIN), Iyanomo, Edo State, Nigeria. Petroleum solvents (Kerosene, Gasoline and Diesel) used for percentage swelling were purchased commercially and were used as received.

Methods: White sand was wet screened using 75µm stainless sieve. The wet screened sample was air-dried, pulverized and oven dried to a constant mass at 105 ^oC to obtain fine particle white sand used as filler.

Characterization of fillers

The fillers, WS and SS were characterized in terms of pH of aqueous slurry, density, moisture content, loss on ignition and iodine adsorption number using standard test methods (ASTM D1509, 1983; ASTM D1510, 1983; ASTM D1512, 1983; Okoh *et al.,* 2014). The fillers were then loaded into the rubber matrix respectively ranging from 0 – 50 phr.

$$\text{Density} = \frac{\text{Weight of Sample}}{\text{Volume of Cylinder}}$$

$$\% \text{ moisture content} = W_1 - W_2 \text{ X } 100$$

Where W_1 is the weight of crucible plus weight of sample before oven drying at 110 ^oC and W_2 is the weight of crucible and sample after drying for 1 hr.

% Loss on Ignition = Initial Weight of Sample – Final Weight of Sample after muffle furnace heating at 1000 ^oC X 100 for 30 minutes.

Compounding and curing of WS – SNR 10 and SS – SNR 10 mixes

Applying known methods (Blow and Hepburn, 1982; Osabohien, 2010; Okoh *et al.,* 2014), standard Nigerian rubber (SNR 10) was compounded using the two-roll mill after the nip clearance has been used to adjust the distance between the front roll and back roll of the two-roll mill which rotates in opposite direction. The cure characteristics (scorch time, cure time and maximum torque) were measured using Alpha Technologies

Rheometer ODR 2000 while curing of the test samples was carried out using electric compression moulding machine (Double day light press) at a temperature of 160 ^{o}C for 15 minutes.

Table 1: Recipe for formulation of WS – SNR 10 and SS – SNR 10 compounds

Ingredients	Quantity (phr)
Natural Rubber (SNR 10)	100.0
Zinc Oxide	4.0
Stearic acid	2.0
Fillers *	0.0 – 50.0
processing oil	2.0
TMQ^{+}	1.5
CBS^{++}	2.0
Sulphur	1.5

+ TMQ = 2,2,4-trimethyl– 1,2dihydroquinoline
++ CBS = N-cyclohexylbenzothiazylsulphenamide
* Filler Content: Filler load of 0, 10, 20, 30, 40 and 50 phr were used for this work.

Determination of the physico-mechanical and percentage swelling properties of vulcanizates

Tensile properties (tensile strength, elongation at break and modulus) of the vulcanizates were measured with Zwick/Roelltensometer (model Z005) using the dumb bell-shaped test pieces following standard test methods (ASTM D1415, 1983; ASTM D1638-99, 1983; Okoh *et al.*, 2014). The Monsanto Duratron 2000 was used to determine hardness of the vulcanizates while abrasion resistance and compression set were determined by Wallace test equipment, C85015/1 and C88053/1 respectively (BS, 1982).

Percentage swelling properties of the natural rubber vulcanizates in petroleum solvents such as gasoline, diesel and kerosene were determined by using standard test method described in BS 903, A16 (BS, 1982; Sogbaike, Okiemen and Edojariogba, 2005; Osabohien and Egboh, 2007; Okoh *et al.*, 2014). The vulcanizates test samples were cut into square shaped, weighed and then immersed in plastic bottles containing the solvents. The plastic bottles were filled to cover the test samples with the solvents and were tightly covered and maintained at room temperature for 48 hrs. The test samples were removed, dried and re-weighed. The change in weight for each sample was expressed as percentage swelling deduced from the following equation 1.

$$\% \text{ swelling} = \frac{W_{2-W_1}}{W_1} \times 100 \ldots\ldots\ldots\ldots\ldots\ldots 1$$

Where W_1 and W_2 are the initial and final weights of the test samples before and after swelling respectively.

Results and Discussion

Results

Table 2 summarizes the physico-chemical properties of the fillers; white sand (WS) and standard silica (SS). The properties investigated include; loss on ignition, moisture content, pH, density, iodine adsorption number and estimated particle size distribution of the fillers. Table 3 showed the cure characteristics of the fillers. The cure times, scorch times and maximum torque of the filled rubber compounds were recorded.

Tables 4-6 showed the physico-mechanical properties of the SNR vulcanizates. The tensile strength, elongation at break, modulus, abrasion resistance,

hardness, compression set, % swelling in gasoline, diesel and kerosene were reported.

Table 2: Physico- chemical properties of the fillers

Parameters measured	**WS**	**SS**
Density (g/cm^3)	2.32	2.21
pH of aqueous slurry	4.70	5.20
% Loss on ignition @ 1000 ^oC	5.00	1.50
% Moisture content @ 110 ^oC	2.05	1.15
Particles size range (µm)	≤75	0.012-0.020
Iodine Adsorption Number (mg/g)	68.52	94.32

Table 3: Cure characteristics of compounded SNR 10 filled with WS and SS

% filler	**0**	**10**	**20**	**30**	**40**	**50**
Scorch time ts_2 (min)	5.20	6.42	6.58	6.89	7.10	7.42
	(5.20)*	(6.57)*	(6.68)*	(6.92)*	(7.15)*	(7.45)*
Cure time t_{90} (min)	7.50	8.18	9.10	9.18	9.20	9.30
	(7.50)*	(8.37)*	(9.25)*	(9.37)*	(9.40)*	(9.47)*
Max torque (kg-cm)	6.42	7.63	7.87	8.44	8.75	8.94
	(6.42)*	(8.53)*	(8.99)*	(9.38)*	(10.54)*	(11.12)*

* Values in parenthesis are for SNR 10 filled with standard silica (SS)

Table 4: Tensile properties of SNR 10 vulcanizates filled with WS and SS

% filler	**0**	**10**	**20**	**30**	**40**	**50**
Tensile Strength (Mpa)	9.80	19.00	22.20	23.20	23.40	21.70
	(9.80)*	(22.70)*	(25.90)*	(28.60)*	(31.80)*	(30.40)*
Modulus M100 (Mpa)	0.40	0.60	0.70	0.70	0.70	0.50
	(0.40)*	(0.70)*	(0.80)*	(0.90)*	(1.02)*	(1.01)*
Elongation at break (%)	1621	1591	1514	1451	1408	1385
	(1621)*	(1619)*	(1610)*	(1573)*	(1525)*	(1513)*

* Values in parenthesis are for SNR 10 filled with standard silica (SS)

Table 5: Physico-mechanical properties of SNR 10 vulcanizates filled with WS and SS

% filler	0	10	20	30	40	50
Abrasion resistance (%)	30.33	33.40	33.66	34.27	34.83	34.59
	(30.33)*	(33.56)*	(33.62)*	(36.55)*	(37.25)*	(36.65)*
Hardness (IRHD)	40.00	46.00	49.00	54.00	57.00	56.00
	(40.00)*	(47.00)*	(50.00)*	(55.00)*	(60.00)*	(59.00)*
Compression set (%)	16.96	14.69	13.68	12.50	12.15	11.73
	(16.96)*	(15.25)*	(14.70)*	(13.96)*	(12.55)*	(12.37)*

* Values in parenthesis are for SNR 10 filled with standard silica (SS)

Table 6: % swelling in petroleum solvents of SNR 10 compounds filled with WS and SS

% Filler Loading	Gasoline	Kerosene	Diesel
0	305.50	260.61	210.55
	(305.50)*	(260.61)*	(210.55)*
10	298.09	244.13	193.68
	(295.45)*	(222.11)*	(171.92)*
20	290.27	230.96	184.68
	(285.10)*	(220.18)*	(169.12)*
30	282.11	221.21	170.09
	(280.69)*	(213.37)*	(158.73)*
40	278.71	212.15	162.74
	(270.25)*	(209.27)*	(155.52)*
50	270.60	209.42	151.62
	(265.18)*	(201.13)*	(150.32)*

*Values in parenthesis represent % swelling in petroleum solvents of SNR 10 filled with SS

Discussion

Physico-chemical properties of the fillers

The results in Table 2 showed that WS filler has higher moisture content than SS filler. The presence of moisture in fillers have been shown to influence the mechanical properties of rubber vulcanizates and this reduces or weakens the polymer - filler matrix adhesion during compounding (Wang, Ponigrahi, Tabil, Crerar, Powell, Kolybaba and Sokhansanj, 2003; Puglia, Biaglotti and Kenny, 2005). The SS aqueous slurry has higher pH value than that of WS. Acidic fillers have been shown to retard cure rates of vulcanizates (Iyasele and Okeimen, 2004) and also have an important influence on the strength properties of vulcanizates (Voet, Morawski and Donnet, 1979; Okoh *et al.*, 2014). Similar observations have been made by previous researchers who reported that acidic fillers retard or reduce cure rates while alkaline fillers increase or enhance cure rates of vulcanizates (Osabohien *et al.*, 2011;

Aguele, Madufor and Adekunle, 2014). The increase in cure and scorch times may have been due to the acidic nature of the fillers under study (Table 3), this is in agreement with earlier observations (Osabohien and Egboh, 2006; Okoh *et al.,* 2014).The loss on ignition at 1000 ^{o}C was higher in WS than SS filler. It is evident that the WS filler contains a little more combustible materials which may be attributed to its natural source (Table 2). Loss on ignition is a measure of the amount of combustible or organic materials present in the sample (Osabohien and Egboh, 2006; Okoh *et al.,* 2014).

However, the result shows that SS filler has higher iodine adsorption number, meaning finer particle sizes and a lighter density (Table 2). Iodine adsorption number is a measure of surface area of fillers. The higher iodine adsorption number is, the higher the surface area, the finer the particle sizes of the filler and the greater the reinforcing potential (Boonstra, 1982; Hepburn, 1984). Surface area of a filler is an important factor influencing the physico-mechanical properties of fillers, hence the larger the surface area, the greater the filler – rubber interactions, implying a higher reinforcing potential (Imanah, 2003; Yamashita and Tanaka, 2002; Osabohien and Egboh, 2006; Okoh *et al.,* 2014). Density of fillers influences the weight property of such filler on rubber. Hence, the SNR 10 – SS compounds will present a lighter rubber article compared to that of SNR 10– WS mixes. This is because the density of SS is less than WS (Table 2).

Cure characteristics of SNR 10 compound

Table 3 shows the result of cure characteristics of the SNR 10 compounds filled with WS and SS at different filler loadings. The scorch and cure times and maximum torque for both WS and SS filled SNR 10 increased with increasing filler loading. This implies cure retardation by both fillers. However, the cure characteristics of the unfilled systems of SNR 10 compounds were lower in terms of scorch time, cure time and maximum torque values than their filled system. These observations agree with previous reports on acidic fillers (Osabohien and Egboh, 2006). It has been known that acidic fillers retard cure. The basis of curing is to form chemical crosslinks which convert the long linear polymer chains into a three-dimensional network structure under pressure by the action of heat to form products with improved elasticity and substantial increase in hardness and modulus (Asore, 2000).

Increase in maximum torques as filler loading is increased shows a good filler – polymer (SNR 10) matrix interaction and a good interfacial bonding between the filler and rubber matrix to form cross-links that can restrict the free mobility of the polymer chains (Wang *et al.,* 2003; Puglia *et al.,* 2005; Okoh *et al.,* 2014). This is an indication of reinforcement. Maximum torque value of SS filler is higher than that of WS filler and this could be related to the particle sizes of the fillers and their surface areas. Because SS has finer particle sizes (Table 2), the rubber – SS interaction is expected to be higher and the higher the reinforcing ability.

Physico-mechanical properties of SNR 10 vulcanizates

The results in Tables 4-6 summarize the physico-mechanical properties of SNR 10 vulcanizates filled separately with WS and SS fillers at different filler loadings. The tensile properties are the measure of the ability of a polymeric material to withstand forces which can pull it apart as a result of applied strain and also to determine the extent the material can stretch before breaking (Wang *et al.,* 2003). The results however showed that the tensile strength and modulus at 100% strain increased with increase in filler loading to optimum level of 40 phr. The increase in tensile strength may be due to small particle size (large surface area) of

filler, enabling possible filler-matrix interaction. Previous research reported by (Yamashita and Tanaka, 2002; Osabohien and Egboh, 2007) postulated that no significant reinforcement would occur if there was no good interaction between the filler and the polymer (rubber) even with increasing addition of fillers. The decrease in tensile strength beyond 40 phr loading may be due to the fact that there was not enough polymer matrix to hold filler particles together. Ishak and Bakar, 1995, reported that reduction in the tensile strength may be due to agglomeration of the filler particles to form a domain that acts like a foreign body or simply the result of physical contact between adjacent aggregates. There was a phase change here which is referred to as phase inversion, and it is explained as a dilution effect due to diminishing volume fraction of the polymer in the vulcanizate, and also due to agglomeration of the filler particles at higher loads (Boonstra, 1984).

However, the results revealed that WS filler showed good reinforcing potential though inferior to SS filler in terms of tensile strength, modulus at 100% strain, hardness and abrasion resistance. The elongation at break of both WS and SS – filled SNR decreased with increase in filler content. This may be due to the restriction to free mobility of the macromolecular chains by the filler particles and thus increase in resistance to stretch on the application of strain. Similar explanation has been reported by Okoh *et al.*, 2014 where the resistance to stretch on the application of strain may be due to strong interactive forces between the rubber matrix and the filler particles.

The abrasion resistance and hardness increased to optimum at 40 phr of filler, while the compression set decreased with increasing filler load in both vulcanizates. Similar observations have been reported by (Imanah, 2003; Okoh *et al.,* 2014; Osabohien *et al.,* 2015). This is also an evidence of reinforcement by the fillers. But the increases were found to be more with the SS – SNR 10 vulcanizates. This may be attributed to the finer (smaller particle) sizes of SS filler as compared to WS (Table 2).

Percentage swelling in the vulcanizates decreased with increase in filler loading for all petroleum solvents used. Transport of small molecules through a polymer membrane occurs due to random molecular motion of each molecule; hence the driving force behind the transport process which involves diffusion, sorption and permeation is the concentration difference between the two phases – solvent and polymer phases (Soney and Sabu, 2001). Previous researchers argued that when a cross-linked polymer is brought into contact with a solvent, a certain amount is absorbed to an extent which is determined by the molecular weight of the solvent and the degree of cross-linking in the polymer (Okeimen and Imanah, 2005; Osabohien *et al.,* 2011). According to (Mathew, Joseph and Joseph, 2006), low molecular size of solventsenables it to diffuse faster into polymervulcanizates; hence increasing swelling. There is report that as the concentration of filler particles increases in the rubber matrix, more obstacles/barriers are created to the diffusing molecules and thus reduces the amount of solvent that penetrate the vulcanizate (Okeimen and Imanah, 2005).

The molecular size of solvents also may influence the diffusion rate of solvent into the polymer matrix. The smaller the molecular size of solvent, the higher the diffusion into the rubber matrix and the higher the swelling may be. This may be the reason why the order of decreasing swelling of vulcanizates in the solvents is gasoline>kerosene>diesel (Table 6). Similar observations were made in earlier works (George and Thomas, 2001; Okeimen and Imanah, 2005; Osabohien *et al.,* 2011).

The diffusion also and transport of solvents in filled polymers depend on the nature of fillers, the degree of adhesion and its compatibility with the polymer matrix (Soney and Sabu, 2001). Hence, nature of cross-links is a factor of swelling in vulcanizates immersed in petroleum solvents. Better cross-links between filler and polymer matrix, gives higher resistance to swelling of the vulcanizates in petroleum solvents (George and Thomas, 2001). And because the SS- filled vulcanizates showed better filler – rubber cross-links, the less swelling in the solvents observed (Table 6).

Conclusion

This work is a contribution to the search for environmentally friendly natural fillers which can substitute/suppliment the highly used reinforcing carbon black and silica fillers in polymer and automobile manufacturing industries. The findings revealed that WS filler showed a reinforcing potential though inferior to that of SS filler when compounded with SNR 10. The superiority of SS filled SNR 10 may be due to the finer particle size and the larger surface area of SS. It is therefore recommended that improved pulverization and screening methods be applied in preparing the WS filler to meet up with that of the synthetic silica filler for rubber compounding.

References

Aguele, F. O., Madufor, C. I. and Adekunle, K. F. (2014). Comparative study of physical properties of polymer composites reinforced with uncarbonised and carbonized coir. *Open Journal of Polymer Chemistry*, **4**: 73 – 82.

Asore, J. E. (2000). An Introduction to Rubber Technology, Josey Books Limited, Benin City, Edo State. Pp. 20-130.

ASTM D1415 (1983). Determination of Swelling Resistance of Rubber Materials. Standard African Rubber Manual, **2**: 1-10.

ASTM D1509 (1983). Standard Method of Testing Moisture Content. American Society for Testing and Materials: West Conshohocken, PA.

ASTM D1510 (1983). Standard Method of Testing Iodine Adsorption Number. American Society for Testing and Materials: West Conshohocken, PA.

ASTM D1512 (1983). Standard Method of Testing pH, 1-10. American Society for Testing and Materials: West Conshohocken, PA.

ASTM D1638-99 (1983). Standard Test Method for Tensile Properties of Elastomers. American Society for Testing and Materials: West Conshohocken, PA.

Blow, C. M. and Hepburn, C. (1982). Rubber Technology and Manufacture, 2nd edition, Butterworth Scientific, London, Pp 300 – 344.

Bonstra, B. B. (1982). Reinforcement by fillers in C. M. Blow and C. Hepburn (Eds). Rubber Technology and Manufacture. 2nd ed, Butterworth Scientific, London, Pp. 227-261.

Boonstra, B. B. (1984). Reinforcement by filler. In rubber technology (2nd edn) morton M(ed). Van Nosteand Co.: New York; Pp. 51 – 108.

BS 1982. British standard methods of testing vulcanized Rubber; British Standard Institution (BSI), London, BS 903-part A 9 – 16.

George, S. C and Thomas, S. (2001). Transport Phenomena through polymeric systems. *Progress in Polymer Science*, **26**(6): 985-1017.

Hepburn, C. (1984). Filler reinforcement of rubber. *Plastics and Rubber International,* **9**:11-13.

Hoffman, W. (1989). Rubber Technology Handbook, Hanswer/Gardener Publisher Incorporated, Ohio, U.S.A, Pp 217-351.

Imanah, J. E. (2003). Studies in the utilization of cocoa pod husk and rubber seed shell as fillers in natural rubber compound. A thesis written in the department of Chemistry and submitted to the school of post graduate studies in partial fulfillment of the requirement for the award of degree Doctor of Philosophy of the University of Benin.

Ishak, Z. A. M. and Bakar, A. A. (1995). An investigation on the potential of rice husk ash as filler for epoxidized natural rubber. *European Polymer Journal,* **31** (3): 259 – 269.

Iyasele, J. U. and Okielmen F. E. (2004). Cure characteristics and Rheological Properties of Mellon Seed Shell-filled Natural Rubber, Proceedings of 27th International conference of Chem. Soc. Of Nig. Benin City, 272-277.

Mathew, L., Joseph, K. U. and Joseph, R. (2006) Swelling Behaviour of Isora/Natural rubber composition in oil used in automobiles. *Bulletin of Materials Science,* **29**(1): 91 – 99.

Okeimen, F. E and Imanah, J. E. (2005). Physico- mechanical properties and equilibrium swelling properties of Natural rubber filled with rubber seed shell carbon. *Journal Polymer Material,* **22**: 409-416.

Okoh, B. E., Osabohien, E. and Egboh, S. H. O (2014). The reinforcing potentials of Velvet tamarind seed shell as filler in natural rubber compounds. *International Journal of Biological and Chemical Sciences,* **8**(5): 2367 – 2376.

Osabohien, E. (2010). Potential of carbonized cherry seed shell as filler in Natural rubber vulcanizates. *Journal of Polymer Materials,* **27**(4): 379 – 389.

Osabohien, E. and Egboh, S. H. O (2007). Characterization of Red earth as filler in natural rubber compounds. *Journal of Chemical Society Nigeria,* **32**(1): 96 – 101.

Osabohien, E. and Egboh, S. H. O. (2006). An Investigation on the Reinforcing Potential of Red Earth as Filler for Natural Rubber Compounds. *Journal of Applied Polymer Science,* **105**: 515-520.

Osabohien, E., Okoh, B. E., Imanah, J. E and Egboh, S. H. O. (2011). The Effects of Epoxidation on the Potentials of Red earth- Natural rubber composites. *Nigerian Journal of Polymer Science and Technology,* **7**(1): 85-100.

Osabohien, E; Okoh, B.E. and Egboh, S.H.O. (2015). *Calamus deerratus* fibre reinforced natural rubber vulcanizates. *International Journal of Biological and Chemical Sciences,* **9**(2): 1094 – 1106.

Puglia, D., Biaglotti, J. Kenny J. M. (2005). Application of Natural Reinforcements in composite materials for Automotive Industry. *Journal of Natural Fibre,* **3**:23 – 65.

Sogbaike, O. E., Okiemen, F. E., Edojariogba, P. O. (2005). Effect of substitution of N330 carbon black with carbonized plantain peels on cure characteristics, physic-mechanical and swelling properties of Natural Rubber vulcanizates. *Chemical Technology Journal,* **1**: 24 – 29

Soney, C. G and Sabu, T. (2001). Transport phenomena through polymeric systems. *Progress in Polymer Science,* **26**: 985-1017.

Voet, A. Morawski, J. C. and Donnet, J. B. (1977). Reinforcement of elastomers by silica. *Rubber Chemistry and Technology*, **50**(2): 342-355.

Wang, B., Ponigrahi, S., Tabil, L. Crerar, W Powell, T. Kolybaba, M. and Sokhansanj, S. (2003) flax fibre reinforced thermoplastic composites proper presented at the 2003 CSAE/ASAE Annual Int. meeting, Furgo, USA, Oct. (3 – 4): 1 – 14.

YamashitanY. and Tanaka, A. (2002). Mechaniclproperties of rubber reinforced with rice husk charcoal. 161th ACS Rubber Division, Spring Technical Meeting. Available at http://www.mat.usp.ac.jp/polymer-composite/yamashitaEPROC.html

Nigerian Journal of Polymer Science and Technology, 2017, Vol. 12, pp 64-74

Received: 10 May 2018 Accepted: 13 October 2018

UTILIZATION OF WASTE GLASS POWDER AS A POZZOLANIC MATERIAL FOR PARTIAL REPLACEMENT OF CEMENT IN CONCRETE.

GAMBO H.I[1*], MAMZA P.A.P.[1] AND GONAH C.M.[2]

[1]Department of Chemistry, Ahmadu Bello University, Zaria, Kaduna, Nigeria.
[2]Department of Glass and Silicate Technology, Ahmadu Bello University, Zaria, Kaduna, Nigeria.

* Corresponding Author: **E-mail:**habibuisari@gmail.com **Phone:** 08039747422

Abstract

The utilization of glass waste powder as cement additives for partial replacement of cement in concrete could be an important step toward the development of sustainable infrastructure systems especially when it's used as a pozzolanic material. When waste glass particles are ball-milled to micro size powder, it is going to undergo pozzolanic reactions with cement hydrates, forming secondary Calcium Silicate Hydrate. This research looked at the chemical analysis using X-Ray fluorescence technique and found minor differences in the chemical composition of soda-lime silicate and borosilicate waste glass. The microstructural characterization was also carried out using Scanning Electron Microscope and X-Ray Diffraction to characterize the concrete samples. It was found that the morphology of concrete samples modified with waste glass powder (10%, and 20%) was denser than the control sample (0%). Also, XRD results indicated that the intensity of the peaks, in particular of portlandite, is significantly reduced in the 10% waste glass sample than the control (10% of portlandite in the control, 2% of portlandite in 10% and 5% of portlandite in 20% waste glass replacement). Various compositions of the samples (Control 0%, 2.5%, 5.0%, 7.5%, 10%, 12.5%, 15%, 17.5% and 20%) of concrete cube and cylinder samples were prepared and tested for strength at 7, 14 and 28 days of curing. The compressive strength test results of the control and the 10% waste glass replacement were 20.95 N/mm^2, 16.44N/mm^2 for 7, 26.52 N/mm^2, 24.14 N/mm^2 14, and 31.38 N/mm^2, 28.82 N/mm^{2}28 days respectively. The tensile strength test results of the control and the 10% waste glass replacement were 2.08 N/mm^2, 1.65N/mm^2 for 7, 2.65N/mm^2 , 2.41 N/mm^2 14, and 3.13N/mm^2, 2.89N/mm^2 28 days respectively. It can be concluded that all the samples can be used for structural purposes, this is because all the samples (except for 2.5% replacement which had 23.12 N/mm^2) which was less than the maximum strength specified by ASTM 24.2 N/mm^2 at 28 days.

Keywords: compressive strength, scanning electron microscope, tensile strength, X-Ray diffraction, X-Ray fluorescence,

INTRODUCTION

Concrete is a homogeneous mixture of aggregates, water, and cement; and also ordinary Portland cement production is associated with high energy demands, the consumption of non-renewable prime materials and the emission of greenhouse gases (essentially CO_2) (Szabo *et al.*,2006).Today's global warming and environmental devastation have become manifested harms in recent years.There is a serious concern about environmental issues, and a switchover from the mass-waste and mass production society of the past to a zero-emanation society is now viewed as significant studies in recent years (Mane and Mane, 2012).

The term "sustainable development" was coined to mean the balance between technological development and conservation of the environment. Ever since, in pursuit of such a balance, the cement industry has been seeking ways to minimize the adverse side effects of its activity (Mahasenan *et al.*,2003).

Glasses of the family SiO_2–CaO–Na_2O take a major share of the total solid wastes disposed worldwide. As glass is not biodegradable, landfilling does not provide the most environmentally friendly solution; so recycling turns out a better alternative (Nunes *et al.,* 2013). Waste glass is a promising alternative cementitious material that requires relatively minor processing infrastructure to make it useful and a lot number of studies have examined the use of waste glass in cement and concrete (Caijun and Keren, 2007), such as a raw material in the manufacture of PC, as an aggregate, inert filler or as partial Portland cement replacement (Nunes *et al.,* 2013). Oliveira *et al.,*(2013), reported that mortars with 10–20% incorporation of fine glass as filler, increased the flexural strength and compressive strength by 29–86% and 31–91% respectively, relative to the conventional mortar. Schwarz and Neithalath (2008), studied the influence of fine glass powder as replacement of Portland cement, they noted that the use of 5–20% of glass did not accelerate the setting or increase the early age strength of cement pastes; however, the glass powder exhibited a pozzolanicity similar or greater than that of fly ash.

The addition of replacement materials to Portland cement brings additional complexity to the chemical reactions developed during the hydration of the composite cements. The dominant product of these reactions is C–S–H gel, which is principally responsible for the mechanical properties of the hydrated cement. C–S–H gel is generated by the interaction of the replacement materials with portlandite, CH, liberated during the hydration of the alite and belite present in the cement (Taylor, 1997).
This study aimed at overcoming the problem of glass waste that is generated from human activities, by determining the addition of borosilicate and soda-lime silicate waste glass as to improve the properties of concrete and their suitability in concrete production. This is to reduce the quantity of un-recycled glass waste, which has been suggested to partially replace cement with waste glass and reduce problems associated with cement manufacture.

MATERIALS AND METHODS

Materials

The materials used in this research include the following: Ordinary Portland cement, fine aggregate, coarse aggregate, water sealant cement, soda-lime silicate, borosilicate waste glass powder and water.

Cement

Ordinary Portland cement was used for the experimental work (OPC, Dangote Brand) conforming to the requirement of BS EN 1260- (2013).

Borosilicate Glass and Soda-lime Silicate Glass wastes

These two glass wastes were obtained from damaged glass, windows, doors and fluorescence waste glass. The glasses were cleaned in water and dried under sun, they were then ground in a ball milling machine. The ground samples were then sieved with 75µm sieve size, in order to eliminate particles that were larger than 75µm. The pulverizedsoda-lme silicate and borosilicate glass samples were then blend together (ratio of 1:1) BS 1881-122:(1983).

Fine Aggregate

The fine aggregate used was natural sand. It was sieved with a 4.75mm BS sieve so as to

remove impurities and larger aggregates. The fine aggregate was obtained from nearby river (ABU Dam). It complies with provisions of BS EN 1260- (2013).

Coarse Aggregate

The coarse aggregates used were crushed gravels which were obtained from single quarry. It is in conformity with the requirement of BS EN 1260- (2013).

Water

The water that was used for mixing the concrete was clean fresh tap water free from injurious oils, chemicals and vegetable matters or other impurities complying with the provisions of BS EN 1008- (2002).

Methods

Production of Concrete samples

Mixing and casting of the concrete samples
The constituent materials required for each sample were measured and weighed on a digital weighing balance i.e cement, sand and aggregate, (borosilicate and soda-lime silicate glass powder) which entails the use of Building Research Establishment (BRE) method of mix design 1:2:4 and water-cement ration of 0.6. The proportion of each constituents were used in the production of concrete specimen using mixing machine, the fresh concrete was casted into 100mm x 100 mm x 100 mm moulds in two layers and was compacted manually by giving it 25 blows with a tapping rod in order to achieve smooth and level compaction for each sample BS 1881 (1996).

i. Curing of Samples

Samples were allowed to set for 24hours before demoulding and immersion in a pool of water tank for 7days, 14 days and 28 days BS 1881-122:(1983).

ii. Concrete Specimens Production

Nine different specimens were produced and tested at various ages of (7, 14 and 28 days). Various compositions of the samples (0%, 2.5%, 5.0%, 7.5%, 10%, 12.5%, 15%, 17.5% and 20%) with specimen A labelled as the control, specimen B samples replaced with borosilicate and soda-lime glass. The variation in the percentage replacement of cement with borosilicate and soda-lime silicate glass was to have a stronger basis for comparison. A total of 108 cubes were casted and 81 cylinders BS 1881-102:(1983).

RESULTS AND DISCUSSION

X-Ray fluorescence (XRF) Analysis

Table 1 shows the chemical composition of cement, soda-lime silicate and borosilicate glass detected in this research. The major oxides detected were combined proportion of silicon oxide (SiO_2), Aluminium oxide (Al_2O_3) and Iron oxide (Fe_2O_3) with percentage value of 73.202%,72.998%,0.411%, 0.201%,and 0.223%, 0.112% respectively. This result is similar to that reported by Novais *et al.*, (2016), except slight difference in the percentage composition of SiO_2 and Al_2O_3. This means that soda-lime silicate and borosilicate glass satisfy the requirement of ASTM C 618-2005.

Table 1:Chemical Composition of Cement, Soda-lime silicate Glass and Borosilicate Glass

Oxides	Percentage Composition (%) Cement	Borosilicate Glass	Soda-lime silicate Glass
Silica (SiO_2)	**20.211**	**72.998**	**73.202**
Aluminium (Al_2O_3)	**4.698**	**0.201**	**0.411**
Iron Oxide (Fe_2O_3)	**3.022**	**0.112**	**0.223**
Sodium Oxide (Na_2O)	**0.189**	**5.722**	**6.843**
Calcium Oxide (CaO)	**61.889**	**3.766**	**6.433**
Magnessium Oxide (MgO)	**2.619**	**0.723**	**1.269**
Potassium Oxide (K_2O)	**0.820**	**0.588**	**0.168**
Sulfur Oxide (SO_3)	**3.889**	**0.135**	**0.158**
Boron Oxide(B_2O_3)	------	**5.251**	------
Loss on Ignition (LOI)	**2.660**	**10.502**	**11.287**

(Gambo *et al.,* 2018)

Compressive Strength Test of Samples

Figure 1 shows the compressive strength of all the sample specimens at 7, 14 and 28 days respectively. The compressive strength test results of the control and the 10% waste glass replacement were 20.95 N/mm^2, 16.44N/mm^2 for 7 days, 26.52 N/mm^2, 24.14 N/mm^2 14 days, and 31.38 N/mm^2, 28.82 N/mm^2 28 days respectively. this can be attributed to the fact that strength increase at the early stage due to higher temperature during placing and setting. It can also be as a result of rapid hydration process in the paste therefore the conventional concrete develop high early strength at early age this is an agreement with the findings of (Utsevu and Taku, 2013 :Vignesh *et al.,* 2014) reported that waste glass powder blended cement concrete have lower strength than the control, at 14 days and 28 days the rate of strength development of the conventional concrete decrease significantly, the strength were 35.69 and 37.73N/mm^2.

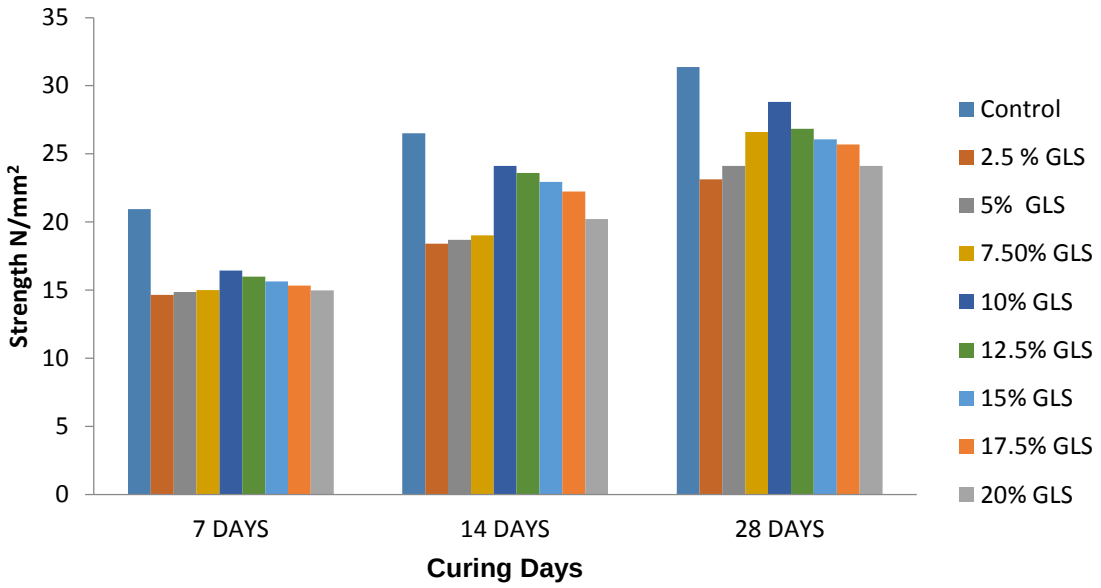

Figure 1: Compressive strength of samples cured in water.

Tensile Strength Test of Samples

Figure 2 shows the tensile strength of all the sample specimens at 7, 14 and 28 days respectively, The tensile strength test results 2.08 and 1.65, 2.65 and 2.41, 3.13 and 2.89 of the control and the 10% waste glass replacement were 2.08 N/mm^2, 1.65N/mm^2 for 7 days, 2.65N/mm^2 , 2.41 N/mm^2 for 14 days, and 3.13N/mm^2, 2.89N/mm^2 for 28 days respectively, this can be attributed to the fact that strength increase at the early stage due to higher temperature during placing and setting. It can also be as a result of rapid hydration process in the paste therefore the conventional concrete develop high early strength at early age this is an agreement with the findings of (Vijayakumar *et al.*, 2013: Madhangopal *et al.*, 2014), reported that waste glass powder blended cement concrete have lower strength than the control, at 14 days and 28 days.

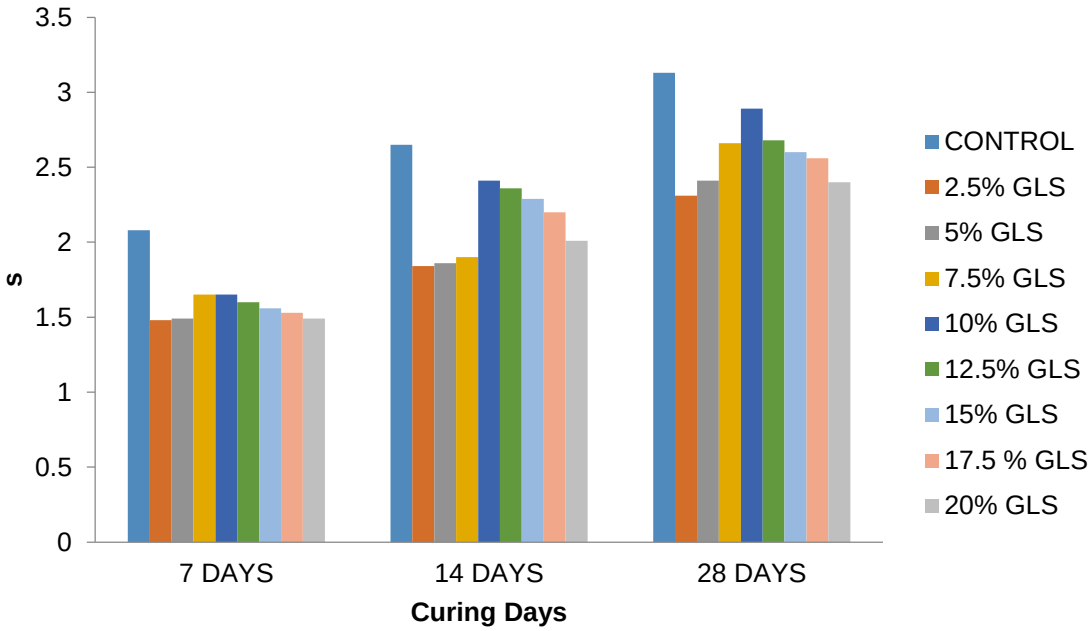

Figure 2: Tensile strength of samples cured in water.

X-Ray Diffraction (X-RD) Analysis

Figures 3, 4, and 5 show the XRD patterns of hydrated cement paste of the Control, 10% and 20% replacement after 28 day respectively.

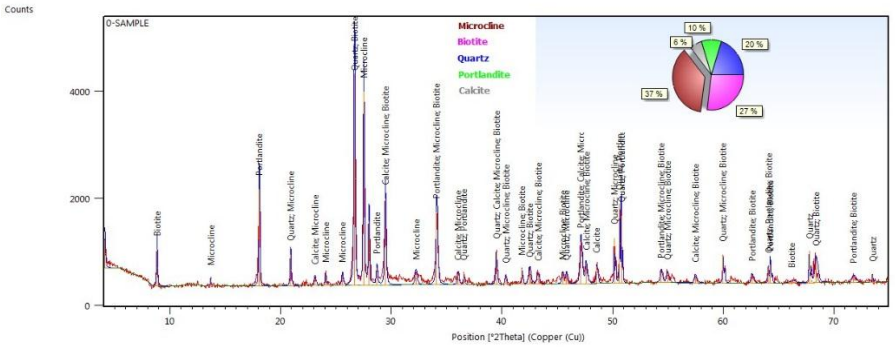

Figure 3: X-ray diffractograms pattern of the control 0% waste glass powder. It shows 10% of portlandite ($Ca(OH)_2$)

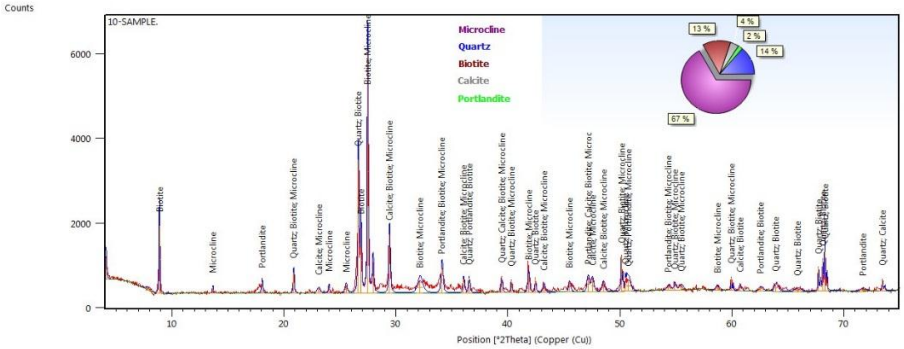

Figure 4: X-ray diffractograms pattern of the 10% waste glass powder. It shows 2% of portlandite($Ca(OH)_2$)

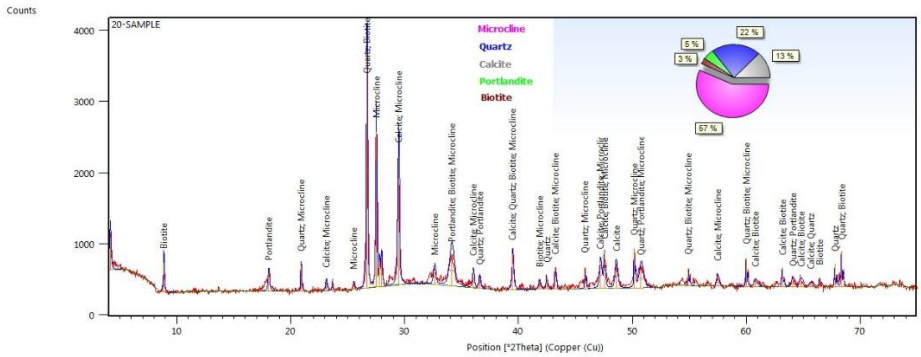

Figure 5: X-ray diffractograms pattern of the 20% waste glass powder. It shows 5% of portlandite ($Ca(OH)_2$).

Fig. 4. shows the X-ray diffractograms pattern of the 10% waste glass powder of concrete sample material cured at room temperature for 28 days, whose in the concrete mixture, several minerals present in the concrete mixture used as a precursor are identified, such as microline, quartz, biotite calcite and portlandite (67%, 14%, 13%, 4% and 2% respectively) type; It is observed that the intensity of the peaks, in particular of portlandite, is significantly reduced in the 10% waste glass sample than the control in fig. 3 (10% of porlandite in the Control and 2% of portlandite in 10% of waste glass replacement).

The reduction of diffraction lines intensity of portlandite is mainly due to the addition of replacement materials to Portland cement which brings additional complexity to the chemical reactions developed during the hydration of the composite cements. The dominant product of these reactions is C–S–H gel, which is principally responsible for the mechanical properties of the hydrated cement. C–S–H gel is generated by the interaction of the replacement materials with portlandite, CH, liberated during the hydration of the alite and belite present in the cement (Taylor, 1997). However, it can be seen from fig 5, that this reduction is also present in the 20%, of waste glass sample which was 5% reduction. This allow us to deduce that, in addition to hydration reactions of alite and belite, a partial dissolution of certain crystalline phases occurs; this is consistent with results reported by other authors for several types of precursors (Ahmari *et al.*, 2012). However, this decrease in intensity has also been attributed to the increase in the SiO_2/Na_2O ratio due to the presence of sodium silicate in the mixture (Komnitsas *et al.*, 2015). The small traces of portlandite ($Ca(OH)_2$) are attributed to the hydrated cement contained in the undissolved concrete mixture particles.

Scanning Electron Microscope (SEM) Analysis

Plates 1, 2, and 3 show the microstructure of the Control 0%, 10% and 20% waste glass powder replacement respectively.

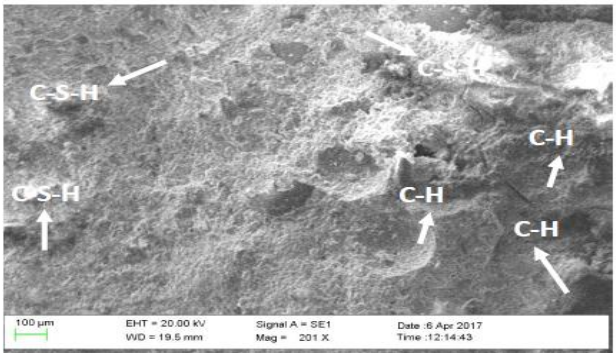

Plate 1: A SEM micrograph of control 0% waste glass powder. CH = $Ca(OH)_2$ C-S-H = Calcium Silicate Hydrate gel

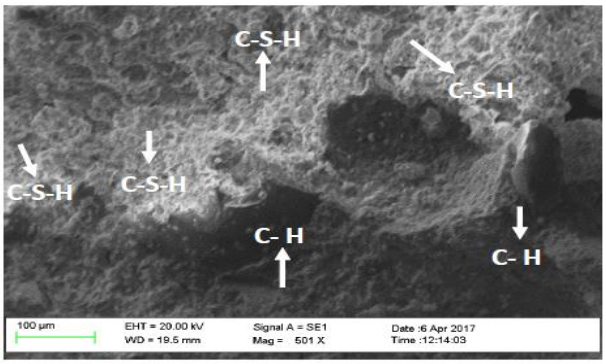

Plate 2: A SEM micrograph of 10% waste glass powder. CH = $Ca(OH)_2$ C-S-H = Calcium Silicate Hydrate gel

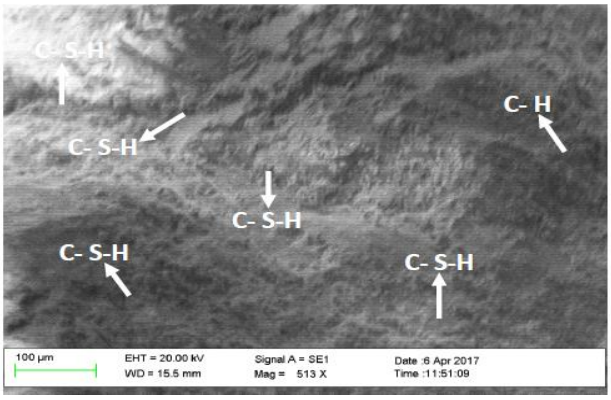

Plate 3. A SEM micrograph of 20% waste glass powder. CH = $Ca(OH)_2$ C-S-H = Calcium Silicate Hydrate gel

Plate 1: shows the micrograph of the control 0% waste glass powder (Pure Portland cement cured at room temperature for 28 days. The grey level of the phases present can be observed. In descending order of brightness, the anhydrous phases, calcium hydroxide, C–S–H gel and porosity (which appears black) can be distinguished, as indicated in plate 1.
The first connected the composition of C–S–H to that of portlandite, marked CH in plate 1 and corresponding to the cement hydration of alite and belite respectively.

These analyses are believed to correspond to a fine intimate mixture of C–S–H and CH formed in space originally occupied by water. It is concluded that it must be finely intermixed with the C–S–H and excess of portlandite $Ca(OH)_2$ of about 10% as indicated in fig. 3.
This results imply that the use of pozolannic materials (SiO_2) reacted with the excess $Ca(OH)_2$ promoted the formation of C–S–H, which was consistent with a high compressive strengths.

In general, the microstructure of 10% (Plate 2.), and 20% (Plate 3.) waste glass replacement were denser than that of the control which was attributed to the presence of abundant and reactive particles of SiO_2 homogeneously dispersed. This result is similar to that of Escalante-Garcia and Sharp (2014).

The microstructure of control sample appeared less dense than the others, which was consistent with the excess of portlandite $Ca(OH)_2$. On the other hand, it was noteworthy that unreacted waste glass powder particles were scarce, and that the smallest ones appeared completely reacted while the larger ones showed thick rims of reaction products (inner products).
This indicates that the SiO_2 strongly promoted the utilization of excess of portlandite $Ca(OH)_2$, but not necessarily the reaction of SiO_2 with portlandite $Ca(OH)_2$. The chemical composition of the rims of the waste glass powder particles had a composition similar to that of (Avila-López *et al.,* 2015) which indicates the presence of silica gel and C–S–H gel.

CONCLUSION

In conclusion the chemical analysis of waste glass powder and cement, samples were determined using X-Ray fluorescence (XRF) technique and found minor differences in the chemical composition of cement, soda-lime silicate and borosilicate glass. The major oxides detected were combined proportion of Silicon oxide (SiO_2), Aluminium oxide (Al_2O_3) and Iron oxide (Fe_2O_3) with percentage value of 73.202%, 72.998%, 0.411%, 0.201%, and 0.223%, 0.112% respectively. The microstructural characterization was also carried out using Scanning Electron Microscope (SEM) and X-Ray Diffraction (XRD) to characterize the concrete samples. It was found that the morphology of concrete samples modified with waste glass powder (10%, 15%, and 20%) was denser than the control sample. Also, XRD results indicated that the intensity of the peaks, in particular of portlandite, is significantly reduced in the 10% waste glass sample than the control (10% of portlandite in the control, 2% of portlandite in 10% and 5% of portlandite in 20% waste glass replacement). Various compositions of the samples (Control 0%, 2.5%, 5.0%, 7.5%, 10%, 12.5%, 15%, 17.5% and 20%) of concrete cube and cylinder samples were prepared and tested for strength at 7, 14 and 28 days of curing. The compressive strength test results of the control and the 10% waste glass replacement were 20.95 N/mm^2, 16.44N/mm^2 for 7, 26.52 N/mm^2 , 24.14 N/mm^2 14, and 31.38 N/mm^2, 28.82 N/mm^2 28 days respectively. The tensile strength test results 2.08 and 1.65, 2.65 and 2.41, 3.13 and 2.89 of the control and the 10% waste glass replacement were 2.08 N/mm^2, 1.65N/mm^2 for 7, 2.65N/mm^2 , 2.41 N/mm^2 14, and 3.13N/mm^2, 2.89N/mm^2 28 days respectively. It can be concluded that all the samples can be used for structural purposes, this is because all the samples (except for 2.5% replacement which had 23.12 N/mm^2) exceeded the maximum strength specified by ASTM 24.2 N/mm^2 at 28 days.

REFERENCE

Ahmari, S. Ren, X., Toufigh, V., and Zhang, L. (2012). Production of Geopolymeric Binder from Blended Waste Concrete Powder and Fly Ash, Constr. Build. Mater. 35 718–729, Http://Dx.Doi.Org/10.1016/J.Conbuildmat.2012.04.044.

ASTM C 618-2005: Specification for Chemical Composition of Pozzolans. ASTM International Headquaters, 100 Barr Harbour Drive, P.O.Box C700 West Conshohocken, Pa 19428-2959, U.S.A.

Avila-López, U., Almanza-Robles, J.M. and Escalante-García J.I. (2015). Investigation of Novel Waste Glass and Limestone Binders Using Statistical Methods / *Construction and Building Materials* 82, 296–303

British Standards European Norm BS EN 1008- (2002). Standard Requirements of Mixing Water, BSI, Garyland and Sons London.

British Standards European Norm BS EN 1260- (2013). Standard Requirements of Aggregates, BSI, Garyland and Sons London.

British Standard Institute 1881-122. (1983). Standard Method of Carring out Moisture and Absorption on Concrete, Linford, Muton Keynes 14 6LE, UK.

Caijun, S., and Keren, Z. (2007). A Review On The Use of Waste Glasses in the Production of Cement and Concrete. Resour Conserv Recycl 52:234–47.

Escalante-Garcia, J.-I., and Sharp J.H (2014). Cement & Concrete Composites 26 967–976.

Gambo, H. I., Mamza, P. A. P., and Gonah, C. M. (2018). Pozzolanic Reactivity of Cement with Soda-lime Silicate and Borosilicate Waste Glass Powder in Concrete Production. *ATBU, Journal of Science, Technology & Education (JOSTE);* Vol. 6(2), June ISSN: 2277-0011.

Komnitsas, K. Zaharaki, D. Vlachou, A. Bartzas, G. and Galetakis, M. (2015). Effect of Synthesis Parameters on the Quality of Construction and Demolition Wastes (CDW) Geopolymers, Adv. Powder Technol. 26 368–376, Http://Dx.Doi. Org/10.1016/J.Apt.2014.11.012.

Madhangopal, K., Nagakiran, B., Sraddha, S.R., Vinodkumar, G., Thajun, P., Kishoresankeerth, S.A., andVaralakshmi, T. (2014). Study the Influence of Waste Glass Powder on the Properties of Concrete IOSR *Journal of Mechanical and Civil Engineering* (Iosr-Jmce) E-Issn: 2278-1684, P-Issn: 2320-334x, Volume 11, Issue 2 Ver. ViPp 34-38.

Mahasenan, N., Smith, S., and Humphreys, K. (2003). The Cement Industry and Global Climate Change: Current and Potential Future Cement Industry CO_2 Emissions, Greenhouse Gas Control Technologies—6th International Conference, Pergamon, Oxford, PP. 995–1000.

Mane, P.S.D. and Mane, R.Y. D. (2012). Comparative Study of Waste Glass Powder Utilized in Concrete *International Journal of Science and Research* 3, 1457-1458

Novais, R. M., Ascensão, G., Seabra, M.P., and Labrincha, J.A. (2016). Waste Glass from End-of-Life Fluorescent Lamps as Raw Material in Geopolymers Waste Management 52 245–255.

Nunes, S., Mafalda, M.A., Duarte, T., Figueiras, H., and Sousa-Couthinho, J. (2013). Mixture Design of Self-Compacting Glass Mortar. Cem Concr Comp 43:1–11.

Oliveira, R., Brito De, J., and Veiga, R. (2013). Incorporation of Fine Glass Aggregate in Renderings. Constr Build Mat 44:329–41.

Schwarz, N., and Neithalath, N. (2008). Influence of a Fine Glass Powder on Cement Hydration: Comparison to Fly Ash and Modeling the Degree of Hydration. Cem Concr Res 38:429–36.

Szabó, L., Hidalgo, I., Ciscar, J.C., andSoria, A. (2006). CO_2 Emission Trading Within the European Union and Annex

B Countries: The Cement Industry Case, Energy Policy 34 72–87.

Taylor, H.F.W. (1997). Cement Chemistry. 2nd Ed. London: Thomas Telford.

Utsevu, J., and Taku, J. K. (2013). Coconut Shell Ash as Partial Replacement of Ordinary Portland cement In Concrete Production. *International Journal of Scientific and Technology Research*, 1 (8), 86-89.

Vignesh, K.N., Aruna, S.V., Manohari, S.P., and Maria, S. (2014). Experimental Study on Partial Replacement of Cement with Coconut Shell Ash in Concrete. *International Journal of Science and Research*. 3(3), 651-661.

Vijayakumar, G., Vishaliny, H., and Govindarajulu, D. (2013).Studies on Glass Powder as Partial Replacement Of Cement In Concrete Production *International Journal of Emerging Technology And Advanced Engineering* (Volume 3issn 2250-2459, ISO 9001:2008 Certified Journal).

Nigerian Journal of Polymer Science and Technology, 2017, Vol. 12, pp 75-84

Received: 01 March 2018 Accepted: 03 September 2018

Mechanical and Cryo-Fracture Properties of *Core-Shell* Clay Filled Epoxy Composites

[§§]Nnamdi Chibuike Iheaturu

Department of Polymer & Textile Engineering, Federal University of Technology, PMB 1526, Owerri, Imo, Nigeria

Abstract

The fracture characteristics and mechanical stability of thermoset composites are of utmost importance in some engineering applications. In this study, novel 3-aminopropyltriethoxysilane coupled nanoporous organically modified calcites, *"core-shell",* clay *"SOBM-Ormocal"* was used to reinforce phenol-free epoxy matrix. Such particulate nanoporous core-shell fillers are meant to diffuse stress concentrations within their host matrices thereby enhancing shear yielding in composite structures. But, on the contrary, this phenomenon greatly limits yielding and post-yield behaviour in particulate filled thermosets giving interesting fracture characteristics which were clearly evident in electron microscopy images obtained after cryo-fracture of the phenol-free epoxy composite samples. A careful assessment of the matting cracked surfaces presented features of brittle fracture even at very low filler loading, with no discernible stretch fibrils or ribs. Instead, crack pinning, tongues, inclusions, river markings, valleys and plateaus and bifurcations, were evident.

Keywords: 3-Aminopropyltriethoxysilane, Nanoporous, Core-Shell, Calcite, Organophilic, Ormocal

Introduction

The use of conventional fillers such as talc, calcium carbonate, mica, layered double hydroxides, sodium or calcium montmorillonite clays, often leads to a temptation of using large quantity of fillers in the polymer matrix, first to cheapen the material, and secondly to have significant improvements in the composite properties, especially mechanical and thermal properties (Dai *et al.*, 2005; Azeez *et al.*, 2012). However, size, shape and form of filler or reinforcement play very significant roles in performance property enhancement (Choudhury *et al.*, 2010; Lee *et al.*, 2003). Polymer composites filled with nano-sized fillers have received considerable attention leading to an upsurge in various engineering applications due to their unique multifunctional property enhancement. Furthermore, it has been widely reported that, the combination of filler nanoscale dimension and high aspect ratio accompanied by surface modification and a high level of nanoscale dispersion and distribution within the polymer matrix usually leads to the improvements in the polymer properties at thresholds of filler volume fractions not more than 5 percent (Azeez *et al.*, 2012; Dai *et al.*, 2005; Fertig & Garnich, 2004; Ha *et al.*, 2007).

Nanoporous fillers with high surface area may also produce good composites at very high filler loading up to 85 percent mass fraction (Carrado, 2000). However, this usually has consequences, and in some cases may be associated with some undesirable properties such as brittleness, unbearable stiffness or loss of opacity in the final nanocomposite material. In an extensive review, Pavlidou and Papaspyrides (2008) reported that the efficiency of properties improvement depends largely on the nature of

[§§] Department of Polymer & Textile Engineering, Federal University of Technology, Owerri, (N. C. Iheaturu, nnamdi.iheaturu@futo.edu.ng)

the filler material, mechanical properties of the filler, the level of adhesion and intimacy between filler and matrix both at the filler-matrix interface, and within the filler material. This has led to various efforts by researchers to improve on the dispersion level of clay platelets in various epoxy matrices. Exfoliation, intercalation and immiscible clay morphologies have been reported as the different possibilities for improved polymer molecule-filler interactions in their host matrix (Paul & Robeson, 2008). The enhanced anatomy and physiology of the internal structure of the polymer composite material by clay intercalation, exfoliation and/or effective interpenetration of the polymeric chains into and within nanoporous core structure of the clay platelets, rather than ordinarily dispersing the clay platelets in the polymer matrix are presumed to be the basis for obtaining composites with good mechanical, dimensional and thermal stability properties (Marouf *et al.*, 2008).

Microstructural Characterization of Composites Fracture – Fractography

Fractography usually begins with a thorough macro and microscopic inspection of the mating surfaces of the fractured composite material. In the case of cracked surfaces, fractography aids the interpretation of the morphology and topographic information of fractured surfaces gleaned at microscopic level (Jansen, 2014). Microstructural defects in epoxy clay composites as a result of particulate solids used as filler or extenders have been seen to be responsible for changes in composites response to loading. Such defects appear as cracks, voids, slipped regions and crazing (Krajcinovic, 1989; Kortschot *et al.*, 1991) Usually, there may be a spatial distribution of these point defects within the entire volume of the composite material leading to possibility of different failure modes; dimple rupture, cleavage, fatigue fracture and decohesive rupture.

However, it has been reported that such fracture modes may be delayed or totally prevented with modified epoxied nanoparticle inclusion that could enhance epoxy composites toughness by way of crack pinning, bridging, crack path deflection, yielding induced shear banding and micro-cracking (Liang & Pearson, 2009, 2010). While, tough and less brittle composites may be due to effective crack bridging by nanoparticle inclusion in an epoxy matrix, the elastic parameters of a polycrystalline nanoporous filler material may be dependent on the type of constituent crystal that makes it a stable mechanical system. It has been reported however, that core clays or nanoporous fillers in thermoplastics or thermoset matrices remain more or less rigid within their host matrices and show non-linear response to an applied force (Liang & Pearson, 2010). On the contrary, Bagheri and Pearson inferred that inter-particle distance of rubber modified nanoporous fillers in epoxy matrix rather than induce micro voids, have a more influential role in toughening epoxy matrices. This investigation was shown via electron microscopy of cryo-fractured surfaces in liquid nitrogen whereby the epoxy composite materials exhibited similar behaviour in fracture toughness tests (Bagheri and Pearson, 1996, 2000). In the investigation by Liang and Pearson, (2009), the crosslink density of epoxy matrix filled with silica nanoparticles was found to be inversely proportional to composites toughness (Liang & Pearson, 2009). This behaviour leads to different fractured surface characteristics of epoxy composite materials. Whereas, at the microscopic level, fracture of brittle and stiff epoxy composites usually takes place without any visible shear yielding and minimal deformation or elongation, macroscopically, the mating fractured surfaces exhibit little separation with minimal distortions (Jansen, 2014). On the contrary, fractured ductile composites would show stretched tips with overhanging fibrils.

Specific objective of this work

Our specific objective is to investigate the mechanical and fracture characteristics of phenol-free amine-cured epoxy composites filled with 3-aminopropyltriethoxysilane (3-APTES) coupled organically modified nanoporous spent oil-base drilling mud otherwise *"core-shell"* organically modified calcite clays - SOBM-ORMOCAL (Iheaturu & Madufor, 2014), in very low temperature environments.

Experimental methods

All chemicals used for this work were of analytical grade. Acetone (CH_3COCH_3) and tetraoxosulphate VI acid (H_2SO_4) were obtained from MERCK KGaA, Darmstadt, Germany. 99% anhydrous ethanol was supplied by Kemetyl A/S, Køge, Denmark. Hexadecyl trimethyl ammonium bromide (HDTMA-Br) ($C_{19}H_{42}N.Br$) dispersant was from SIGMA-ALDRICH, while 3-Aminopropyltriethoxosilane (3-APTES), with structural formula shown in Fig. 1, was supplied by Alfa Aesar GmBH & Co. KG, Karlsruhe, Germany.

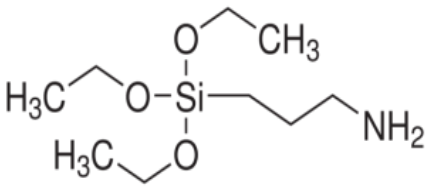

Figure 1: Structural formula of 3-Aminopropyltriethoxysilane (3-APTES), Linear Formula: $H_2N(CH_2)_3Si(OC_2H_5)_3$, Molecular Mass: 221.37g, Density: 0.946 gmL^{-1} at 25°C, Boiling point: 217°C per 760 mmHg

The epoxy resin used for this study is a two (2) component laminating PRO-SET epoxy system from PRO-SET Inc., Bay City, MI, USA. The components are 135/229 epoxy resin and phenol-free amine hardener, which are formulated for laminating synthetic composite structures. The 135/229 mixture, provides a working time of approximately 120 minutes at 22.2°C bonding. According to ASTM D-2427-71, 135/229 has pot life of 59 minutes for 100g mixture. Particle size distribution of the core clay filler material obtained via calcination of spent oil base mud (SOBM) cuttings was 10.94% of particles less than 100µm, out of which maximum size of the smallest 6.78% corresponding to 45µm were 3-aminopropyltriethoxosilane (3-APTES) coupled organically modified SOBM core-clay referred herein as *"core-shell"* clay filler, otherwise SOBM Filler-1. Specific gravity of the core clay is $2.77gcm^{-3}$.

Energy Dispersive X-Ray (EDX) Analysis and Scanning Electron Microscopy (SEM) of SOBM "Core-Shell" Clay

Chemical composition and image analysis of 40µm sized core-clay samples were carried out using the Hitachi SU-70 and Zeiss EVO-60 Scanning Electron Microscope, with accelerating voltage up to 15KV in back scattered mode.

Method for Epoxy Composite Moulding

3-APTES organically modified clays obtained by calcination of spent oil-base drilling mud (SOBM) were introduced into the epoxy resin at various mass fractions of 0.8 mass percent, 1.6 mass percent, 4.0 mass percent, and 8.0 mass percent corresponding to 1g, 2g, 5g and 10g of the total 126g mass of both epoxy and hardener. Method for aminosilane coupling on the organically modified hydrocalcites-rich spent oil-base drilling mud (SOBM) "core-shell" clay, *Ormocal* – christened "SOBM Filler -1", earlier reported (Iheaturu and Madufor,

2014). Epoxy composites preparation method reported by Khanbabaei *et. al.*, (2007), was modified by first of all subjecting a mixture of the epoxy resin pre-polymer and core-shell clay to ultrasonication. A first stage mechanical high speed mixing was carried out at 200rpm for 15minutes. This first stage mixing enables sorption of epoxy pre-polymer into the crevices of the core clay before hardener addition into the mixture. Then, 26g of phenol-free amine hardener was added to the epoxy clay mixture and stirred vigorously with the high speed mechanical mixer. This second stage mechanical mixing was done at 200rpm but this time, for 10minutes in order to homogenize the entire composites formulation. The stirring time was reduced to avoid turbulence and emergence of air bubbles as a result of vigorous stirring action of the stirrer. These steps are clearly represented in Figure 2.

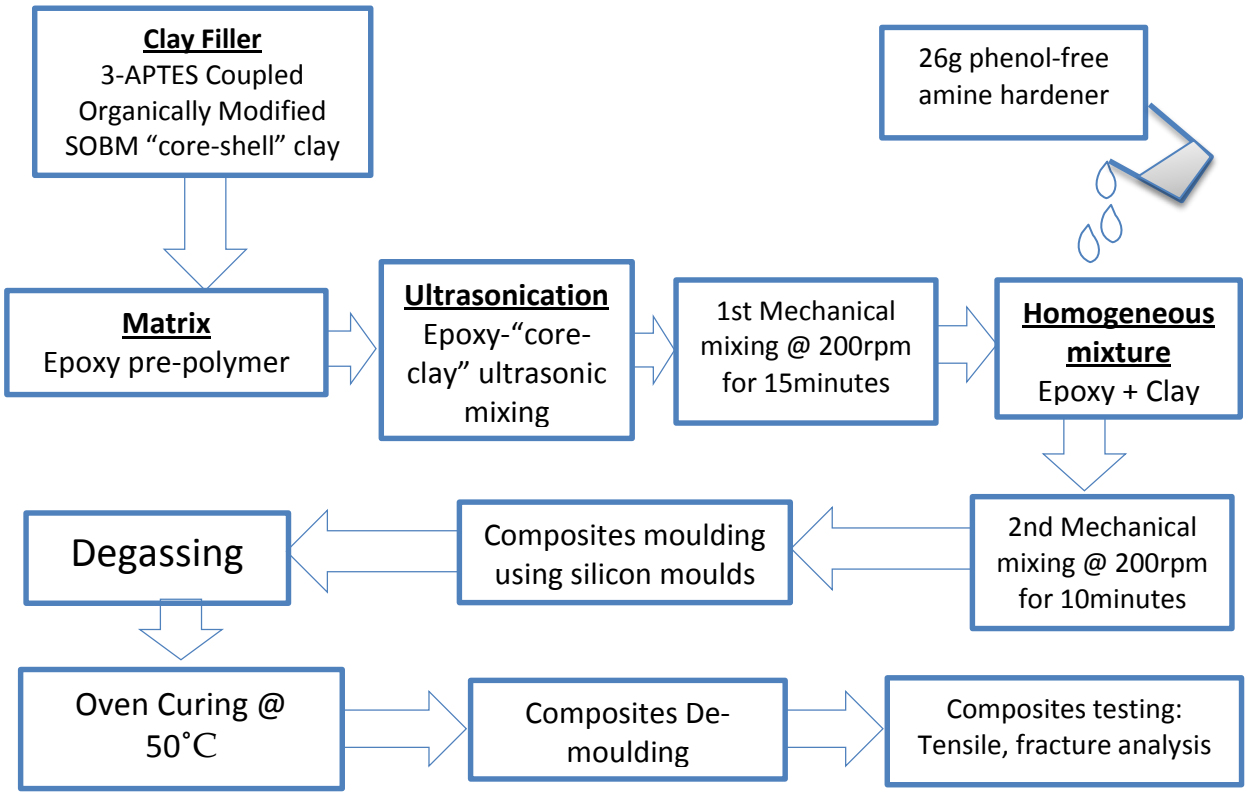

Figure 2: Schematic representation of epoxy composites preparation

To obtain dog-bone shaped composites for testing, the mixture of 100g epoxy and 26g hardener with different mass percent of 3-APTES coupled *"core-shell"* clay filler; 0, 0.8, 1.6, 4.0 and 8.0 mass percent, was poured into silicone moulds. The mouldings were degassed for a few minutes to allow micro-bubbles trapped in the resin-clay mixture in the course of moulding, to escape. Composite curing was done in a laboratory oven at a controlled temperature of 50˚C for 12 hours before releasing them from the mould.

Energy dispersive x-ray (EDX) and scanning electron microscopy (SEM) analysis

High resolution micrograph with resolution of up to 50µm, were obtained with the Hitachi SU-70 and Zeiss EVO 60 SEM in back scattered electron (BE) mode.

Tensile Testing of 3-APTES Coupled Core-Shell Clay Filled Epoxy Composites – ASTM D638

Prior to testing, dog-bone shaped epoxy core-shell clay filled samples were conditioned at liquid nitrogen temperatures of -196˚C for 30 minutes. Tensile tests were carried out with ZWICK/ROELL Z100 equipment according to ASTM D638, at cross-head speed of 500µm/min, grip-to-grip separation of 60mm, and E-modulus speed of 2mm/min. The E-modulus was electronically measured by the extensometer directly connected to the neck of dog-bone sample. All measurements were zeroed before testing.

Fractography

Fractured surfaces were examined using the Zeiss scanning electron microscope, model: EVO 60, with 10KV accelerating voltage. This procedure exposed the topography and surface characteristics of the tensile-tested-to-failure fractured surfaces.

Results and Discussion

Results of EDX and SEM Analysis

Chemical composition of core-shell clay filler by EDX Analysis as obtained by Hitachi SU-70 SEM is presented in Table 1.

Table 1: Chemical composition of SOBM core clay by EDX

Element	*ZAF*	*Weight %*	*Atom %*
Aluminium (Al)	1.827	4.68	7.64
Silicon (Si)	1.521	22.92	35.99
Potassium (K)	1.110	3.13	3.53
****Calcium (Ca)***	1.067	27.87	30.66
Titanium (Ti)	1.193	1.23	1.13
Iron (Fe)	1.123	15.17	11.97
Molybdenum (Mo)	1.442	7.60	3.49
Barium (Ba)	1.356	17.40	5.59
Total		**100.00**	**100.00**

The elemental composition shows almost equal weight fractions (weight %) of 22.92% silicon (Si) and 27.87% calcium (Ca) in the calcined SOBM clay. Iron (Fe) content was 15.17%, while 17.40% barium (Ba) content may have come from barites used as weighting agent in mud formulation.

High resolution micrograph from SEM with resolution of up to 50µm, obtained with the Hitachi SU-70 and Zeiss EVO 60 SEM in back scattered electron (BE) mode are presented in Figures 3 (a.) and (b.).

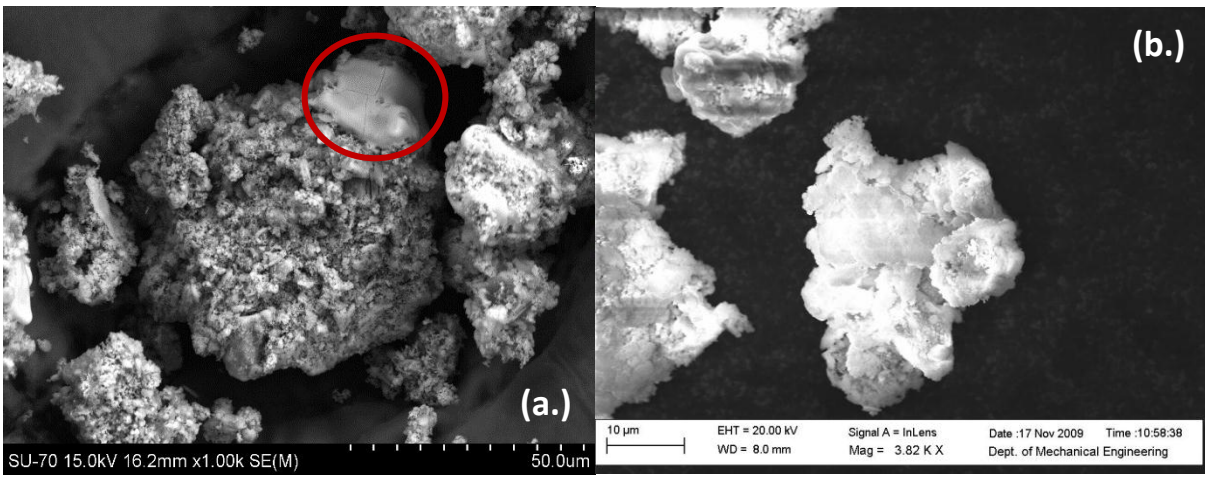

Figure 3: Images of (a.) Calcined SOBM "core" clay and (b.) 3-APTES coupled SOBM "core-shell" clay. Marked zone indicate frozen-in melt region as a result of high temperature treatment

Tensile Properties of Epoxy Composite Samples

The average values of three (3) consecutive tests for one composite formulation, of which ±5% of the average were plotted in Figure 4, representing tensile behaviours of 3-APTES coupled SOBM core-shell clay filled epoxy composites measured at the crosshead speed of 500μmmin^{-1}, while the variations in tensile strength, ultimate strength, percentage strain, E-modulus and toughness with respect to nanoporous core-shell clay filler content in the phenol-free epoxy matrix interpreted from the graph are presented in Table 2.

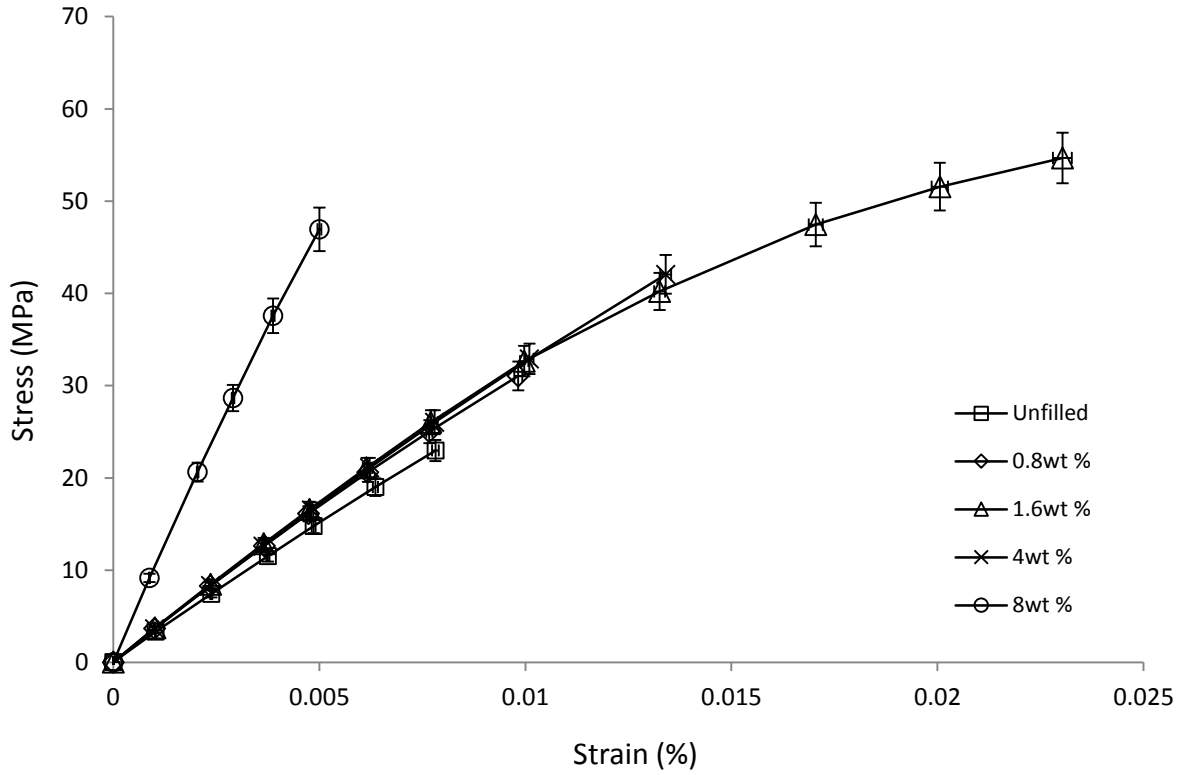

Figure 4: Comparative stress-strain behaviour of 3-APTES coupled core clays

Table 2: Mechanical properties of 3-APTES coupled-SOBM core clay epoxy composites

Composite Sample ID /wt %/	*Strain /%/*	*Ultimate Strength /MPa/*	*E-modulus /GPa/*	*Toughness /MPa.10^{-2}/*
0	0.010	28.666	2.871	0.100
0.8	0.012	35.724	3.069	0.099
1.6	0.023	54.682	3.327	0.194
4	0.015	46.081	3.105	0.128
8	0.005	48.069	10.018	0.048

From Figure 4, there is a clear difference between the tensile strength of unfilled phenol-free epoxy and that of filled epoxy material. Similarly, the effect of gradual increase in filler volume fraction on some mechanical properties of the composites is also evident as shown in Table 2. Almost all the samples showed considerable resistance

to deformation. Whereas the E-modulus value associated with stiffness property of the unfilled phenol-free epoxy matrix was 2.871GPa. The gradual inclusion of the 3-APTES coupled core-shell clay filler, led to increase in E-modulus. However, 4wt% of the core-shell clay filler material, gave a reduced E-modulus of 3.105GPa which may be attributed to dysfunctional filler-matrix interactions due to processing flaws or presence of un-imploded and unreleased micro bubbles trapped within the core-clay structure. The E-modulus increased to 3.327GPa when the filler volume fraction was doubled up to 1.6wt%. As the mass fraction of SOBM Filler-1 increased, the material absorbed more tensile energy than the unfilled epoxy. It is therefore obvious that the core-shell clay material has significant effect at increasing the stiffness of the epoxy composite material. The epoxy composite material with the highest ultimate strength of 54.682MPa is that filled with 1.6wt% 3-APTES coupled core-shell clay filler. However, as filler volume fraction increased up to 8wt %, the composite's ability to withstand the acting tensile force and absorb energy reduced. The normalized strain rate of 4.47 is highest also for the epoxy composite material filled with 1.6wt% core-shell clay filler. This normalized strain value was calculated as a percentage of the unfilled epoxy matrix.

Fracture analysis

Surface characteristics of fractured unfilled phenol-free epoxy and that of 3-APTES coupled nanoporous core-shell clay filled epoxy composites observed with the scanning electron microscope are presented in Figures 5, 6 and 7 respectively. Macroscopically, the cracked samples were characterized by relatively smooth surfaces for the unfilled and all filled epoxy composite samples. But at the microscopic level, as shown in the SEM images, certain features became visible. For the unfilled epoxy, a point of crack initiation is visible in *Figure 5*. Also, visible are diagonal lines of striations, ridges, incisions and river marks in a pattern similar to that resulting from cleavage fracture as a result of sudden impact. However, certain features show that some impurities may have, in one way or the other, found their way into the epoxy matrix-filler mixture during preparation and / or casting.

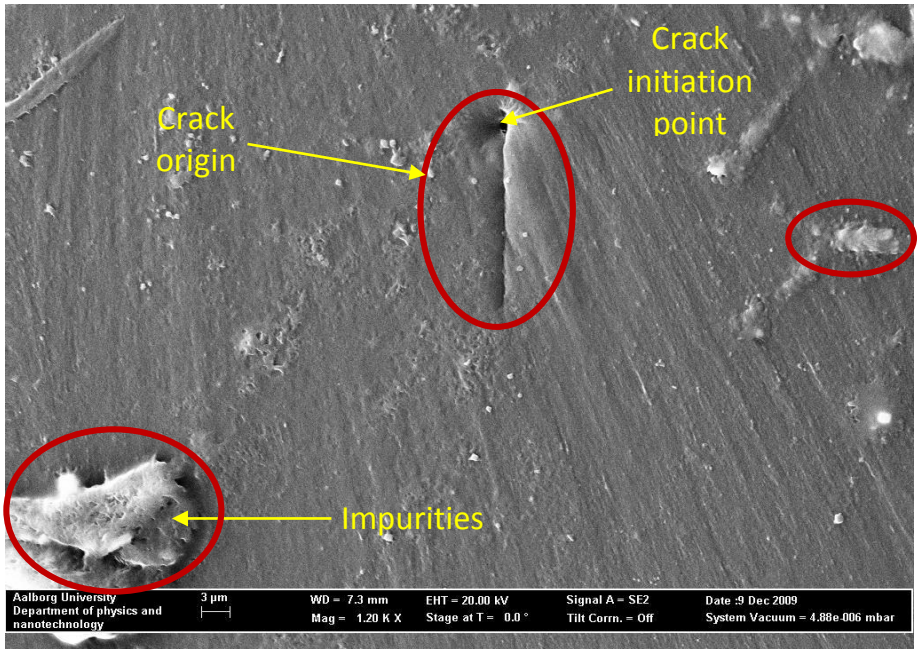

Figure 5 SEM micrograph of fractured unfilled phenol-free epoxy composite

SEM image of 0.8wt% and 1.6wt% silane coupled SOBM clay, as shown in *Figures 6(a.) and (b.)* respectively, indicate the existence of micro-cracks which originated from multiple plateaus and valleys at different elevations with respect to one another. The surfaces are characterized by convex contours whose edges are the grain boundaries of nucleating cracks. Clearly visible also are dimples formed from the existence of micro-voids. These dimples are initiated as a direct consequence of tear and shear loading at the points of nucleating cracks.

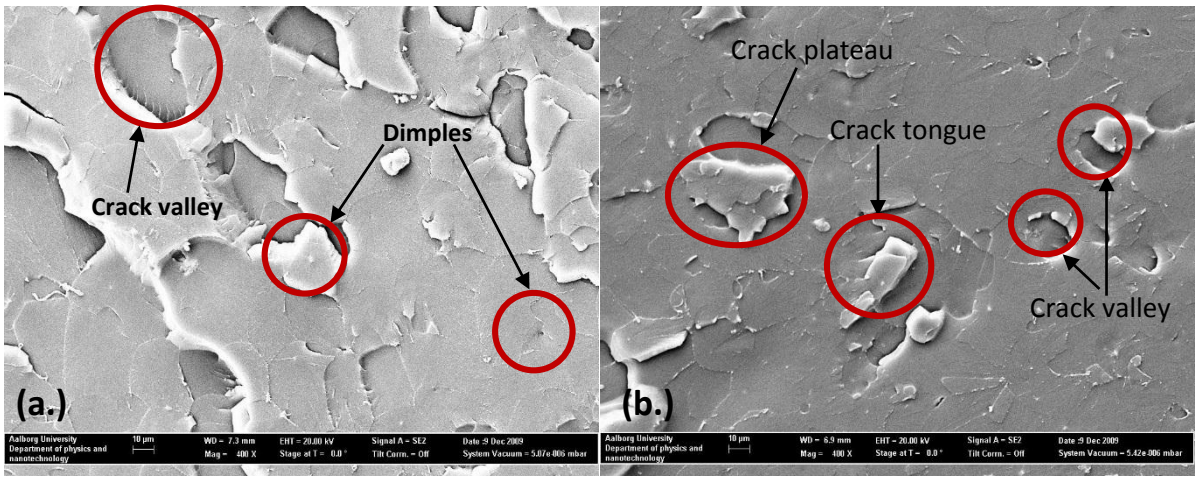

Figure 6: SEM micrograph of fractured epoxy composite surface filled with (a.) 0.8wt% and (b.) 1.6wt% of 3-APTES coupled SOBM core-shell clay filler

From Figure 6, the number of dimples which is governed by number and distribution of nucleating micro-voids is high. On the other hand, fractography of 3-APTES coupled SOBM core-shell-clay filled epoxy composites as presented in Figures 7 (a.) and (b.) respectively, are those of relatively plain surfaces indicating non-linear behaviour of the filled epoxy composites, showing micro-cracks, dips and tongues. It can be inferred that the micro and macro cracks, dips and tongues are indicative of well dispersed and well distributed core-shell clay filler material used as reinforcement in the epoxy matrix.

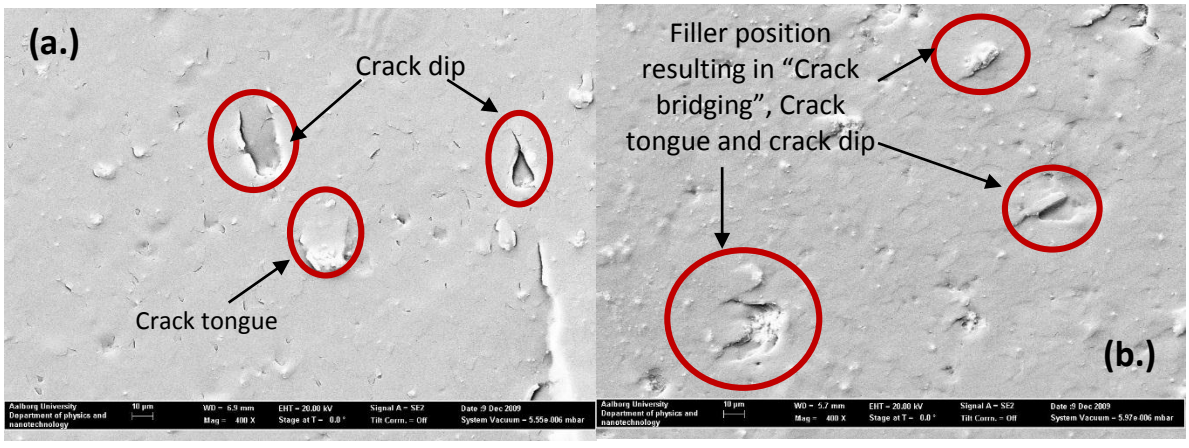

Figure 7: SEM micrograph of fractured epoxy composite surface filled with (a.) 4 /wt% and (b.) 8 /wt% of 3-APTES coupled SOBM core-shell clay filler

4wt% and 8wt% 3-APTES coupled SOBM core-shell clay filled epoxy is indicative of diffused crack propagation along grain boundaries as a result of SOBM core-shell clay particles imbedded in the epoxy matrix. When a fatigue crack approaches such a particle, it is briefly retarded if the particle remains intact, or accelerated if the particle cleaves. In this case, there seems to be a very clear sign of crack path deflection as a result

of SOBM porous clay particle bridging. The crack path deflections may have led to elongated dimples and crack tongues signifying shear fracture as shown in *Figures 6 (a.) and (b.)*. Visible also are multiple points of crack pinning which may be showing a distributed stress concentration along grain lines as a result of SOBM clay nanoporous morphology in the form of foamed clay materials. Evidently, the clays may have helped to diffuse crack propagation along grain boundaries and crack paths.

Conclusion

We have presented phenol-free epoxy composites filled with nanoporous core-shell calcite-aluminosilicate clays and their cryo-fracture character at very low temperatures. Tensile test results show brittle behavior of core-shell clay filled epoxy composites. SEM images confirmed reasons for brittle mechanical behavior with the absence of shear yielding. It is therefore evident that as the silane coupled SOBM clay concentration increased from 0.8wt% to 1.6wt% volume fraction, and with effective SOBM filler dispersion, the clay particles transmitted stresses throughout epoxy matrix while at the same time bridging crack propagation. Normally, in the course of fracture, this phenomenon may delay catastrophic failure of polymer nanocomposite materials, making room for plastic deformation or yielding. However, brittleness of the core-shell clay filled epoxy composite material became more pronounced with increased core-shell clay filler loading above 1.6wt%.

Conflict of Interest

The authors are in agreement with the publication and thereby declare that there is no conflict of interest in publishing this scholarly research article.

Acknowledgement

We acknowledge funding from AppliedSignals International Inter-Disciplinary Research Group (ASIIRG), Project: #22013/AS, Institut f. Maskintecknik and the Department of Physics and Nanotechnology, Aalborg University, Denmark for making their laboratory available for scanning electron microscopy. The supervisory roles of Assoc. Prof. Jens Chr. Rauhe and Laboratory Technologist Thomas Quaede of Aalborg Universitet, Denmark (AAU), are also acknowledged.

References

Azeez, A. A., Rhee, K. Y., Park, S. J., & Hui, D. (2012). Epoxy clay nanocomposites – processing, properties and applications: A review. *Composites Part B: Engineering*, *Article in*, 1–13. https://doi.org/10.1016/j.compositesb.2012.04.012

Bagheri, R., & Pearson, R. (1996). Role of particle cavitation in rubber-toughened epoxies: 1. Microvoid toughening. *Polymer*, *37*(20), 4529–4538. https://doi.org/10.1016/0032-3861(96)00295-9

Bagheri, R., & Pearson, R. (2000). Role of particle cavitation in rubber-toughened epoxies: II. Inter-particle distance. *Polymer*, *41*(1), 269–276. https://doi.org/10.1016/S0032-3861(99)00126-3

Carrado, K. A. (2000). Synthetic organo- and polymer – clays: preparation, characterization, and materials applications. *Applied Clay Science*, *17*(1–2), 1–23. https://doi.org/10.1016/S0169-1317(00)00005-3

Choudhury, A., Bhowmick, A. K., Ong, C., & Soddemann, M. (2010). Effect of various nanofillers on thermal stability and degradation kinetics of polymer nanocomposites. *Journal of Nanoscience and Nanotechnology*, *10*(8), 5056–5071.

Dai, F., Xu, Y., Zheng, Y., & Yi, X.-S. (2005). Study on morphology and mechanical properties of high functional epoxy based clay

nanocomposites. *Chinese Journal of Aeronautics*, *18*(3), 279–282. https://doi.org/10.1016/S1000-9361(11)60310-5

Fertig, R. S., & Garnich, M. R. (2004). Influence of constituent properties and microstructural parameters on the tensile modulus of a polymer/clay nanocomposite. *Composites Science and Technology*, *64*, 2577–2588. https://doi.org/10.1016/j.compscitech.2004.06.002

Ha, S., Ryu, S., Park, S., & Rhee, K. (2007). Effect of clay surface modification and concentration on the tensile performance of clay/epoxy nanocomposites. *Materials Science and Engineering A*, *448*(1–2), 264–268. https://doi.org/10.1016/j.msea.2006.10.052

Iheaturu, N. C. (2013). *Synthesis, Preparation and Characterization of Nanoporous Core-Shell-Clay Epoxy Composites*. Federal University of Technology, Owerri, Nigeria.

Iheaturu, N. C., & Madufor, I. C. (2014). Novel Organically Modified Core-Shell Clay for Epoxy Composites — "SOBM Filler 1." *International Scholarly Research Notices*, *2014*, 1–8. https://doi.org/10.1155/2014/282817

Jansen, J. (2014). Root Cause Analysis: Success in failure. *Plastics Engineering*, 21–26. Retrieved from www.4spe.org

Khanbabaei, G., Aalaie, J., Rahmatpour, A., Khoshniyat, A., & Gharabadian, M. A. (2007). Preparation and properties of epoxy-clay nanocomposites. *Journal of Macromolecular Science, Part B: Physics*, *46*(5), 975–986. https://doi.org/10.1080/00222340701457287

Kortschot, M. T., Beaumont, P. W. R., & Ashby, M. F. (1991). Damage mechanics of composite materials. III: Prediction of damage growth and notched strength. *Composites Science and Technology*, *40*(2), 147–165. https://doi.org/10.1016/0266-3538(91)90094-6

Krajcinovic, D. (1989). Continuum Damage Mechanics: What, When and Why? *Mechanics of Materials*, *8*, 117–197.

Lee, M., Hu, X., Yue, C., Li, L., & Tam, K. (2003). Effect of fillers on the structure and mechanical properties of LCP/PP/SiO2 in-situ hybrid nanocomposites. *Composites Science and Technology*, *63*(3–4), 339–346. https://doi.org/10.1016/S0266-3538(02)00222-1

Liang, Y. L., & Pearson, R. A. (2009). Toughening mechanisms in epoxy–silica nanocomposites (ESNs). *Polymer*, *50*(20), 4895–4905. https://doi.org/10.1016/j.polymer.2009.08.014

Liang, Y. L., & Pearson, R. A. (2010). The toughening mechanism in hybrid epoxy-silica-rubber nanocomposites (HESRNs). *Polymer*, *51*(21), 4880–4890. https://doi.org/10.1016/j.polymer.2010.08.052

Marouf, B. T., Bagheri, R., & Pearson, R. A. (2008). Mechanical and thermal properties of montmorillonite-epoxy nanocomposites. *International Journal of Modern Physics B*, *22*(18 & 19), 3247. https://doi.org/10.1142/S0217979208048176

Paul, D. R., & Robeson, L. M. (2008). Polymer nanotechnology: Nanocomposites. *Polymer*, *49*(15), 3187–3204. https://doi.org/10.1016/j.polymer.2008.04.017

Pavlidou, S., & Papaspyrides, C. D. (2008). A review on polymer – layered silicate nanocomposites. *Progress in Polymer Science*, *33*, 1119–1198. https://doi.org/10.1016/j.progpolymsci.2008.07.008

Nigerian Journal of Polymer Science and Technology, 2017, Vol. 12, pp 85-92

Received: 20 August 2018 Accepted: 17 October 2018

Comparative Study of Conventional Paver Block with Coir Fibre Filled Waste Low-Density Polyethylene Paver Blocks

Yibowei, Moses E[1***]., Biotidara Frank O[1]., Ichetaonye Simon I[1]., Ugo Kingsley U[1]., Adekoya, Joseph G[1]., Idemudia, Lawrence O[1], Nwigwe, Uzoma S[2]

[1] *Department of Polymer and Textile Technology, Yaba College of Technology, Lagos State, Nigeria.*

[2] *Department of Mechanical & Mechatronics Engineering, Federal University Ndufu-Alike Ikwo, Ebonyi State, Nigeria.*

Abstract

Plastic waste materials pose great challenge worldwide as they affect both human and marine life, in every environment where waste is indiscriminately disposed of. The use of coir fibre and WLDPE for the production of paver block has been studied. **Rockwell hardness**, **water absorption**, and **compression tests** were conducted on samples developed with cement and WLDPE with 5%,10% and 15% coir fibre-content. This is supported with Phenom Pro Desktop **SEM**. The convention paver block recorded a hardness value of 97.3RHN while the 15% filled WLDPE block had the highest hardness value of 91.3RHN compared to other WLDPE blocks. The water absorption result showed that the 5% filled WLDPE blocks absorbed 2.20%, the cement block had 4.96% water absorption and the 15% filled block recorded absorption of 8.20%%. The WLDPE blocks, however, showed better compression strength than the cement blocks. The 5% filled WLDPE had the highest compression strength of 20.1MPa with the cement block recording a value of 9. 56MPa.Results from this study show that WLDPE offers better and cheaper alternative for the production of paver blocks.

Keywords: Waste Low-Density Polyethylene (WLDPE), Compression strength, paver block.

Introduction

The production and demand of plastics globally have increased consistently since the first plastic material was produced. Hence, an increase in the amount of plastic waste generated. Greyor, Jambeck, and Law (2017) calculates that 8.3 billion metric tonnes of plastic have been produced in the 65 years since when plastics were mass produced, 6.3 billion metric tonnes of plastic waste has been generated as of 2015, only 9% have been recycled, 12% incinerated and 79% deposited in landfills or natural environment.

As plastic is non-biodegradable, its disposal has been a problem. The 79% deposited in landfills and other natural environment pose grave environmental hazards, however, these hazards can be reduced through a thorough recycling process. Plastic recycling is the process of recovering plastic wastes and turning old or scrap plastic into useable products that can re-enter the manufacturing chains. The recycling of plastics is capable of creating more job opportunities and minimize the hazards associated with improper disposal of plastic wastes (Temitope et al.,2015).

*** *Department of Polymer and Textile Technology, Yaba College of Technology, Lagos State, Nigeria* (Yibowei, Moses E, mosesyibowei@yabatech.edu.ng and mosesyibowei@gmail.com)

The increasing demand for alternative construction materials other than Ordinary Portland Cement (OPC) has led to research in the application of plastics as construction materials. Typically cement contain an average of 84% Portland cement clinker; the clinker manufacturing process releases 0.9 tonnes of CO_2 per tonne of clinker (Mehta and Walters,2008). The emission of CO_2 is responsible for global warming. In order to protect the environment, it is necessary that new materials with improved mechanical be developed. The use of waste plastics for making paver blocks has several advantages over conventional cement paver blocks. Some of the advantages include relative cheapness, less time required for production, comparative lightweight to that of cement paver blocks, and reduction in the emission of greenhouse gases (Temitope et al.,2005).

One challenge with the use of waste plastics as replacement for fine or coarse aggregate in concrete or mortar mix is the reducing compressive and flexural strength with increasing plastic addition. Pramod et al., (2013) used recycled plastic aggregate as replacement for coarse aggregate in the production of concrete. Results showed decrease in 7days and 28days compressive strength with as coarse aggregate was replaced with recycled plastic. Similar result was obtained by Ramesh et al., (2004) and Zainab and Enus (2007). Zainab and Enus attributed the decreasing compressive and flexural strength to poor adhesion between plastic and cement.

Low-Density Polyethylene (LDPE) which is used in the production of plastic bags and films make up a large chunk of all plastic waste in Nigeria. This is as a result of millions of used polyethylene being thrown on a daily basis onto the streets of virtually every city, town and villages in Nigeria (Babatunde and Biala,2010; Bassey et al.,2017). Sources of these waste include Residential, commercial, institutions and industries. About 70% of Nigerian adults drink, at least a sachet of water per day resulting to almost 50 to 60 million used polyethylene sachets disposed of daily across the country (Bassey, et al., 2017).

Coir is the name given to the fibrous material that constitutes the thick mesocarp (middle layer) of the coconut fruit (Cocos nucifera). The husk of the coconut contains approximately 75 percent fibre and 25 percent fine material (Maher,2008). Coir fibre has the highest toughness of natural fibres and they have been used as reinforcement in low-cost concrete structures (Ali, et al., 2012).

In this work, an attempt has been made to manufacture paver blocks by using waste LDPE up to 70% by weight, with fine aggregates and coir fibres. The blocks produced were tested for their compressive strength, hardness and water absorption.

Experimental

Materials

The Waste Low-Density Polyethylene (WLDPE) was sourced from different residences and industries and dumpsites in Lagos. Coir fibres were also collected from Badagry market in Lagos, Nigeria. The entangled fibres were separated by hand, washed with distilled water and cut to 1-inch lengths. River sand was sieved to get a particle size of 3.5mm

Fig 1: Shredded WLDPE

Fig 2: Developed WLDPE block

Fig 3: Coir Fibre

Material preparation/ Methodology

The collected waste plastic was washed, shredded and dried. Sand was poured into a metal barrel and heated to 200^{O}C for 15mins and the shredded plastic was introduced. The mixture was heated and stirred for 15mins to get a paste. Different weight percentage composition of coir fibres; 5%,10% and 15% were added to the paste, stirred for 2mins and poured into a 194mm x 134mmx 40mm I-section paver mould. Proper compaction was done to ensure that the paste fills the entire mould and no air was trapped. Samples were taken out of the mould and allowed to cure at ambient temperature for 7 days.

Test procedure

Hardness

A hardness test was carried out on the samples to measure the resistance to indentation with a Qualitest, Rockwell Hardness Tester and it was determined by measuring the permanent depth of the indentation. A sample was placed on the sample holder and a sharp dent was made by a load of 1500N on the sample. Each sample was tested at different points, the hardness values were recorded and the average was calculated. The sample hardness was tested on either end of the samples and also at the centre.

Compression

The compression test was determined on each sample using a motorized crushing machine. Samples were weighed and placed between two plates which applied load across the entire surface area of the two opposite faces of the test sample causing the sample to deform.

Water absorption

The water absorption was determined according to ASTM D570.Samples cut to 5mm by 5mm were dried in an oven for 1hr at 50^{o}C and allowed to cool. They were immersed in 100ml of water for 24 hrs they were taken out, wiped clean with a cloth and re-weighed. The water absorption was calculated using the Eq. (1).

$$\% \text{ Water Absorption} = \frac{w_2 - w_1}{w_1} \times 100 \quad \text{Eq. (1)}$$

W_2 = Wet weight (g)

W_1 = Dry weight (g)

Morphology

The morphology of the samples was determined using a Phenom Pro Desktop Scanning Electron Microscope (SEM) with a magnification range up to 150,000x and light optical magnification between 20-134x. A 10mm diameter and 5mm thick sample was mounted on the stub using a metallic adhesive, the stub was place on a

sample holder and the height of the sample was adjusted so that it was just 2mm from the surface of the holder. A 10KV electron beam was focused on the samples with the view depth of 521µm to view the surface.

Results

Compressive Strength

The WLDPE samples did not fracture, unlike the cement blocks, rather they continued to flatten out as the load was applied. However, there was a consistent reduction in the compressive strength as fibre loading increased. The reduction in compressive strength as fibre loading increased could be as a result of poor interfacial adhesion between the fibre and plastic (Meenalochani & Vijayasimha Reddy, 2017). The 5% WLDPE had the least compression strength compared to other WLDPE samples. Comparing the WLDPE blocks with the cement blocks, the WLDPE block had better compressive strength.

Table 1: Compressive strength of cement and WLDPE samples

Sample	WLDPE Ratio	Coir Ratio	Sand Ratio	Cement Ratio	Compression Strength(Mpa)
Cement block	NIL	NIL	4	1	9.6
WLDPE (5%)	1	0.07	0.4	NIL	20.1
WLDPE (10%)	1	0.14	0.3	NIL	16.2
WLDPE (15%)	1	0.21	0.2	NIL	10.8

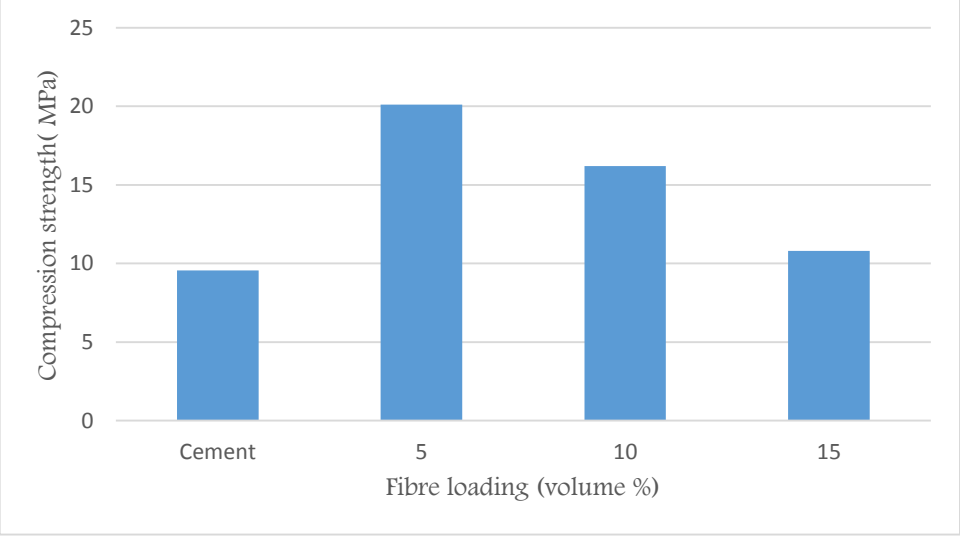

Fig. 4: showing graph of compression strength against fibre loading

Hardness

Figure 5 shows the graph of hardness against fibre loading. The cement blocks

had the highest hardness value. Again, the hardness of the 5% WLDPE sample was the lowest due to the presence of large pores in the sample. There was little change in the hardness of the 10% and 15% filled WLDPE.

Table 2: Hardness values of cement and WLDPE samples.

Sample	WLDPE Ratio	Coir Ratio	Sand Ratio	Cement Ratio	Hardness (HRN)
Cement block	NIL	NIL	4	1	97.3
WLDPE (5%)	1	0.07	0.4	NIL	88.5
WLDPE (10%)	1	0.14	0.3	NIL	90.0
WLDPE (15%)	1	0.21	0.2	NIL	91.3

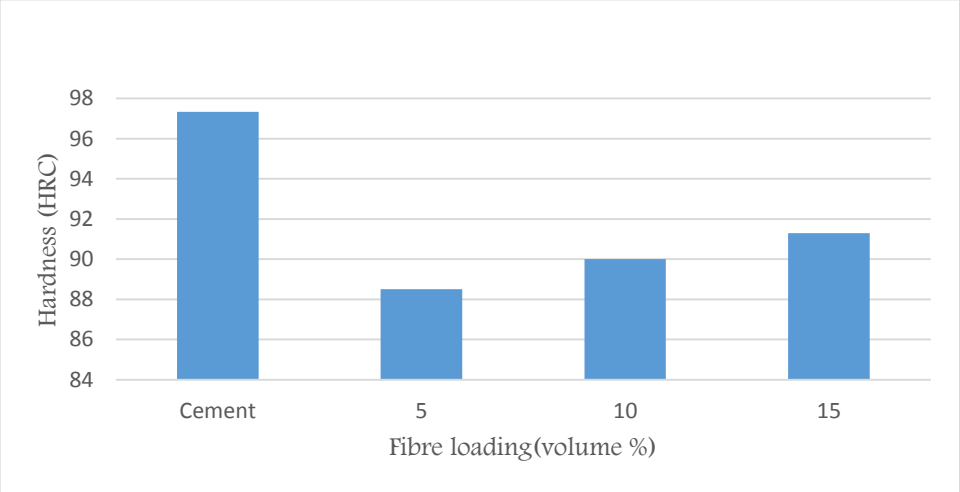

Fig. 5: showing graph of hardness against fibre loading

Water absorption

The water absorption result showed that the cement block absorbed more water than the WLDPE samples. It also showed that fibre addition led to increasing water absorption. Coir like most natural fibres has high hydroxyl content making it susceptible to absorb water. The water absorption tends to increase with increased fibre content (Meenalochani & Vijayasimha Reddy, 2017). Comparing the cement block with the WLDPE block, results showed that the WLDPE blocks absorbed less water.

Table 3: Water absorption value of cement and WLDPE samples

SAMPLE	WLDPE RATIO	COIR RATIO	SAND RATIO	CEMENT RATIO	WATER ABSORPTION (%)
Cement block	NIL	NIL	4	1	4.96
WLDPE (5%)	1	0.07	0.4	NIL	2.19
WLDPE (10%)	1	0.14	0.3	NIL	3.33
WLDPE (15%)	1	0.12	0.2	NIL	8.20

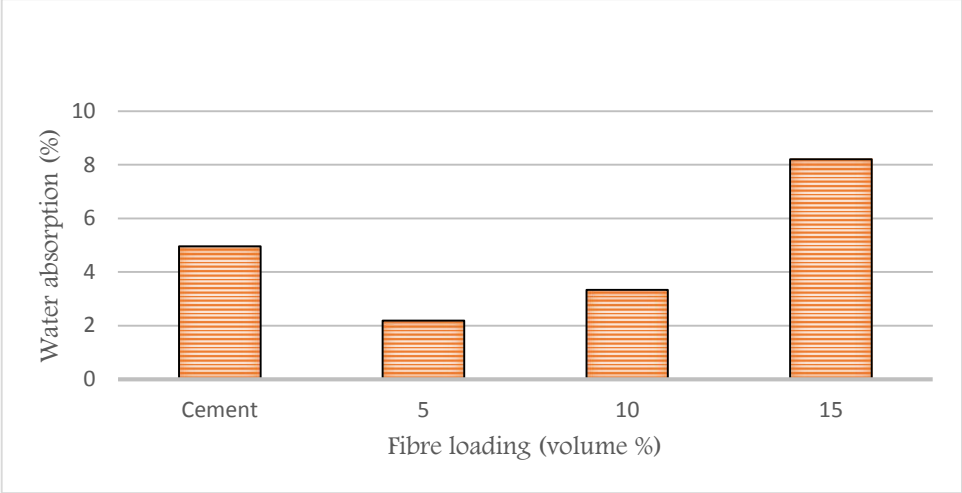

Fig. 6: showing graph of water absorption against fibre loading

Micrograph

Fig. 7, 8 and 9 shows the micrograph of 15%,5% and 10% filled plastic blocks respectively after failure. Fig 7 show fibre pull out from the plastic matrix due to poor interfacial adhesion. Fig. 8 also shows the growth of crack along the surface of the plastic. There was also poor interfacial adhesion between the fine aggregate and WLDPE, thus causing the fine aggregate to slide out of the matrix during compression, as can be seen in fig. 9, this explains why the blocks flattened out during the compression test and almost lost its shape.

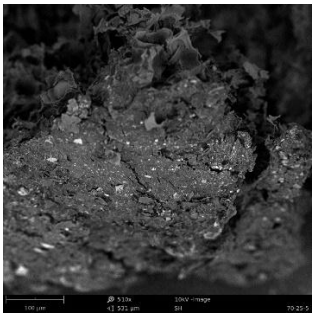

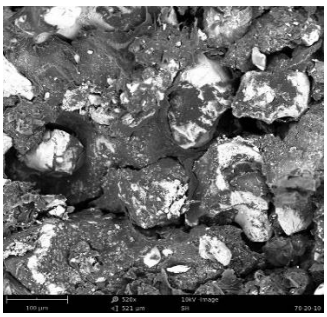

Fig. 7: Microstructure of 15% filler Fig. 8: Microstructure of 5% filler Fig 9: Microstructure of 10% filler

CONCLUSION

Waste LDPE can serve as a good replacement or alternative to the use of cement for the production of paver blocks. The incorporation of fibres such as coir could help increase the hardness of the material but does not improve the compressive strength beyond 5% loading for paver blocks. However, better results can be achieved when the interfacial adhesion between the fibres and WLDPE is enhanced with the use of a coupling agent.

References

Ali, M., Liu, A., Sou, H. & Nanawi, C., 2012. Mechanical and dynamic properties of coconut fibre reinforced concrete. *Construction and Building Materials,* Volume 30, pp. 814-825.

Babatunde, A. M. & Biala, M. I., 2010. Externality effects of sachet water consumption and the choice of policy instruments in Nigeria:Evidence from Kwara. *Journal of Economics,* 1(2), pp. 113-131.

Bassey, Gitu,I.,Egbe,Jerome,G.,Ewa,Desmond.E.,Ettah & Emmanuel,B., 2017. Reprocessing of Low Density Polyethylene(LDPE) waste materials for the formation of PVC ceiling blocks using saw dust as reinforcement. *Journal of Architecture and Civil Enginnering,* 3(4), pp. 9-15.

Geyer, R., Jambeck, J. & Law, K. L., 2017. Production,use and fate of all plastics ever made. *Science Advances.*

Maher, M., Prasad, M. & Raviv, M., 2008. Organic soilless media components. *Soilless Culture,* pp. 459-504.

Meenalochani, K. S. & Vijayasimha Reddy, B. G., 2017. A review on water absorption behaviour and its effect on mechanical properties of natural fibre reinforced composites. *International Journal of Innovative Research in Advanced Engineering,* 4(4), pp. 143-147.

Mehta, P. K. & Walters, M., 2008. Roadmap to sustainable concrete construction industry. *The Concrete Specifier,* 61(1), pp. 48-57.

Pramod, S.,Patil,J.R.,Mali,Gavesh,V.,Tapkire,H.R. & Kumavat., 2013. Innovative techniques of waste plastic used in concrete mixture. *International Journal of Research in Engineering and Technology.*

Ramesh , R. L.,Asharani,K.M.,Dhiraj,K.V.,Pruthri,S.D. & Sahana,R., 2001. *Recycled plastic used as coarse aggregate for constuctional concrete,* Bangalore: s

Temitope, A. K., Abayomi, O. O., Ruth, A. O. & Adeola, A. P., 2015. A pilot recycling of pure water sachets/bottles into composite floor blocks:A case study from selected dumping site in Ogbomosho. *Journal of Material Sciences and Engineering,* 4(6).

Zainab, Z. I. & Enus, A. A., 2007. *Use of waste plastic as concrete mixture or agggregate replacement,* Baghdad: